A Unified Analysis of the B = 2 System

By

Chang-Heon Oh

Dissertation submitted to the Faculty of the

Virginia Polytechnic Institute and State University

in partial fulfillment of the requirements for the degree of

DOCTOR OF PHILOSOPHY

IN

PHYSICS

APPROVED:

Richard A. Arndt, Co-Chairman

John R. Ficenec, Co-Chairman

L. David Roper

David A. Jenkins

Ron L. Workman

Key Words: K-matrix, Partial Wave, Nucleon, Pion, Deuteron

A Unified Analysis of the B = 2 System

By

Chang-Heon Oh

Richard A. Arndt and John R. Ficenec, Co-Chairmen

Physics

(ABSTRACT)

Results are presented for a unified analysis of the reactions $pp \to pp$, $\pi d \to \pi d$ and $\pi d \to pp$ over the center-of-mass energy interval from pion threshold to approximately 2.4 GeV. These results for $\pi d \to pp$ and πd elastic scattering are superior to previous VPI analyses of these reactions. In particular, the overall phase in $\pi d \to pp$ has now been determined. Comparisons and predictions are made with previous (separate and unified) analyses of this two-baryon system. Several partial wave amplitudes show resonance-like behavior in these reactions.

Acknowledgments

I would like to thank my advisor, Dr. R.A. Arndt, for his individual guidance and patience over the past years. I would also like to thank my graduate student advisor and co-chairman, Dr. J.R. Ficenec, for his concern and encouragement. Credit should be given to my CAPS group members, Drs. R.L. Workman and I.I. Strakovsky, for their many discussions and generous help on this study. Thanks also goes to Drs. L.D. Roper, D.A. Jenkins, and T. Mitzutani for helpful suggestions and comments. I would like to express my deep appreciation to Chris Thomas who has always been ready to help, and R.A. Link for his support in setting up the computers.

I wish to thank again Drs. R.A. Arndt and L.D. Roper for their especially kind care for me as their last graduate student.

I have benefited from financial assistance provided by the U.S. Department of Energy and the Physics Department at VPI&SU.

Finally, a special thank goes to my dear wife and son who made this dissertation successful. Credit is also given to my relatives.

I will always be in debt to my loving parents. They have always believed in me and encouraged me to achieve with great love and patience. This thesis is dedicated to them.

Contents

List of Figures

List of Tables

Chapter 1

INTRODUCTION

Although nuclear physics has been studied for almost a century, there are many unsolved problems. The intermediate energy range is a particularly useful area to understand nuclear physics, as interactions in this energy region are studied through different kinds of theoretical approaches (such as the potential model). This is the transition region between low energy physics which cannot be solved using standard perturbation techniques and high energy physics where some process can be studied using perturbative QCD. In the intermediate energy range there are only a few low angular momentum states available and a few open channels, thereby simplifying the analysis.

Scattering is a general tool used to study the dynamics of the interactions which govern the behavior of particle systems. All the information from scattering is characterized by the scattering amplitudes which depend on the kinematical variables, such as scattering angle and energy, and also on the quantum numbers describing the states of the particles participating in the collision process.

Analysis of scattering information allows one to examine the predictions of different theoretical approaches of strong interactions between subatomic particles. It also allows one to suggest experimentation that can differentiate between theoretical models and provide practical information for models. For this purpose, it is necessary to analyze scattering information from the entire available data set over an appropriate energy range without resorting to other theoretical inputs or models.

Only a complete, unbiased analysis can provide amplitudes that can be compared with theoretical models and can guide effective experimentation.

The first step in the understanding nuclei is to understand the two nucleon (NN) system. The nucleon is a baryon(B). All the baryons and mesons (the p meson is an example) are hadrons that experience the strong interaction. To study strong interactions, the simplest choice is the two nucleon system. It has a long history of study in nuclear physics, and is easily accessible to experimentation. However, overall phases in inelastic channels are still undetermined. In addition, there is a resonance-like behavior in the two nucleon interaction. The very existence (or non-existence) of actual "resonant" (or "pseudo-resonant") states has been a hot issue in the Nuclear Physics community over the last half century.

A unified partial wave analysis of the two baryon system is required to understand the two nucleon structure and the resonance-like states. By constructing a unified system and simultaneously analyzing the results of reactions in the form of detailed partial waves, a consistent picture should emerge. However, until the present time, no such unified analysis has been presented.

In the intermediate energy range, it is useful to employ a multi-channel formalism in analyzing all existing data simultaneously. In the present work, we have used the K-matrix formalism in order to unify the analysis of several reactions ($pp \to pp$ [1], p$d \to$ pd [2], and p$d \to pp$ [3]) which have, in the past, been considered separately - the most updated versions of the analyses for these reactions are provided by SAID[4]. The center-of-mass energy $\sqrt{s}$ range was chosen to include all of VPI results for the pion-induced reactions with pion kinetic energies (T_π) from 0 to 500 MeV.

This thesis contains eight chapters and four appendices. A survey of previous work, relevant to this thesis, is presented in Chapter 2. Chapter 3 gives the formalisms for the observables of three reactions. All the scattering information is decomposed into angular momentum states, namely a partial wave decomposition. On the other hand, the two nucleon system contains spin. Depending on the polarization of the scattering states, independent measurements are reconstructed using helicity amplitudes. Chapter 4 gives the multi-channel *K*-matrix formalisms for the unified analysis. Chapter 5 gives the data distribution of the three reactions. Results of the partial wave analysis for a unified two baryon (B = 2) system will be explained in Chapter 6; and in this chapter, the unified and separate analyses will be compared, and the phase ambiguity in the separate $\pi d \to pp$ analysis[3] will be described. In chapter 7, the detailed energy dependence of the amplitudes will be explained with Argand plots. Study of resonance-like behaviors in the two baryon system and the predictions for the observables will also be provided in this chapter. Chapter 8 concludes the present work with a discussion of the results from the unified analysis of the $B = 2$ system, and with suggestions for future work and experiments.

Chapter 2

BACKGROUND

An understanding of the NN interaction is fundamental to studies of the more general πNN problem[5]. Two nucleon elastic($NN \rightarrow NN$) scattering is the simplest choice for the purpose of studying the two baryon system, since nuclei are built from protons and neutrons. Below 1 GeV, in proton laboratory kinetic energy (T_p) for the NN system, the dominant channels contributing to NN inelasticity are πd and $N\Delta$ [6]. The Δ is a resonant state with spin $3/2$ that decays predominantly to the πN .

The pion is the lowest mass strongly interacting meson and is considered a carrier of the strong interaction between nucleons.

Another important object to study in nuclear physics is the deuteron. The deuteron is the nucleus of the heavy hydrogen atom (deuterium); the stable but lightly-bound combination of one proton and one neutron. It is the simplest multi-nucleon system, and the only known bound state of two nucleons with baryon number two (B = 2) and isospin zero (I = 0). The deuteron's binding energy is 2.224 MeV[7].

The proton-proton elastic ($pp \rightarrow pp$), pion-deuteron elastic ($\pi d \rightarrow \pi d$), and pion-deuteron to proton-proton ($\pi d \rightarrow pp$) reaction have long been recognized as an important arena to study the strong nuclear force. One reason is they are the simplest examples of the strong interaction easily accessible to experimentation. These interactions are obviously important to our understanding of the hadronic force. Explicit first principle calculations of the physical observables, cross sections, and polarizations are not yet possible. Recent analyses for *NN* elastic[1], πd elastic[2], and $\pi d \to pp$ inelastic[3] scattering have been performed by the VPI&SU group; and the most updated versions of the analyses of these reactions are provided by SAID[4].

Our knowledge of the *B* = *2* system has been enhanced through partial-wave analyses of the *NN* and πd subsystems. One interesting feature of these analyses is the appearance of resonance-like behavior in a number of partial-waves. Similar structures have been seen in *NN* and πd elastic scattering as well as the reaction $\pi d \to pp$.

Above T_p = 280 MeV, the two nucleon reaction can produce a pion. It produces πNN, πd, and $N\Delta$. Since the interaction range is governed by the strong interaction, the $\pi^- d$ elastic reaction is identical with $\pi^+ d$ elastic reaction before Coulomb correction. Both the *NN* and πd reactions produce πNN, $N\Delta$, $\pi N\Delta$, *NN**(1440), *NN**(1520), *etc*. All these channels are usually accounted for by a single " $N\Delta$ " channel. This catch-all channel is indeed mainly the $N\Delta$ channel.

The most important thresholds are illustrated schematically in Figure 1. Figure 1 shows the energy scale in terms of the total center-of-mass energy ($\sqrt{s} = W$) and the incident kinetic energies of the proton (T_p) and the pion (T_π) in

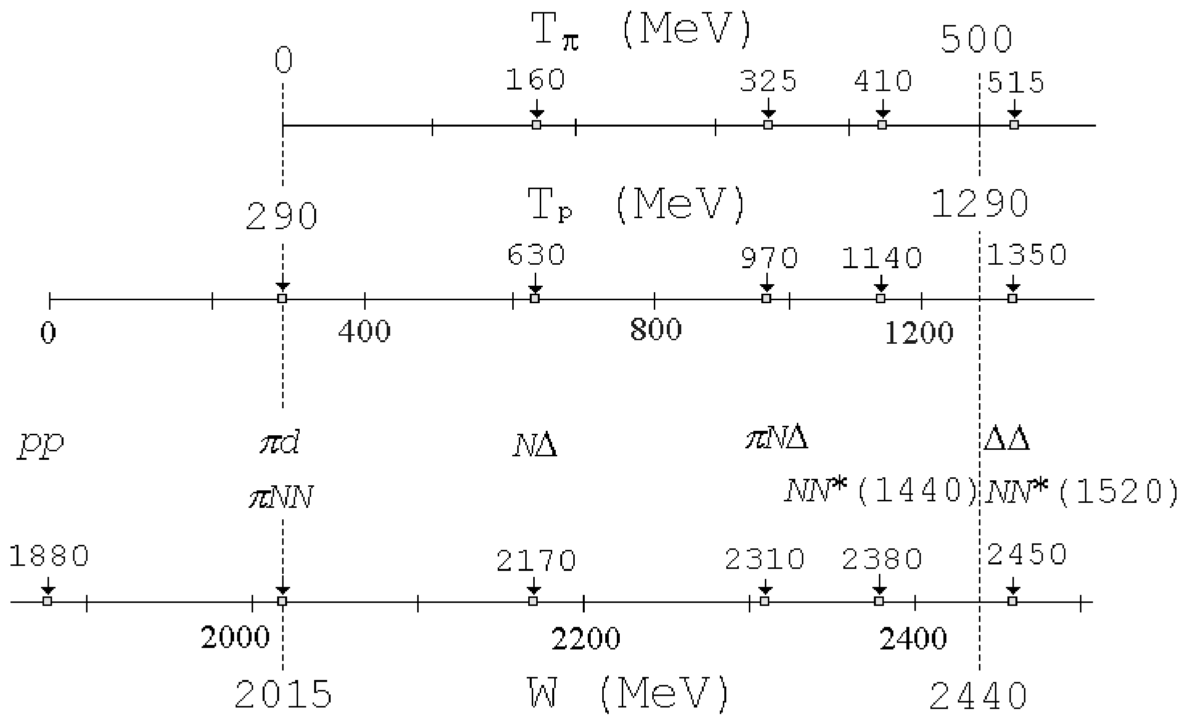

Figure 1. Energy scale in terms of the total center-of-mass energy ($\sqrt{s} = W$) and the incident kinetic energies of the proton (T_p) and the pion (T_p) in the *pp* and p*d* initial states, respectively. The vertical dashed lines show the energy range of the analysis. The locations of relevant thresholds are also presented. Relations among the total center-of-mass energy ($\sqrt{s} = W$) and the incident kinetic energies of the proton (T_p) and the pion (T_p) in the *pp* and p*d* initial states are presented in Appendix A.

the pp and πd initial states, respectively. The vertical dashed lines show the energy range of the analysis. The locations of relevant thresholds are also illustrated. Relations among the total center-of-mass energy ($\sqrt{s} = W$) and the incident kinetic energies of the proton (T_p) and the pion (T_π) in the pp and πd initial states are given in Appendix A.

Figure 2 shows that the catch-all channel is indeed mainly $N\Delta$ channel, where the total cross sections for pp and πd scattering are broken into their components. $N\Delta$ is the most dominantly produced system from both the πd and NN reactions, while other produced systems are infrequent below T_p = 1290 MeV. Figure 2 (a) displays the total pp cross sections, σ_{tot} (solid) and total elastic cross sections σ_{tot}^{el} (dashed) correspond to the unified (C500) solution. Data for σ_{tot} (open circles) are taken from the SAID[4] data base. Dash-dotted line, corresponding to the C500 solution, shows the total cross section ($\sigma_{tot}^{pp\to\pi d}$) for $pp \to \pi d$. The corresponding data from the SAID database are plotted as open triangles. The remainder ($\Delta\sigma$) is given by $\sigma_{tot} - \sigma_{tot}^{el} - \sigma_{tot}^{pp\to\pi d}$ and plotted as a dotted line. Total cross sections for the reactions $pp \to \Delta^+ p + \Delta^{++} n$ [7] are plotted as dark circles. Details of the observables will be provided in Chapter 3.

Figure 2 (b) describes total πd cross sections. σ_{tot} (solid) and total elastic cross sections σ_{tot}^{el} (dashed) correspond to the unified (C500) solution. Data for σ_{tot} (open circles) are taken from the SAID[4] data base. Dash-dotted line (C500) shows the total cross section ($\sigma_{tot}^{\pi d \to pp}$) for $\pi d \to pp$. The corresponding data from the SAID database are plotted as open triangles. The remainder ($\Delta\sigma$) is

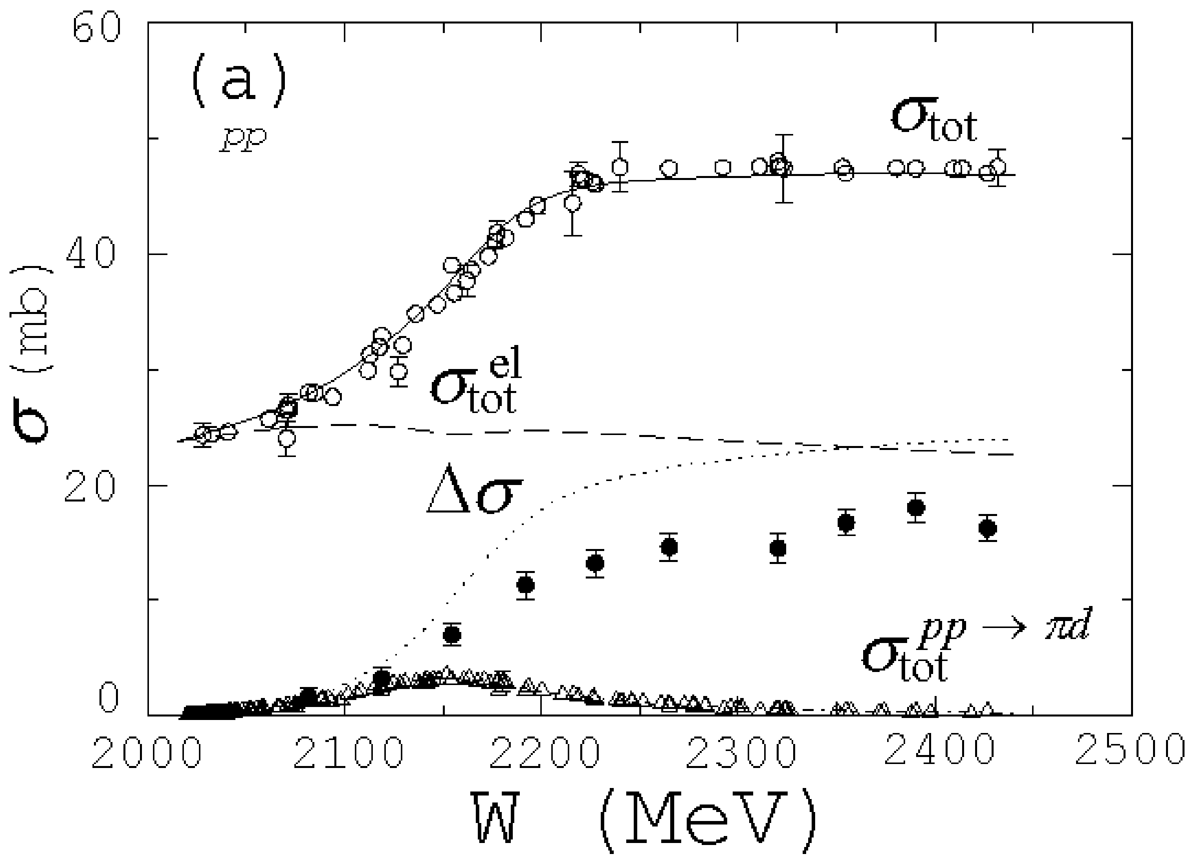

Figure 2 (a). Total *pp* cross sections σ_{tot} (solid) and total elastic cross sections σ_{tot}^{el} (dashed) correspond to the Unified (C500) solution. Data for σ_{tot} (open circles) are taken from the SAID[4] data base. Dash-dotted line, corresponding to the C500 solution, shows the total cross section ($\sigma_{tot}^{pp\rightarrow\pi d}$) for $pp \rightarrow \pi d$. The corresponding data from the SAID database are plotted as open triangles. The remainder ($\Delta\sigma$) is given by $\sigma_{tot} - \sigma_{tot}^{el} - \sigma_{tot}^{pp\rightarrow\pi d}$ and plotted as a dotted line. Total cross sections for the reactions $pp \rightarrow \Delta^{+} p + \Delta^{++} n$ [6] are plotted as dark circles. Details of the observables will be provided in Chapter 3.

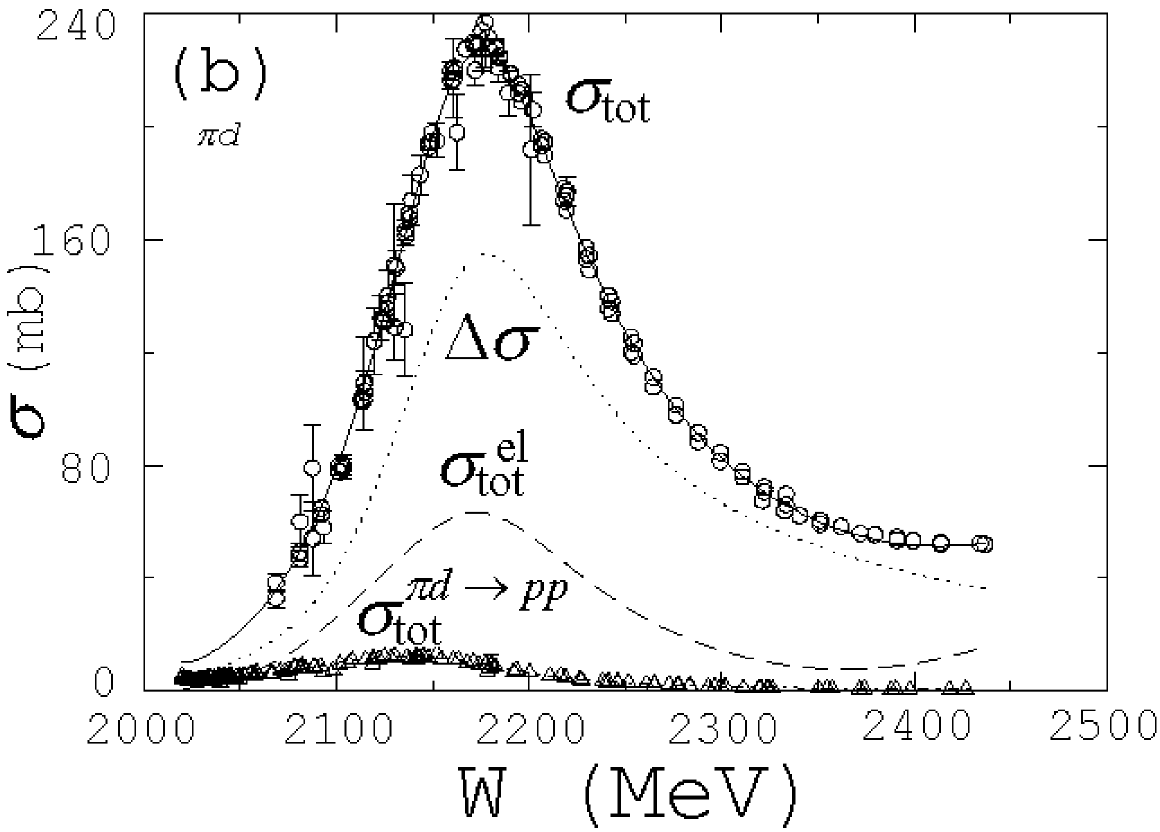

Figure 2 (b). Total πd cross sections σ_{tot} (solid) and total elastic cross sections σ_{tot}^{el} (dashed) correspond to the Unified (C500) solution. Data for σ_{tot} (open circles) are taken from the SAID[4] data base. Dash-dotted line (C500) shows the total cross section ($\sigma_{tot}^{\pi d \to pp}$) for $\pi d \to pp$. The corresponding data from the SAID database are plotted as open triangles. The remainder ($\Delta\sigma$) is given by $\sigma_{tot} - \sigma_{tot}^{el} - \sigma_{tot}^{\pi d \to pp}$ and plotted as a dotted line. Details of the observables will be provided in Chapter 3.

given by $\sigma_{tot} - \sigma_{tot}^{el} - \sigma_{tot}^{\pi d \to pp}$ and plotted as a dotted line. Details of the observables will be provided in Chapter 3.

The resonance-like behaviors of the three systems (NN, πd and $N\Delta$) are similar; and therefore appear to have a common interaction mechanism that can be studied by multi-channel analysis. A nucleon state is described by a Baryon Number (B), Isospin (I), and total angular momentum (J). The observation, that the resonance-like behaviors, for a given value of J, in $pp \to pp$, $\pi d \to pp$, and $\pi d \to \pi d$ are similar, implies the resonance-like states in these reactions are, in fact, a single state of the two nucleon system that has the values of $B = 2$, $I = 1$.

The resonance-like behaviors in the two baryon system have been variously described as "resonant" (due to the creation of dibaryon resonances) and "pseudo-resonant" (due to the $N\Delta$ intermediate state). The very existence (or non-existence) of the dibaryon system has been one of the hottest issues of debate in the Nuclear Physics community in the last half century. More details about this issue will be presented in Chapter 7.

Clearly, we are not the first to consider this problem. A multi-channel analysis of these three reactions, in a narrow energy range near the $N\Delta$ threshold, was recently reported by J. Nagata *et al.*[8]. This work used a mix of model-based and phenomenological results to investigate possible narrow structures around $\sqrt{s}$ ≈ 2.16 GeV in these reactions. They analyzed the analyzing power A_y of elastic *pp* scattering at an angle of roughly 39° in the center-of-mass system.

An older work by B.J. Edwards[9] used the multi-channel *K*-matrix formalism to study the $J^P = 2^+$ and 3^- states associated with dibaryon candidates where J is total angular momentum and P is parity. They performed a pp-$N\Delta$ two-channel analysis and tried to find poles for the $J^P = 2^+$ and 3^- states. They neglected the effect of πd channel in the first trial. By including the πd channel in addition to the pp-$N\Delta$, a three-channel approach was performed in the second trial.

N. Hiroshige's group performed several analyses[10]. They studied the $J^P = 2^+$, 3^-, and 2^- states. Their agreement with the elastic πd amplitudes was poor.

Actually, the use of multi-channel analysis has long history in the analysis of scattering information. An early analysis of this type was discussed and performed by R.A. Arndt in the 1960s[11]. The authors of the reference 11 had performed a pp-$N\Delta$ two-channel analysis to fit the elastic pp reaction data. Recent work of this type was reported in reference 1 and the most recent result is provided by SAID[4]. A πd-$N\Delta$ two-channel analysis has also been used in fitting the elastic πd reaction data. This was reported in reference 2 and an updated result is provided by SAID[4].

The approach needed to address these questions begins with the development of a complete data base of $pp \to pp$, $\pi d \to pp$, and $\pi d \to \pi d$ scattering results. It requires the examination of these resonance-like states from three different reactions by constructing a unified system and simultaneously analyzing the results in the form of detailed partial waves. However, until the present analysis, no such a unified analysis has been presented.

The present analysis differs from those carried out previously in a number of important respects. We analyzed all the possible partial waves completely and simultaneously from a complete collection of scattering data. We did not restrict our study to partial-waves containing interesting structures.

For pp elastic scattering, all waves with J $\leq$ 7 were used. Partial waves with J $\leq$ 5 were retained for both πd elastic scattering and $\pi d \to pp$. In addition, the *K*-matrix parameters were determined solely from our fits to the available data bases for each separate reaction. No results of outside analyses or any model approaches were used as constraints. As a result, the amplitudes found in our *K*-matrix fits are as "unbiased" as those coming from the separate analyses[4].

Chapter 3

FORMALISMS FOR THE OBSERVABLES

In quantum mechanics, a scattering process is described by a scattering amplitude. This amplitude depends on the kinematical variables, such as scattering angle and energy, and also on the quantum numbers describing the states of the particles participating in the collision process. It is convenient to expand the initial and final wave functions into angular momentum states.

The scattering amplitude at fixed values of the energy and scattering angle requires several independent measurements depending on the reaction. These independent measurements are described in terms of the helicity amplitudes.

§ 3-1. Partial Wave Decomposition for the Three Reactions

A brief review of elementary scattering theory, which describes the partial wave decomposition and observables in scattering reactions, follows. The solution of the Schrödinger equation for a scattering reaction (see any nuclear physics text book, for example, reference 11) is given by

$$\psi(r) \xrightarrow{r\to\infty} e^{ikz} + f\,\frac{e^{ikr}}{r}$$

where $k = p/\hbar$ and p is momentum of the incident particle that is along the z-axis. Here the first term describes incident plane wave along the z-axis and the second term describes the scattered spherical wave. The scattering amplitude is defined as f, which is a function of energy and scattering angle.

The expansion of the incident plane wave for $r >> R$, where R is the range of the potential that is finite, has the following asymptotic behavior ;

$$\psi_i = e^{ikz} \xrightarrow[kr\to\infty]{} \frac{1}{2ikr}\sum_{l=0}^{\infty} i^l (2l+1)\left(e^{i\left(kr-\frac{l}{2}\pi\right)} - e^{-\left(kr-\frac{l}{2}\pi\right)}\right) P_l(\cos\theta)$$

where θ is the scattering angle. Here the first (second) term describes the outgoing (incoming) spherical wave.

A similar expansion of the final wave function, in presence of absorption yields ;

$$\psi_f \longrightarrow \frac{1}{2ikr}\sum_{l=0}^{\infty} i^l (2l+1)\left(\eta_l e^{2i\delta_l} e^{i\left(kr-\frac{l}{2}\pi\right)} - e^{-\left(kr-\frac{l}{2}\pi\right)}\right) P_l(\cos\theta)$$

At large distance, the effects of the scattering potential alter the outgoing l^{th} wave by a phase shift $2\delta_l$ and by an attenuation η_l (or absorption parameter), if some absorption has taken place.

The scattered wave ψ_{sc} is given by difference $\psi_f - \psi_i$;

$$\psi_{sc} = \frac{1}{k}\sum_{l=0}^{\infty}(2l+1)\frac{\eta_l e^{2i\delta_l} - 1}{2i} P_l(\cos\theta)\frac{e^{ikr}}{r}.$$

The scattering amplitude is

$$f(\varepsilon,\theta) = \sum_{l=0}^{\infty}(2l+1)\frac{\eta_l e^{2i\delta_l} - 1}{2ik} P_l(\cos\theta)$$

where ε is the energy of the incident particle. Alternatively, we can define the dimensionless scattering amplitude in a given l^{th} angular momentum state, called partial wave amplitude, as;

$$f_l = T_l = \frac{\eta_l e^{2i\delta_l} - 1}{2i} \ .$$

Generally, T_l is used as a notation for the partial wave amplitude.

The partial wave decomposition of the pp, πd, and $N\Delta$ systems are given in Table 1. In Table 1, the state notations are ${}^{2S+1}L_J$ where S is the total spin quantum number, J is the total angular momentum quantum number of the system, and the letter for L (S, P, D, F, G, H) represent the orbital angular moments quantum number (0, 1, 2, 3, 4, 5) in units of $\hbar$. Details of the partial wave decomposition of the elastic pp, πd reactions and $\pi d \to pp$ reaction are presented in Appendix B.

One important restriction for the elastic pp reaction is parity (P) conservation. Elastic pp scattering occurs between two identical particles. The Pauli principle requires that the total wave function of this system should be antisymmetric[13]. So only spin singlet (odd under exchange) even angular momentum states (even under exchange) or spin triplet (even under exchange) odd angular momentum states (odd under exchange) can be present for the elastic pp system. Details of these constraints are presented in Appendix B.

Table 1. Partial wave decomposition of the pp, pd, and $N\Delta$ systems.

J^P	pd	pp	$N\Delta$
0^+	$^3P_0$	$^1S_0$	$^5D_0$
0^-		$^3P_0$	$^3P_0$
1^+	$^3P_1$ $^3P_1$		$^3S_1$, $^3D_1$ $^5D_1$
1^-	$^3S_1$, $^3D_1$ $^3S_1$, $^3D_1$	$^3P_1$ $^3P_1$	$^3P_1$ $^5P_1$, $^5F_1$
2^+	$^3P_2$, $^3F_2$ $^3P_2$, $^3F_2$ $^3P_2$, $^3F_2$	$^1D_2$ $^1D_2$ $^1D_2$	$^3D_2$ $^5S_2$, $^5D_2$ $^5D_2$, $^5G_2$
2^-	$^3D_2$ $^3D_2$	$^3P_2$, $^3F_2$ $^3P_2$, $^3F_2$	$^3P_2$, $^3F_2$ $^5P_2$, $^5F_2$
3^+	$^3F_3$ $^3F_3$		$^3D_3$, $^3G_3$ $^5D_3$, $^5G_3$
3^-	$^3D_3$, $^3G_3$ $^3D_3$, $^3G_3$ $^3D_3$, $^3G_3$	$^3F_3$ $^3F_3$ $^3F_3$	$^3P_3$, $^3F_3$ $^5P_3$, $^5F_3$ $^5F_3$, $^5H_3$
4^+	$^3F_4$, $^3H_4$ $^3F_4$, $^3H_4$ $^3F_4$, $^3H_4$	$^1G_4$ $^1G_4$ $^1G_4$	$^3G_4$ $^5D_4$, $^5G_4$ $^5G_4$, $^5I_4$
4^-	$^3G_4$ $^3G_4$	$^3F_4$, $^3H_4$ $^3F_4$, $^3H_4$	$^3F_4$, $^3H_4$ $^5F_4$, $^5H_4$

§ 3-2. Helicity Amplitudes for the Three Reactions

Since a nucleon has spin, the scattering amplitudes of the two nucleon system can be described in a simple matrix form in spin space. To reconstruct the scattering amplitude at fixed values of the energy and scattering angle, one requires several independent measurements depending on the reaction. These independent measurements are described in terms of the helicity amplitudes.

The dependence of the scattering amplitude on the helicity amplitudes is greatly restricted by various invariance requirements most of which are connected with conservation laws. All the possible observables in the two nucleon interactions are described in terms of the restricted number of helicity amplitudes. Also each helicity amplitude is determined by the summation of proper partial wave combinations.

3-2-1. Helicity Amplitudes for the Elastic *pp* Reaction

In the case of the two nucleon interaction, it is convenient to use a nucleon-nucleon scattering matrix. The scattering matrix for the *pp* elastic reaction is [14]

$$\begin{aligned} M\left(\mathbf{q}_f,\mathbf{q}_i\right)=\frac{1}{2}\Big[&\left(a+b\right)+(a-b)(\sigma_1\cdot\mathbf{n})(\sigma_2\cdot\mathbf{n})+(c+d)(\sigma_1\cdot\mathbf{m})(\sigma_2\cdot\mathbf{m})\\ &+(c-d)(\sigma_1\cdot\mathbf{l})(\sigma_2\cdot\mathbf{l})+e\left\{\left(\sigma_1+\sigma_2\right)\cdot\mathbf{n}\right\}\Big]. \end{aligned}$$

Here, $\mathbf{q}_i$ ($\mathbf{q}_f$) is a unit vector in the direction of the incident (scattered) particle momenta in the c.m.s.(center-of-mass system). a, b, c, d, e denote amplitudes, which are the functions of center-of-mass energy, ε, and the scattering angle, θ. The c.m.s. basis vectors are

$$\mathbf{l} = \frac{\mathbf{q}_i + \mathbf{q}_f}{\left|\mathbf{q}_i + \mathbf{q}_f\right|} \qquad \mathbf{m} = \frac{\mathbf{q}_i - \mathbf{q}_f}{\left|\mathbf{q}_i - \mathbf{q}_f\right|} \qquad \mathbf{n} = \frac{\mathbf{q}_i \times \mathbf{q}_f}{\left|\mathbf{q}_i \times \mathbf{q}_f\right|}.$$

σ_1 (σ_2) is the Pauli spin matrix acting on the first (second) nucleon wave function.

This nucleon-nucleon scattering matrix is denoted by helicity. The helicity λ for a nucleon is $+\frac{1}{2}$ if the spin projection is parallel to the momentum, $-\frac{1}{2}$ if it is anti-parallel. Using '+' for $+\frac{1}{2}$ and '–' for $-\frac{1}{2}$ helicity, the scattering matrix is

$$\mathbf{M} = \begin{pmatrix} \langle ++|M|++\rangle & \langle ++|M|+-\rangle & \langle ++|M|-+\rangle & \langle ++|M|--\rangle \\ \langle +-|M|++\rangle & \langle +-|M|+-\rangle & \langle +-|M|-+\rangle & \langle +-|M|--\rangle \\ \langle -+|M|++\rangle & \langle -+|M|+-\rangle & \langle -+|M|-+\rangle & \langle -+|M|--\rangle \\ \langle --|M|++\rangle & \langle --|M|+-\rangle & \langle --|M|-+\rangle & \langle --|M|--\rangle \end{pmatrix}.$$

The helicity amplitudes are denoted $\langle \lambda_3 \lambda_4 |M| \lambda_1 \lambda_2 \rangle$, where λ_1 describes the incident particle, λ_2 describes the target, λ_3 describes the scattered particle and λ_4 describes the recoil particle. The helicity amplitudes can be expanded into a partial wave sum as

$$\langle \lambda_3 \lambda_4 |M| \lambda_1 \lambda_2 \rangle = \frac{1}{2ik} \sum_J (2J+1) \langle \lambda_3 \lambda_4 | T^J(E) | \lambda_1 \lambda_2 \rangle d^J_{\lambda\mu}(\theta)$$

where $\lambda = \lambda_1 - \lambda_2$, $\mu = \lambda_3 - \lambda_4$ and $d^J_{\lambda\mu}(\theta)$ are rotation matrices satisfying

$$d^J_{\lambda\mu}(\theta) = (-1)^{\lambda-\mu} d^J_{\lambda\mu}(\theta) = (-1)^{\lambda-\mu} d^J_{-\lambda\,-\mu}(\theta).$$

These amplitudes are greatly restricted by various invariance requirements most of which are connected with conservation laws. Parity conservation implies

$$\left\langle -\lambda_3 \; -\lambda_4 \left| T^J(E) \right| -\lambda_1 \; -\lambda_2 \right\rangle = \left\langle \lambda_3 \, \lambda_4 \left| T^J(E) \right| \lambda_1 \, \lambda_2 \right\rangle ;$$

time reversal invariance implies

$$\left\langle \lambda_1 \, \lambda_2 \left| T^J(E) \right| \lambda_3 \, \lambda_4 \right\rangle = \left\langle \lambda_3 \, \lambda_4 \left| T^J(E) \right| \lambda_1 \, \lambda_2 \right\rangle .$$

The Pauli principle implies

$$\left\langle \lambda_4 \, \lambda_3 \left| T^J(E) \right| \lambda_2 \, \lambda_1 \right\rangle = \left\langle \lambda_3 \, \lambda_4 \left| T^J(E) \right| \lambda_1 \, \lambda_2 \right\rangle .$$

These relations imply that the helicity amplitudes satisfy

$$\left\langle -\lambda_3 \; -\lambda_4 \left| M \right| -\lambda_1 \; -\lambda_2 \right\rangle = (-1)^{\lambda_1 - \lambda_2 - \lambda_3 + \lambda_4} \left\langle \lambda_3 \, \lambda_4 \left| M \right| \lambda_1 \, \lambda_2 \right\rangle$$

$$\left\langle \lambda_1 \, \lambda_2 \left| M \right| \lambda_3 \, \lambda_4 \right\rangle = (-1)^{\lambda_1 - \lambda_2 - \lambda_3 + \lambda_4} \left\langle \lambda_3 \, \lambda_4 \left| M \right| \lambda_1 \, \lambda_2 \right\rangle$$

$$\left\langle \lambda_4 \, \lambda_3 \left| M \right| \lambda_2 \, \lambda_1 \right\rangle = (-1)^{\lambda_1 - \lambda_2 - \lambda_3 + \lambda_4} \left\langle \lambda_3 \, \lambda_4 \left| M \right| \lambda_1 \, \lambda_2 \right\rangle$$

Taking these symmetry relations into account and indicating only the signs of the nucleon helicities requires only five components for the scattering matrix:

$$M_1 \equiv \langle ++|M|++\rangle = \langle --|M|--\rangle$$

$$M_2 \equiv \langle ++|M|--\rangle = \langle --|M|++\rangle$$

$$M_3 \equiv \langle +-|M|+-\rangle = \langle -+|M|-+\rangle$$

$$M_4 \equiv \langle +-|M|-+\rangle = \langle -+|M|+-\rangle$$

$$\begin{aligned} M_5 &\equiv \langle ++|M|+-\rangle = \langle -+|M|--\rangle = \langle --|M|+-\rangle = \langle -+|M|++\rangle \\ &= -\langle --|M|-+\rangle = -\langle +-|M|++\rangle \\ &= -\langle ++|M|-+\rangle = -\langle +-|M|--\rangle \end{aligned}$$

In the analysis, we use a notation H for the helicity amplitude. Relations for the helicity amplitudes (H) in terms of the elements of the scattering matrix (M) and the partial waves amplitudes, which were described in section 3-1, are[15]:

$$H_1 = \frac{1}{2}\left(M_1 - M_2 - M_4\right) = \sum_{J=\text{even}} \left(2J+1\right) T_J P_J\left(\cos\theta\right)$$

$$H_2 = \frac{1}{2} M_3 = \sum_J \left\{ \left(2j+1\right) T_{JJ} \left(P_J\left(\cos\theta\right) - \frac{\cos\theta P_J^1\left(\cos\theta\right)}{J\left(J+1\right)} \right) \right.$$
$$\left. + \left(\left(J+1\right) T_{J,J-1} + J T_{J,J+1} - 2\sqrt{J\left(J+1\right)}\varepsilon_J \right) \frac{P_J^1\left(\cos\theta\right)}{J\left(J+1\right)} \right\}$$

$$H_3 = \frac{1}{2}\left(M_1 + M_2 + M_3 - M_4\right) = \sum_J \left\{ \left(2j+1\right) T_{JJ} \frac{P_J^1\left(\cos\theta\right)}{J\left(J+1\right)} \right.$$
$$\left. + \left(\left(J+1\right) T_{J,J-1} + J T_{J,J+1} - 2\sqrt{J\left(J+1\right)}\varepsilon_J \right) \left(P_J\left(\cos\theta\right) - \frac{\cos\theta P_J^1\left(\cos\theta\right)}{J\left(J+1\right)} \right) \right\}$$

$$H_4 = -M_5 = \sum_J J\left(J+1\right)\left(T_{J,J-1} - T_{J,J+1}\right) \frac{P_J^1\left(\cos\theta\right)}{J\left(J+1\right)} \sin\theta$$

$$H_5 = \frac{1}{2}\left(M_1 + M_2\right) = \sum_J \left(J T_{J,J-1} + \left(J+1\right) T_{J,J+1} + 2\sqrt{J\left(J+1\right)}\varepsilon_J \right) P_J\left(\cos\theta\right)$$

Here, $P_J^1\left(x\right) = \left(1 - x^2\right)^{\frac{1}{2}} \frac{d}{dx} P_J\left(x\right)$ is the first order associated Legendre function, when $x = \cos\theta$.

Partial waves, when described in terms of total angular momentum J, are

T_J : Partial waves of spin singlet state where $J \geq 0$ and even parity,

T_{JJ} : Partial waves of spin triplet $J = L$ state where $J > 0$ and odd parity,

$T_{J,J-1}$: Partial waves of spin triplet $J = L + 1$ state where $J > 0$ and even parity,

ϵ_J : Partial waves of spin flipped mixture state of $J = L + 1$ and $J = L - 1$ where $J > 0$ and even parity,

$T_{J,J+1}$: Partial waves of spin triplet $J = L - 1$ where $J \geq 0$ and even.

Since the proton is a spin one-half particle, it can be polarized in three Pauli spin directions. When the unpolarized condition is included, the four possible polarization conditions suggest that there are 256 ($=4^4$) possible conditions to observe the elastic pp reaction[16]. General descriptions of these observables are presented in Appendix C.

There are 25 measured observables for the elastic pp reaction available in SAID and summarized in Table 2-1. In Table 2-1, notations for particles are as follows; **P** is Polarization, $\boldsymbol{p_1}$ is the incident proton beam, $\boldsymbol{p_2}$ is the target proton, $\boldsymbol{p_1'}$ is the scattered proton, and $\boldsymbol{p_2'}$ is the recoil proton. Notations for polarization are as follows; *P* means polarization, *D* means depolarization tensor, *A* means asymmetry in cross section, *C* means polarization correlation, *K* means polarization transfer, and *M* means contribution to the polarization of scattered particle. Bold notations are used in SAID[4]. Details of all notations, including polarization conditions and direction normal vectors, are explained in Appendix C.

3-2-2. Helicity Amplitudes and Observables for the Elastic p *d* Reaction

Due to parity conservation, four independent helicity amplitudes are required for this reaction. Thus, for reconstruction of the scattering amplitude at fixed values of the energy and scattering angle, one requires seven independent measurements. The helicity amplitude, $H_{\mathrm{ab}}(\mathrm{q})$, is labeled by the deuteron helicities (a and b) in the initial and final states[17]. Here the angle q is the center-of-mass scattering angle of the outgoing pion.

$$H_{11} \equiv H_1 = \frac{1}{2}\sum_{J\geq 1}\Big\{(J+1)T^J_{J-1,J-1} + JT^J_{J+1,J+1} + (2J+1)T^J_{J,J} + 2\sqrt{J(J+1)}\,T^J_{J-1,J+1}\Big\}d^J_{1,1}$$

$$H_{10} \equiv H_2 = -\frac{1}{2}\sum_{J\geq 1}\Big\{\sqrt{2(J+1)}\,(T^J_{J+1,J+1} - T^J_{J-1,J-1}) + \sqrt{2}\,T^J_{J-1,J+1}\Big\}d^J_{1,0}$$

$$H_{1-1} \equiv H_3 = \frac{1}{2}\sum_{J\geq 1}\Big\{(J+1)T^J_{J-1,J-1} + JT^J_{J+1,J+1} - (2J+1)T^J_{J,J} + 2\sqrt{J(J+1)}\,T^J_{J-1,J+1}\Big\}d^J_{1,-1}$$

$$H_{00} \equiv H_4 = \sum_{J\geq 1}\Big\{JT^J_{J-1,J-1} + (J+1)T^J_{J+1,J+1} - 2\sqrt{J(J+1)}\,T^J_{J-1,J+1}\Big\}d^J_{0,0}$$

Here, $d^J_{\mathrm{a},\mathrm{b}}$ is the reduced rotation matrix. $T^J_{L^{\mathrm{p}'},L^{\mathrm{p}}}$ is the partial wave amplitude and $L^{\mathrm{p}'}$ (L^{p}) means angular momentum of p*d* final (initial) state.

By the symmetry relations,

$$H_{\mathrm{ab}} = (-1)^{\mathrm{a}+\mathrm{b}} H_{-\mathrm{a}-\mathrm{b}} \qquad (\mathrm{a},\mathrm{b} \neq 0)$$

and $H_{0\mathrm{b}} = -H_{\mathrm{b}0}$.

Table 2-1. Available observables and polarization for the elastic pp reaction

	$\boldsymbol{p_1}$ $\boldsymbol{p_2}$	**P**$\boldsymbol{p_1}$ $\boldsymbol{p_2}$	$\boldsymbol{p_1}$ **P**$\boldsymbol{p_2}$	**P**$\boldsymbol{p_1}$ **P**$\boldsymbol{p_2}$
$\boldsymbol{p_1'}$ $\boldsymbol{p_2'}$	I (0000) $ds/d\Omega$ s_T s_T^{el}	A **P**	A (P)	A A_{xx} : (00ss) A_{zz} : (00kk) A_{zx} : −(00sk)
P$\boldsymbol{p_1'}$ $\boldsymbol{p_2'}$	P (P)	**D** (D_{n0n0}) **A**: ($D_{\mathrm{s'0k0}}$) **AP**: ($D_{\mathrm{k'0k0}}$) **R**: ($D_{\mathrm{s'0s0}}$) **RP**: ($D_{\mathrm{k'0s0}}$)	K	M **MSSN**: (s'0ns) **MSKM**: (k'0ns)
$\boldsymbol{p_1'}$ **P**$\boldsymbol{p_2'}$	P (P)	K **AT**: −(0s"k0) **RT**: (0s"s0) **DT**: (0nn0)	D **D0SK**: (0s"0k)	N **NNKK**: (0nkk) **NSNK**: (0s"nk) **NSKN**: (0s"kn)
P$\boldsymbol{p_1'}$ **P**$\boldsymbol{p_2'}$	C A_{yy} (nn00) C_{KP} (lm00)	C	C	C $\Delta s_{tot}^{\mathrm{L}}$: $= s\begin{pmatrix}\rightarrow\\ \leftarrow\end{pmatrix} - s\begin{pmatrix}\rightarrow\\ \rightarrow\end{pmatrix}$ $\Delta s_{tot}^{\mathrm{T}}$: $= s(\uparrow\ \downarrow) - s(\uparrow\ \uparrow)$

P : Polarization
$\boldsymbol{p_1}$: Incident Proton (Beam) $\boldsymbol{p_2}$: Target Proton
$\boldsymbol{p_1'}$: Scattered Proton $\boldsymbol{p_2'}$: Recoil Proton
P : Polarization D : Depolarization Tensor A : Asymmetry in Cross Section
C : Polarization Correlation K : Polarization Transfer
M : Contribution to the Polarization of Scattered Particle

Directions : ($\boldsymbol{p_1'}$, $\boldsymbol{p_2'}$, $\boldsymbol{p_1}$, $\boldsymbol{p_2}$)

in Lab. ; $\mathbf{q}$ for $\boldsymbol{p_1}$ (z-axis; k) $\mathbf{q}'$ for $\boldsymbol{p_1'}$ (k′) $\mathbf{q}''$ for $\boldsymbol{p_2'}$ (k″)

in c.m. ; $\mathbf{n} = \dfrac{\mathbf{q}_i \times \mathbf{q}_f}{\left|\mathbf{q}_i \times \mathbf{q}_f\right|}$ (y-axis; n) $\mathbf{l} = \dfrac{\mathbf{q}_i + \mathbf{q}_f}{\left|\mathbf{q}_i + \mathbf{q}_f\right|}$ (K, l) $\mathbf{m} = \dfrac{\mathbf{q}_i - \mathbf{q}_f}{\left|\mathbf{q}_i - \mathbf{q}_f\right|}$ (P, m)

Also $\mathbf{s} = \mathbf{n} \times \mathbf{q}$ (x-axis; s) $\mathbf{s}' = \mathbf{n} \times \mathbf{q}'$ (s′) $\mathbf{s}'' = \mathbf{n} \times \mathbf{q}''$ (s″)

The relations between helicity amplitudes and observables available in SAID are as follows. For the unpolarized cross section;

$$\frac{d\sigma}{d\Omega} = \sigma_g I_0$$

where $I_0 \equiv t_{00}^{00} = 2|H_1|^2 + 4|H_2|^2 + 2|H_3|^2 + |H_4|^2$

and $\sigma_g = \frac{1}{3}\left(\frac{\hbar c}{q_\pi}\right)^2$, q_π is the pion momentum in c.m.

$$\sigma_T = 4\pi\sigma_g\left[2\,\mathrm{Im}\,H_1(0) + \mathrm{Im}\,H_4(0)\right]$$

$$\sigma_T^{el} = 4\pi\sigma_g \int_0^\pi I_0 \sin\theta \, d\theta$$

For the polarization of deuteron, the tensor operator requires four 3×3 matrices which can be expressed in terms of the spin operator S and the unit matrix[18];

$$1 = \begin{pmatrix} 1 & 0 & 0 \\ 0 & 1 & 0 \\ 0 & 0 & 1 \end{pmatrix}, \qquad S_x = \frac{1}{\sqrt{2}}\begin{pmatrix} 0 & 1 & 0 \\ 1 & 0 & 1 \\ 0 & 1 & 0 \end{pmatrix},$$

$$S_y = \frac{i}{\sqrt{2}}\begin{pmatrix} 0 & -i & 0 \\ i & 0 & -i \\ 0 & i & 0 \end{pmatrix}, \qquad S_z = \begin{pmatrix} 1 & 0 & 0 \\ 0 & 0 & 0 \\ 0 & 0 & -1 \end{pmatrix}.$$

The explicit forms of the tensor operators in terms of components of the spin operator S are expressed by T in the spherical coordinate system, and by P in the cartesian coordinate system[18];

$$T_{00} = 1 \qquad P_\alpha = S_\alpha$$

$$T_{10} = \sqrt{\frac{3}{2}}S_z \qquad P_{\alpha\alpha} = 3S_\alpha^2 - 2$$

$$T_{1\pm1} = \mp\frac{\sqrt{3}}{2}\left(S_x \pm iS_y\right) \qquad\qquad P_{\alpha\beta} = \frac{3}{2}\left(S_\alpha S_\beta + S_\beta S_\alpha\right)$$

$$T_{20} = \frac{1}{2}\left(3S_z^2 - 2\right)$$

$$T_{2\pm1} = \mp\frac{\sqrt{3}}{2}\left\{\left(S_x \pm iS_y\right)S_z + S_z\left(S_x \pm iS_y\right)\right\}$$

$$T_{2\pm2} = \frac{\sqrt{3}}{2}\left(S_x \pm iS_y\right)^2$$

In the cartesian coordinate system, α and β labels each cartesian direction (x, y, z). In the spherical coordinate system, generally

$$T_{\alpha\beta} = (-1)^{\beta}\, T^{+}_{\alpha-\beta}\,.$$

The relations between some observables for a polarized deuteron and the helicity amplitudes are as follows:

$$iT_{11} = -\sqrt{6}\,\mathrm{Im}\left\{H_2^*\left(H_1 - H_3 + H_4\right)\right\}\Big/ I_0$$

$$T_{20} = \sqrt{2}\left(|H_1|^2 - |H_2|^2 + |H_3|^2 - |H_4|^2\right)\Big/ I_0$$

$$\tau_{22} = \sqrt{\frac{1}{6}}T_{20} + T_{22}$$

$$\tau_{21} = T_{21} + \frac{1}{2}\tau_{22} = \frac{1}{2}\sqrt{\frac{1}{6}}T_{20} + T_{21} + \frac{1}{2}T_{22}$$

$$T_{21} = -\sqrt{6}\,\mathrm{Re}\left\{H_2^*\left(H_1 - H_3 - H_4\right)\right\}\Big/ I_0$$

$$T_{22} = \sqrt{3}\left\{2\,\mathrm{Re}\left(H_1^* H_3^* - |H_2|^2\right)\right\}\Big/ I_0$$

$$T_{20}^{lab} \equiv t_{20}^{lab} = \frac{3\cos^2\theta_R}{2}T_{20} + 2\sqrt{\frac{3}{2}}\sin\theta_R\cos\theta_R T_{21} + \frac{3}{2}\sin^2\theta_R T_{22}$$

Here, θ_R is the deuteron recoil angle in the laboratory system.

There are eight measured observables for the elastic πd reaction available in SAID and summarized in Table 2-2.

Table 2-2. Available observables and polarization for the elastic πd reaction

	π $\boldsymbol{d}$	π $\mathbf{P}\boldsymbol{d}$
π'	I $d\sigma/d\Omega$	D iT_{11} T_{20}
$\boldsymbol{d'}$	σ_T σ_T^{el}	τ_{22} τ_{21} T_{20}^{lab}

P : Polarization
π : Incident Pion (Beam)
π' : Scattered Pion
D : Polarization Tensor
d : Target Deuteron
d′: Recoil Deuteron

3-2-3. Helicity Amplitudes and Observables for the $\pi d \to pp$ Reaction

Due to parity conservation, six independent helicity amplitudes are required to describe the $\pi d \to pp$ reaction. The symbol $F_{\alpha,\beta;\lambda}(\theta)$ is used for the helicity amplitudes for the $\pi d \to pp$ reaction[19]. Here, α and β lables the two proton spin states and λ lables the spin state of the deuteron. To analyze this system, the time reversed reaction is analyzed, $pp \to \pi d$. The scattering angle θ is the pion production angle in the center-of-mass system.

$$F_{\frac{1}{2},\frac{1}{2};1} \equiv H_1 = \frac{1}{4\pi} \sum_{J\,(\text{even})} (2J+1) h_1^J d_{0,-1}^J \,,$$

$$F_{\frac{1}{2},\frac{1}{2};0} \equiv H_2 = \frac{1}{4\pi} \sum_{J\,(\text{even})} (2J+1) h_2^J d_{0,0}^J \,,$$

$$F_{\frac{1}{2},\frac{1}{2};-1} \equiv H_3 = \frac{1}{4\pi} \sum_{J\,(\text{even})} (2J+1) h_3^J d_{0,1}^J \,,$$

$$F_{-\frac{1}{2},\frac{1}{2};0} \equiv H_4 = \frac{1}{4\pi} \sum_{J\,(\text{odd})} (2J+1) h_4^J d_{0,1}^J \,,$$

$$F_{\frac{1}{2},-\frac{1}{2};-1} \equiv H_5 = \frac{1}{4\pi} \sum_{J} (2J+1) h_5^J d_{1,1}^J \,,$$

$$F_{\frac{1}{2},-\frac{1}{2};1} \equiv H_6 = \frac{1}{4\pi} \sum_{J} (2J+1) h_6^J d_{1,-1}^J \,.$$

Here, $d_{\alpha,\beta}^J$ are the reduced rotation matrices. These helicity amplitudes satisfy the symmetry relations

$$F_{\alpha,\beta;\lambda} = (-1)^{\alpha+\beta+\lambda} F_{-\alpha,-\beta;\lambda} \,.$$

The symbol for the partial wave amplitude is $T^J_{L^{pp},S_{pp};L^\pi}$. Labels are L^{pp}, S_{pp}, and J corresponding to the pp state of ${}^{2S_{pp}+1}L_J^{pp}$; and L^π is used for the πd state. Decomposition of the helicity amplitudes and the partial wave amplitudes are as follows. For even J

$$h_1^J = \sqrt{\frac{J+1}{2J+1}} T^J_{J,0;J-1} + \sqrt{\frac{J}{2J+1}} T^J_{J,0;J+1} - \sqrt{\frac{J}{2J+1}} T^J_{J-1,1;J} + \sqrt{\frac{J+1}{2J+1}} T^J_{J+1,1;J} \,,$$

$$h_2^J = \sqrt{\frac{2J}{2J+1}} T^J_{J,0;J-1} + \sqrt{\frac{2J+2}{2J+1}} T^J_{J,0;J+1} ,$$

$$h_3^J = \sqrt{\frac{J+1}{2J+1}} T^J_{J,0;\,J-1} + \sqrt{\frac{J}{2J+1}} T^J_{J,0;\,J+1} + \sqrt{\frac{J}{2J+1}} T^J_{J-1,1;\,J} - \sqrt{\frac{J+1}{2J+1}} T^J_{J+1,1;\,J}\,,$$

$$h_4^J = 0\,,$$

$$h_5^J = \sqrt{\frac{J+1}{2J+1}} T^J_{J-1,1;\,J} + \sqrt{\frac{J}{2J+1}} T^J_{J+1,1;\,J}\,,$$

$$h_6^J = (-1)^{J+1} h_5^J\,.$$

For odd J

$$h_1^J = 0\,,$$

$$h_2^J = 0\,,$$

$$h_3^J = 0\,,$$

$$h_4^J = \sqrt{\frac{2J}{2J+1}} T^J_{J,1;\,J-1} - \sqrt{\frac{2J+2}{2J+1}} T^J_{J,1;\,J+1}\,,$$

$$h_5^J = \sqrt{\frac{J+1}{2J+1}} T^J_{J,1;\,J-1} + \sqrt{\frac{J}{2J+1}} T^J_{J,1;\,J+1}\,,$$

$$h_6^J = (-1)^{J+1} h_5^J\,.$$

The relations between helicity amplitudes and observables are as follows. For the unpolarized cross section,

$$\frac{d\sigma}{d\Omega} = \sigma_\gamma I_0,\ \text{where}\ I_0 \equiv t^{00}_{00} = \sum_i H_i^2\,,$$

$$\sigma_\gamma = \frac{1}{6}\left(\frac{\hbar c}{q_\pi}\right)^2,$$ and q_π is the pion momentum in c.m. ; and

$$\sigma_T = 2\pi\sigma_\gamma \int_0^{\frac{\pi}{2}} I_0 \sin\theta\, d\theta\,.$$

The total cross section in a pure spin state

$$\Delta\sigma_{tot}^{L} = \sigma\begin{pmatrix}\rightarrow\\ \leftarrow\end{pmatrix} - \sigma\begin{pmatrix}\rightarrow\\ \rightarrow\end{pmatrix} = -2\int A_{zz}\frac{d\sigma}{d\Omega}d\Omega$$

$$= -4\pi\sigma_g\int_0^{\frac{\pi}{2}}\left(I_0 - 2H_1^2 - 2H_2^2 - 2H_3^2\right)\sin\theta d\theta,$$

$$\Delta\sigma_{tot}^{T} = \sigma\left(\uparrow\ \ \downarrow\right) - \sigma\left(\uparrow\ \ \uparrow\right) = -\int\left(A_{xx} + A_{yy}\right)\frac{d\sigma}{d\Omega}d\Omega$$

$$= -4\pi\sigma_g\int_0^{\frac{\pi}{2}}\left(H_2^2 - 2\,\mathrm{Re}\,H_1^* H_3\right)\sin\theta d\theta\ .$$

For the polarized proton or deuteron , one must consider both the spin $1/2$ and the spin 1 case. The polarized deuteron (spin 1) case is explained in section 3-2-2. For the polarization of proton, Pauli spin matrices for the spin $1/2$ particle are;

$$1 = \begin{pmatrix}1 & 0\\ 0 & 1\end{pmatrix},\quad \sigma_x = \begin{pmatrix}0 & 1\\ 1 & 0\end{pmatrix},\qquad \sigma_y = \begin{pmatrix}0 & -i\\ i & 0\end{pmatrix},\qquad \sigma_z = \begin{pmatrix}1 & 0\\ 0 & -1\end{pmatrix}.$$

The explicit forms of the tensor operators in terms of components of the spin operator S are expressed by T in the spherical coordinate system[18];

$$T_{00} = 1,$$

$$T_{10} = \sigma_z,$$

$$T_{1\pm1} = \mp\frac{1}{\sqrt{2}}\left(\sigma_x \pm i\sigma_y\right).$$

For a polarized proton,

$$A_{y0} \equiv \sqrt{2}it_{00}^{11} = 2\,\mathrm{Im}\left(H_1H_5^* + H_2H_4^* + H_3H_6^*\right)\Big/ I_0\ ,$$

where in $t_{\mathrm{dg}}^{\mathrm{ab}}$ the indices a, b label the proton spin state (T_{ab}) in the spherical coordinate system; and d, g label the deuteron spin state (T_{dg}) in the spherical coordinate system.

For a polarized deuteron,

$$iT_{11} \equiv it_{11}^{00} = \sqrt{\frac{3}{2}}\,\mathrm{Im}\left(H_1H_2^* + H_2H_3^* - H_4H_5^* + H_4H_6^*\right)\Big/ I_0\ .$$

For two polarized protons,

$$A_{xx} = \left\{- H_2^2 + H_4^2 + 2\,\mathrm{Re}\left(H_1H_3^* - H_5H_6^*\right)\right\}\Big/ I_0\ ,$$

$$A_{yy} = \left\{- H_2^2 - H_4^2 + 2\,\mathrm{Re}\left(H_1H_3^* + H_5H_6^*\right)\right\}\Big/ I_0\ ,$$

$$A_{zz} = \left(- H_1^2 - H_2^2 - H_3^2 + H_4^2 + H_5^2 + H_6^2\right)\Big/ I_0\ ,$$

$$A_{xz} = 2\,\mathrm{Re}\left(- H_1H_5^* - H_2H_4^* - H_3H_6^*\right)\Big/ I_0\ .$$

For one polarized proton and a polarized deuteron,

$$K_{xx} \equiv P_x^x = \sqrt{2}\,\mathrm{Re}\left(H_1H_4^* + H_2H_5^* + H_2H_6^* + H_3H_4^*\right)\Big/ I_0\ ,$$

$$K_{yy} \equiv P_y^y = \sqrt{2}\,\mathrm{Re}\left(H_1H_4^* - H_2H_5^* + H_2H_6^* - H_3H_4^*\right)\Big/ I_0\ ,$$

$$K_{xz} \equiv P_z^x = 2\,\mathrm{Re}\left(- H_1H_5^* + H_3H_6^*\right)\Big/ I_0\ .$$

Where in $P_{\mathrm{b}}^{\mathrm{a}}$ the index α labels the polarization of the deuteron, and b labels the polarization of the proton.

There are 14 measured observables available in SAID for the $\pi d \rightarrow pp$ reaction. These are summarized in Table 2-3.

Table 2-3. Available observables and polarization for the $\pi d \rightarrow pp$ reaction

	$\boldsymbol{p1'}$ $\boldsymbol{p2'}$	$\boldsymbol{p1'}$ $\mathbf{P}\boldsymbol{p2'}$ or $\mathbf{P}\boldsymbol{p1'}$ $\boldsymbol{p2'}$	$\mathbf{P}\boldsymbol{p1'}$ $\mathbf{P}\boldsymbol{p2'}$
π ***d***	*I* $d\sigma/d\Omega$ σ_T	*P* A_{y0}	*P* A_{xx} A_{yy} A_{zz} A_{xz}
π **P*d***	*A* iT_{11}	*A* K_{xx} K_{yy} K_{xz} ε	*C* $\Delta\sigma^{\mathrm{L}}_{tot} = \sigma\begin{pmatrix}\rightarrow\\ \leftarrow\end{pmatrix} - \sigma\begin{pmatrix}\rightarrow\\ \rightarrow\end{pmatrix}$ $\Delta\sigma^{\mathrm{T}}_{tot} = \sigma(\uparrow\ \downarrow) - \sigma(\uparrow\ \uparrow)$

P : Polarization
π : Incident Pion (Beam) — ***d*** : Target Deuteron
$\boldsymbol{p1'}$: Scattered Proton — $\boldsymbol{p2'}$: Recoiled Proton

I : Unpolarization — *P* : Polarization
A : Asymmetry in Cross Section — *C* : Polarization Correlation
ε : Geneva and TRIUMF Spin *p* - *d* Transfer Epsilion Parameters[19]

Chapter 4

FORMALISMS FOR

A UNIFIED ANALYSIS

In order to analyze the reaction $\mathrm{p}d \rightarrow pp$ along with elastic pp and $\mathrm{p}d$ scattering, we have constructed a *K*-matrix formalism having pp, $\mathrm{p}d$ and $N\Delta$ channels. The energy-dependence of our global fit was obtained through a coupled-channel *K*-matrix form in order to ensure that unitarity would not be violated. The "$N\Delta$" channel is added to account for all channels other than pp and $\mathrm{p}d$. As mentioned in Chapter 2, the most important thresholds are illustrated schematically in Figure 1. Unitarity and multi-channel matrix formalisms are briefly explained in Appendix D.

As the elastic pp partial-wave analysis is far superior to the $\mathrm{p}d$ elastic and $\mathrm{p}d \rightarrow pp$ analyses, we have carried out fits in which the pp partial-waves were held fixed. (The partial wave decomposition of the pp, $\mathrm{p}d$, and $N\Delta$ systems are given in Table 1 and explained in Chapter 3.)

As described below, the pp amplitudes were used to fix some elements of the *K*-matrix, while the others were determined from a fit to the combined $\mathrm{p}d$ elastic and $\mathrm{p}d \rightarrow pp$ data bases.

States of a given total angular momentum and parity (J^P) were parameterized by a 4x4 K-matrix (K_J) which coupled to an appropriate $N\Delta$ channel as explained in Appendix D. Spin-mixed(2x2) pp states couple to unmixed πd states, and unmixed pp states couple to spin-mixed(2x2) πd states, so the $\pi d - pp$ system is always represented by a 3x3 matrix. For example, the T-matrix (T_J) for $J^P = 2^+$ (unmixed pp states) is given by

$$
\begin{array}{cc}
 & \begin{array}{ccc} pp & \pi d_- & \pi d_+ \end{array} \\
T_2 = & \begin{pmatrix} {}^1D_2 & {}^1D_2\,p & {}^1D_2\,f \\ {}^1D_2\,p & {}^3P_2 & \varepsilon_2 \\ {}^1D_2\,f & \varepsilon_2 & {}^3F_2 \end{pmatrix} \begin{array}{l} pp \\ \pi d_- \\ \pi d_+ \end{array}
\end{array}
$$

whereas the T-matrix for $J^P = 2^-$ (mixed pp states) is

$$
\begin{array}{cc}
 & \begin{array}{ccc} pp_- & pp_+ & \pi d \end{array} \\
T_2 = & \begin{pmatrix} {}^3P_2 & \varepsilon_2 & {}^3P_2 d \\ \varepsilon_2 & {}^3F_2 & {}^3F_2 d \\ {}^3P_2 d & {}^3F_2 d & {}^3D_2 \end{pmatrix} \begin{array}{l} pp_- \\ pp_+ \\ \pi d \end{array}
\end{array}
$$

The subscripts $\pm$ denote states with $L = J \pm 1$. In the above, the mixing parameters (ε) for elastic pp and πd scattering are different. For the reaction $\pi d \to pp$ the notation (${}^{2S_{pp}+1}L_J^{pp} l^{\pi}$) is used.

Adding an $N\Delta$ channel results in a 4x4 T-matrix. Dropping the J-subscript, we write the K-matrix as

$$
K = \begin{pmatrix} K_{pp} & K_0 \\ \tilde{K}_0 & K_i \end{pmatrix},
$$

where K_{pp} is the elastic pp scattering sub-matrix, K_0 and $\tilde{K}_0$ are row and column vectors, and K_i is the sub-matrix of channels involving pd and $N\Delta$ states. Since we assume that the $N\Delta$ channel accounts for all unmeasured scattering, we can have a real symmetric K-matrix that satisfies the unitarity condition. A general reduced K-matrix formalism[12] gives the following relation for the elastic pp reduced K-matrix $\overline{K}_{pp}$,

$$\overline{K}_{pp} = K_{pp} + iK_0(1 - iK_i)^{-1}\tilde{K}_0 .$$

The K-matrix can be re-expressed as a T- matrix

$$T = \begin{pmatrix} T_{pp} & T_0 \\ \tilde{T}_0 & T_i \end{pmatrix}$$

using the relation $\mathbf{T} = \mathbf{K}(1 - i\mathbf{K})^{-1}$. We then have the correspondence

$$T_{pp} = \overline{K}_{pp}\left(1 - i\overline{K}_{pp}\right)^{-1} .$$

In order to ensure an exact fit to the pp elastic T-matrix, given by our most recent analysis of NN elastic scattering to 1.6 GeV[4], we take

$$K_{pp} = T_{pp}\left(1 + iT_{pp}\right) - iK_0(1 - iK_i)^{-1}\tilde{K}_0 .$$

The matrix elements are then expanded as polynomials in the pion energy times appropriate phase-space factors. The pd elastic and p$d \to pp$ T-matrix elements are extracted from T_0 and T_i .

To adjust the threshold factor, we applied momentum matrix r , that gives a threshold corrected K'-matrix

$$\mathbf{K}' = \mathrm{r}^{1/2}\mathbf{K}\mathrm{r}^{1/2}.$$

This r-matrix (sometimes it is called as phase factor matrix) is composed of the barycentric momentum of each state. In the total angular momentum representation, the r-matrix has the following form for the unmixed pp states coupled to spin-mixed(2x2) $\mathrm{p}d$ states;

$$\mathrm{r}^{2l+1} = \begin{pmatrix} q_{\mathrm{p}d}^{2J-1} & & & \\ & q_{\mathrm{p}d}^{2J+3} & & \\ & & q_{pp}^{2J+1} & \\ & & & q_{N\Delta}^{2l+1} \end{pmatrix}.$$

Here, we use the realtion

$$\boldsymbol{q}^2 = \frac{\left\{s-(m_1+m_2)^2\right\}\left\{s-(m_1-m_2)^2\right\}}{4s},$$

(this is explained in Appendix A) for the pp and $\mathrm{p}d$ states; and the Chew-Mandelstam function is used to obtain $q_{N\Delta}$ [20].

We obtain the parameters through a “best fit” to the experimental data. We define our “best fit” in a least-square sense. The standard approach uses a c^2 minimization technique, where c^2 is defined as the following[21]

$$\mathrm{c}^2(p) = \sum_{i=1}^{N^D}\left(\frac{\mathrm{a}^n\mathrm{q}^i(p)-\mathrm{q}^i_{\exp}}{\Delta\mathrm{q}^i_{\exp}}\right)^2 + \sum_{j=1}^{N_\mathrm{a}}\left(\frac{\mathrm{a}^j-1}{\Delta\mathrm{a}^j_{\exp}}\right)^2,$$

where

$\mathrm{q}^i(p)$ = value of i^{th} observable determined by the set of parameters,

$\mathrm{q}^{i}_{\mathrm{exp}}$ = experimental value of i^{th} observable,

$\Delta\mathrm{q}^{i}_{\mathrm{exp}}$ = experimental standard deviation (statistical error) of i^{th} data point

a^{n} = normalization parameter for experiment $n = n(i)$, $i = 1, \ldots, N_{\mathrm{a}}$

N^{D} = total number of data points being fit

N_{a} = total number of normalization parameters

$\Delta\mathrm{a}_{\mathrm{exp}}$ = experimental systematic error

Chapter 5

DATA DISTRIBUTION

A complete and up-to-date data base is used in the present analysis. A detailed description of the whole data base for the three reactions is given in SAID[4] and reported in reference 1, 2, and 3. We have fitted the amplitudes for $pp \to pp$ and the existing data bases for $\pi d \to pp$, and $\pi d \to \pi d$, using the *K*-matrix formalism explained in Chapter 4.

The overall χ^2 for our unified analysis is actually superior to that found in previous single-reaction analyses. This is due to the improved parameterization scheme. A comparison is given in Table 3.

We should emphasize that the amplitudes for pp elastic scattering are the same as the separate elastic pp analysis given in SAID, with solution name WI96[4]. As mentioned above, this feature was built into our *K*-matrix parameterization.

Number of data points for each observable is given in Table 4. Number of data points for each observable in the elastic pp reaction is presented in Table 4-1. χ^2 comes from WI96 solution. In SAID, most of observables of the elastic pp reaction follow Bystricky's notation[14]. Details of polarizations are explained in Appendix C.

Table 3. Comparisons of the unified (C500) and previous (separate) analyses. WI96 for $pp \to pp$ [4], SM94 for $\pi d \to \pi d$ [2], and SP96 for $\pi d \to pp$ [4]. The relevant energy ranges are: T_π = 0 – 500 MeV, T_p = 288 – 1290 MeV, and $\sqrt{s}$ = 2015 – 2440 MeV, respectively.

Reaction	Separate χ^2 / Data	Unified χ^2 / Data
$pp \to pp$	17380/10496	17380/10496
$\pi d \to \pi d$	2745/1362	2418/1362
$\pi d \to pp$	7716/4787	7570/4787

Comparison of the number of data points and χ^2 for each observable in the elastic πd reaction is presented in Table 4-2. The separate analysis, SM94, was reported in reference 2. The unified analysis is C500. The energy range is 0 to 500 MeV in T_π. A comparison of the number of data points and χ^2 for each observable in the $\pi d \to pp$ reaction is presented in Table 4-3. The separate analysis is SP96. The energy range is 0 to 500 MeV in T_π. We should indicate that the ε data[23(a)] were not directly included in the analysis. Instead, we included the amplitudes constructed from this data[23(b)] in our fits.

The energy-angle distributions of the complete data set for the three reactions are presented in Figure 3. The energy-angle distribution of the complete data set for the elastic pp reaction, which served as the basis for the WI96 solution, is presented in Figure 3-1. Dark marks indicate the new data since the

SM94 solution; (a) Differential cross section $d\sigma/d\Omega_{cm}$, (b)polarization of one particle, (c) depolarization tensor for one initial and one finial particles, (d) asymmetry tensor for polarized initial particles or finial particles. The vertical arrows indicate the range of the analysis. This figure shows that the distribution of measurement in the data base is complete in energy and angle for the elastic pp reaction.

The energy-angle distribution of the total data set for the elastic πd reaction is presented in Figure 3-2; (a) Differential cross section $d\sigma/d\Omega_{cm}$, (b)deuteron vector analyzing power iT_{11}, (c) deuteron tensor analyzing power T_{20}, (d) combined deuteron tensor analyzing powers $\tau_{22} = \sqrt{\frac{1}{6}}T_{20} + T_{22}$. There are sharp cutoffs in the number of data in the elastic πd reaction. Due to these sharp cutoffs, our analysis is limited to 500 MeV in pion laboratory energy.

The energy-angle distribution of the total data set for the $\pi d \to pp$ reaction is presented in Figure 3-3. Dark marks indicate the new data since the SP93 solution; (a) Differential cross section $d\sigma/d\Omega_{cm}$; (b) deuteron vector analyzing power iT_{11}, (c) proton analyzing power A_{y0}, (d) spin correlation parameter for two protons A_{zz}. The vertical arrow indicates the upper limit of the analysis. There are also sharp cutoffs in the number of data in the $\pi d \to pp$ reaction, for example A_{zz}.

Table 4-1. Number of data points for each observables in the $pp \rightarrow pp$ reaction. χ^2 comes from the WI96 solution.

Observables			0 ~ 1600 MeV		290 ~ 1290 MeV	
Common	Bystricky[14]	SAID	Data	(χ^2)	Data	(χ^2)
$d\sigma/d\Omega$	I_{0000}	DSG	3216	(6196)	2276	(4241)
	P_{p000}	P	4377	(6737)	3767	(5585)
	$D_{n0n0} = D_{0n0n}$	D	551	(757)	460	(617)
	$K_{0nn0} = K_{n00n}$	DT	323	(545)	288	(499)
A_{yy}	$C_{nn00} = A_{00nn}$	AYY	905	(1467)	791	(1200)
A_{xx}	A_{00ss}	AXX	127	(178)	106	(124)
A_{zz}	A_{00kk}	AZZ	993	(1683)	844	(1279)
A_{zx}	$-A_{00sk} = -A_{00ks}$	AZX	460	(900)	357	(661)
C_{KP}	$-C_{lm00} = -C_{ml00}$	CKP	8	(9)	7	(6)
	$D_{s'0s0}$	R	399	(548)	349	(500)
	$D_{k'0s0}$	RP	97	(153)	77	(145)
	$D_{s'0k0}$	A	382	(560)	341	(510)
	$D_{k'0k0}$	AP	87	(112)	87	(112)
	$K_{0s''s0}$	RT	4	(3)	4	(3)
	$-K_{0s''k0}$	AT	98	(101)	66	(66)
	$M_{s'0sn} = C_{k'nk0}$	MSSN	152	(176)	144	(167)
	$-M_{s'0kn} = -C_{k'ns0}$	MSKN	171	(216)	163	(211)
σ_T^{el}		SGTE	11	(20)	11	(20)
σ_T		SGT	59	(216)	52	(185)
$\Delta\sigma_{tot}^{\mathrm{L}}$		SGTL	50	(502)	43	(461)
$\Delta\sigma_{tot}^{\mathrm{T}}$		SGTT	47	(305)	44	(297)
	$D_{0s''0k}$	D0SK	99	(163)	66	(114)
	$-C_{nk''0s}$	NSNK	38	(112)	22	(87)
	$-N_{0nkk} = M_{n0ss}$	NNKK	45	(123)	31	(100)
		A0ST*	12	(21)	12	(21)

(Table 4-1 continued)

(Table 4-1 continued)

Observables			0 to 1600 MeV		290 to 1290 MeV	
Common	Bystricky	SAID	Data	(χ^2)	Data	(χ^2)
		A0KT*	12	(22)	12	(22)
		KS0T*	12	(16)	12	(16)
		KK0T*	12	(27)	12	(27)
		MSNT*	12	(14)	12	(14)
		MNKT*	12	(10)	12	(10)
		MKNT*	12	(27)	12	(27)
Total			12839	(22160)	10519	(17514)

* LAMPF Variables by Los Alamos[21]

Table 4-2. Number of data points and χ^2 comparison for each observable in the $\pi d \to \pi d$ reaction. The separate analysis is SM94 that was reported in reference 4. The unified analysis is C500. The energy range is from 0 to 500 MeV in T_π .

Obser-vables	$\pi^+ d \to \pi^+ d$			$\pi^- d \to \pi^- d$		
	Data	χ^2		Data	χ^2	
		Unified	Separate		Unified	Separate
$d\sigma / d\Omega$	516	840	839	236	461	643
σ_T	57	81	146	67	72	135
σ_T^{el}	3	1	0.5	3	9	5
iT_{11}	280	565	650	5	8	10
T_{20}	42	100	81	-	-	-
τ_{21}	47	89	64	-	-	-
τ_{22}	76	128	113	-	-	-
T_{20}^{lab}	30	64	60	-	-	-
Total	1051	1869	1952	311	550	793

Table 4-3. Number of data points and χ^2 comparison for each observable in the $\pi d \to pp$ reaction. The separate analysis is SP96. The unified analysis is C500. The energy range is 0 to 500 MeV in T_π .

Obser-vables	Ref. 3	Present		
	Data	Data	χ^2	
			Separate	Unified
$d\sigma/d\Omega$	1051	1420	2256	2499
σ_T	150	176	322	288
$\Delta\sigma_{tot}^{L}$	14	2	0.1	2.8
$\Delta\sigma_{tot}^{T}$	5	0	-	-
A_{y0}	1749	1750	2329	2349
A_{xx}	62	49	31	41
A_{yy}	185	185	222	194
A_{zz}	340	340	530	652
A_{xz}	257	257	377	336
iT_{11}	155	166	439	379
K_{xx}	9	4	23	17
K_{yy}	10	10	19	7
K_{xz}	5	5	10	12
K_{zx}	5	0	-	-
ε	136	136	501	446
H_i *	264	264	292	284
Total	4541	4787	7716	7570

* means helicity amplitudes from reference 23(b).

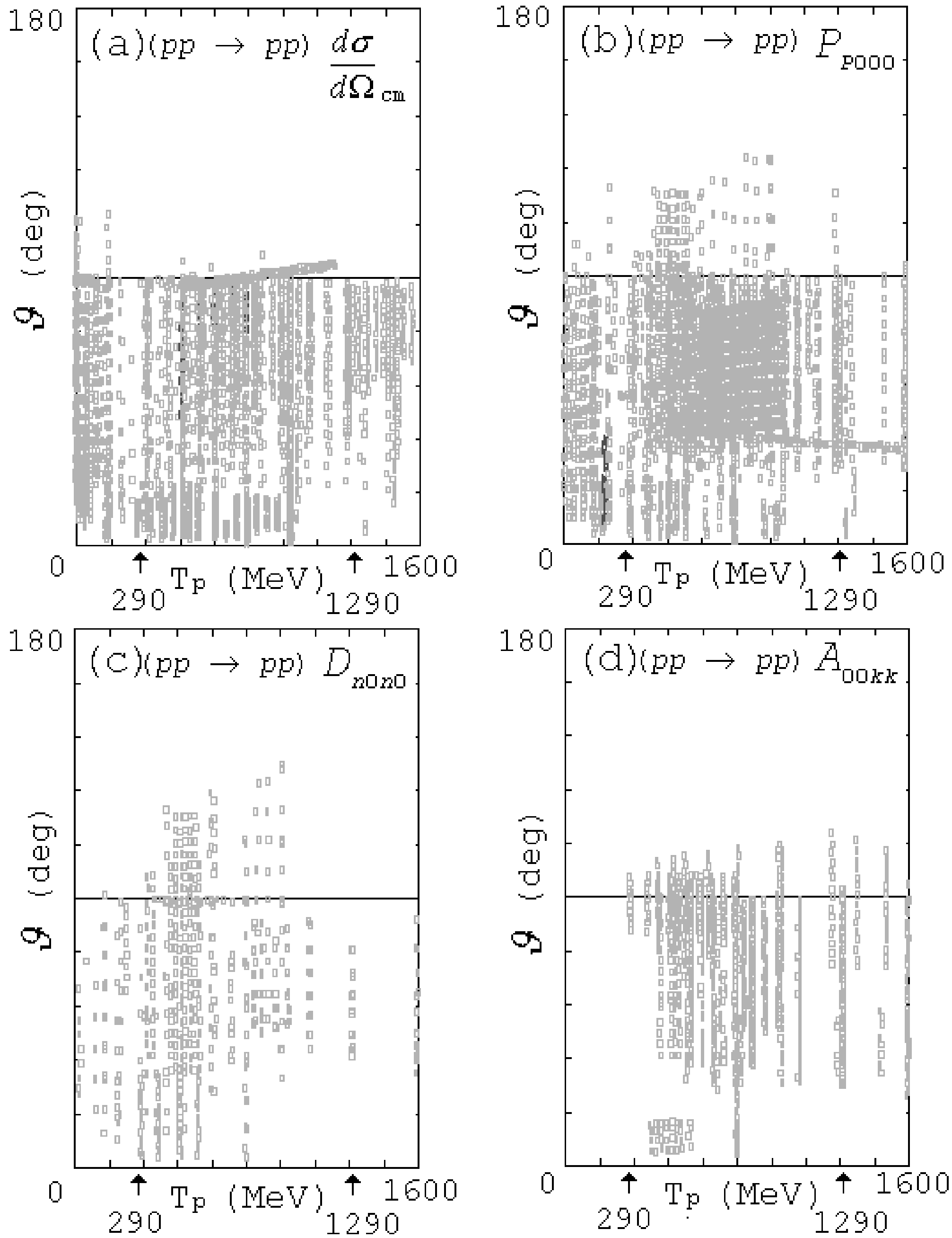

Figure 3-1. Energy-angle distribution of the complete data set for the elastic *pp* reaction which served as the basis for the WI96 solution. Dark marks indicate the new data since SM94 solution. (a) Differential cross section $d\mathrm{s}/d\Omega_{\mathrm{cm}}$, (b)polarization of one particle, (c) depolarization tensor for one initial and one final particle, (d) asymmetry tensor for polarized initial particles or finial particles. The vertical arrows indicate the range of the analysis.

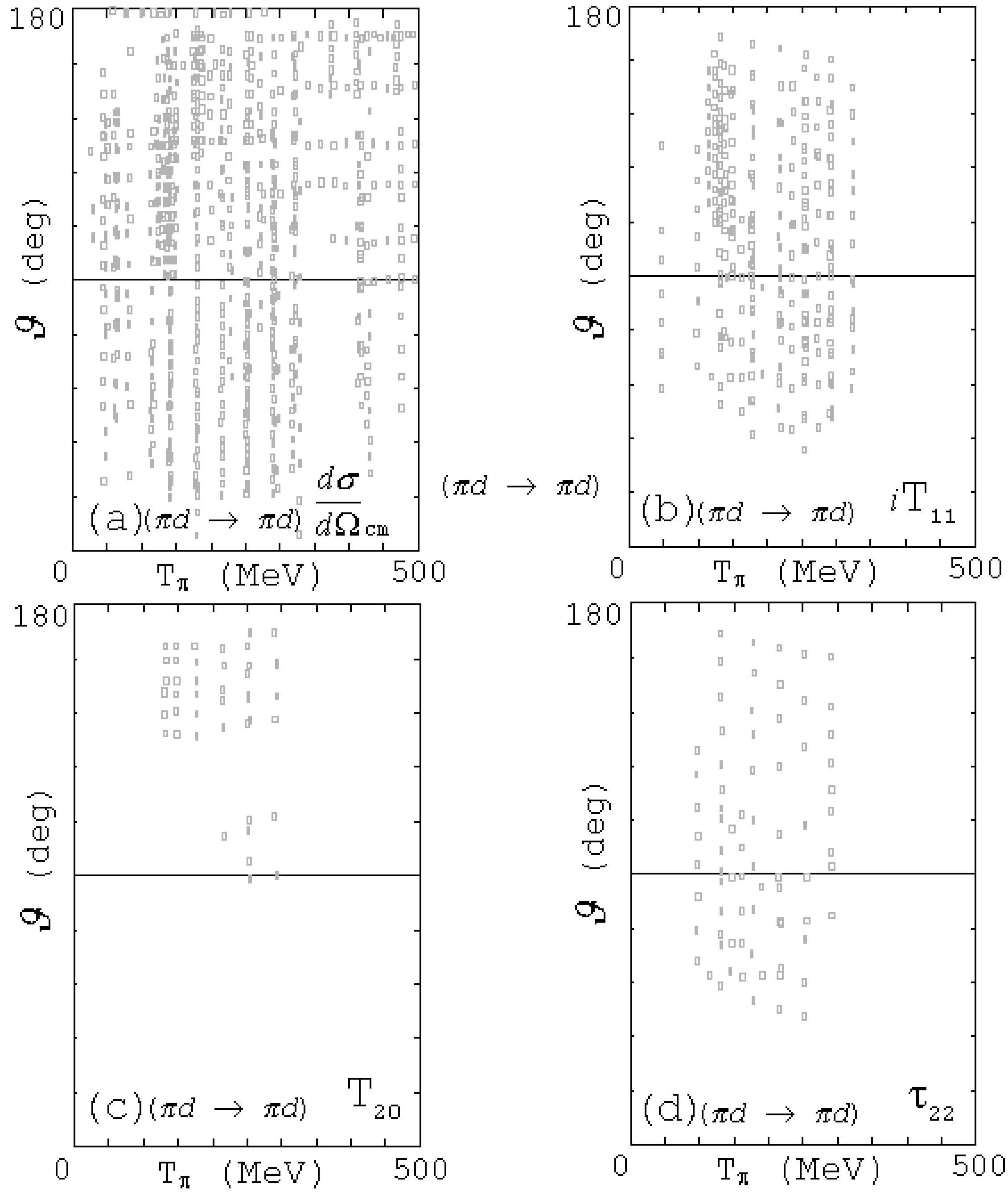

Figure 3-2. Energy-angle distribution of the total data set for the elastic πd reaction. (a) Differential cross section $d\sigma / d\Omega_{\mathrm{cm}}$, (b)deuteron vector analyzing power iT_{11}, (c) deuteron tensor analyzing power T_{20}, (d) combined deuteron tensor analyzing powers $\tau_{22} = \sqrt{\frac{1}{6}} T_{20} + T_{22}$.

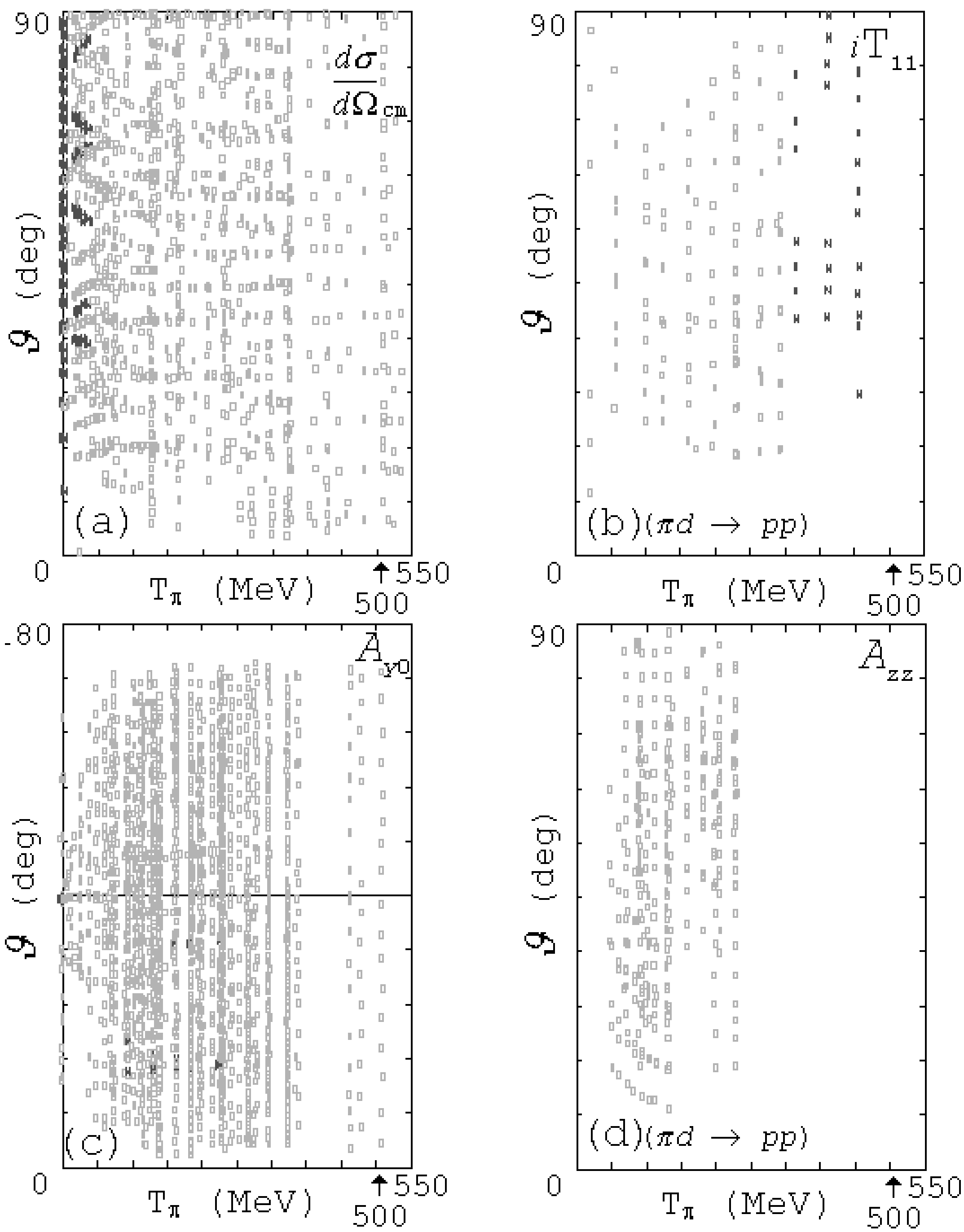

Figure 3-3. Energy-angle distribution of the total data set for the $\text{p}d \rightarrow pp$ reaction. Dark marks indicate the new data since SP93 solution. (a) Differential cross section $d\text{s}/d\Omega_{\text{cm}}$; (b) deuteron vector analyzing power iT_{11}, (c) proton analyzing power A_{y0}, (d) spin correlation parameter for two protons A_{zz}. The vertical arrow indicates the upper limit of the analysis.

Chapter 6.

PARTIAL WAVE AMPLITUDES

We have fitted the amplitudes for $pp \to pp$ and the existing data bases for $\mathrm{p}d \to pp$, and $\mathrm{p}d \to \mathrm{p}d$, using the *K*-matrix formalism explained in Chapter 4. The elastic $\mathrm{p}d$ and $\mathrm{p}d \to pp$ data bases used in this analysis are described in Chapter 5.

We started with SP94 solutions[4] for three reactions. For the elastic pp reaction, the SP94 solution was replaced by the WI96 solution, the newest updated solution for this reaction. The elastic $\mathrm{p}d$ SP94 solution, based on T_{p} = 0 to 500 MeV, 1339 data points with c^2 = 5292, used 66 parameters. This solution was updated and replaced by the SM94 solution[2]. The $\mathrm{p}d \to pp$ SP94 solution, based on T_{p} = 0 to 550 MeV, 4459 data points with c^2 = 7077, used 52 parameters. This solution was updated and replaced by SP96 solution[4].

For pp elastic scattering, all waves with J $\leq$ 7 were used. Partial waves with J $\leq$ 5 were retained for both $\mathrm{p}d$ elastic scattering and $\mathrm{p}d \to pp$. We used a total of 116 parameters to fit the data of both $\mathrm{p}d$ elastic scattering and $\mathrm{p}d \to pp$. Partial wave amplitudes for the unified system are displayed in Figure 4. The energy range is from 0 to 500 MeV in T_{p} and 290 to 1290 MeV in T_p for the (a) 0^+, (b) 1^+, 3^+, 5^+, (c) 1^-, (d) 2^+, (e) 2^-, (f) 3^-, (g) 4^+, (h) 4^-, and (i) 5^-

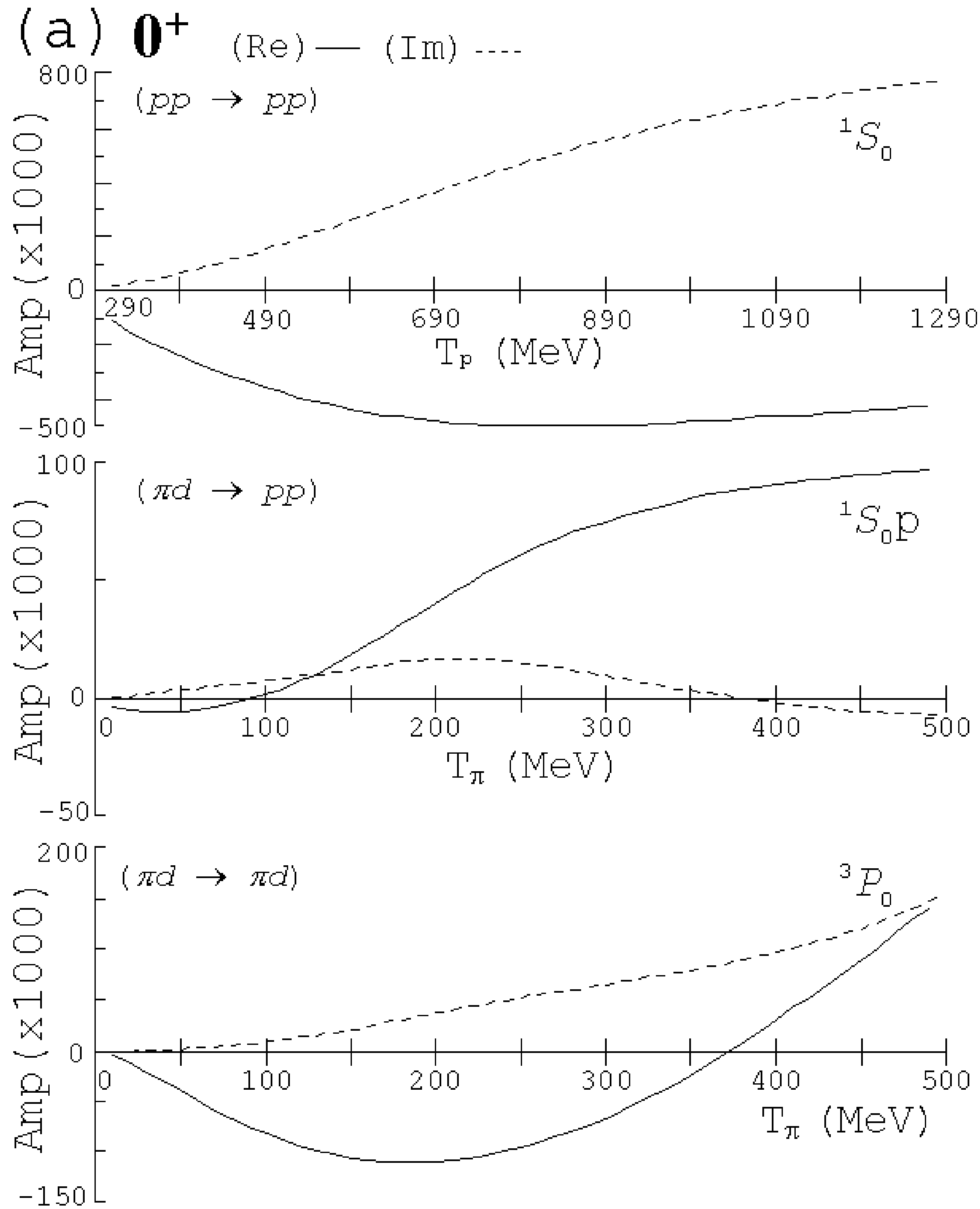

Figure 4. Partial wave amplitudes for the unified system from 0 to 500 MeV in T_p and 290 to 1290 MeV in T_p : (a) 0^+, (b) 1^+, 3^+, 5^+, (c) 1^-, (d) 2^+, (e) 2^-, (f) 3^-, (g) 4^+, (h) 4^-, and (i) 5^- system. Since 1^+, 3^+ and 5^+ systems only contain the $\mathrm{p}d \to \mathrm{p}d$ reaction, they are presented together in (b).

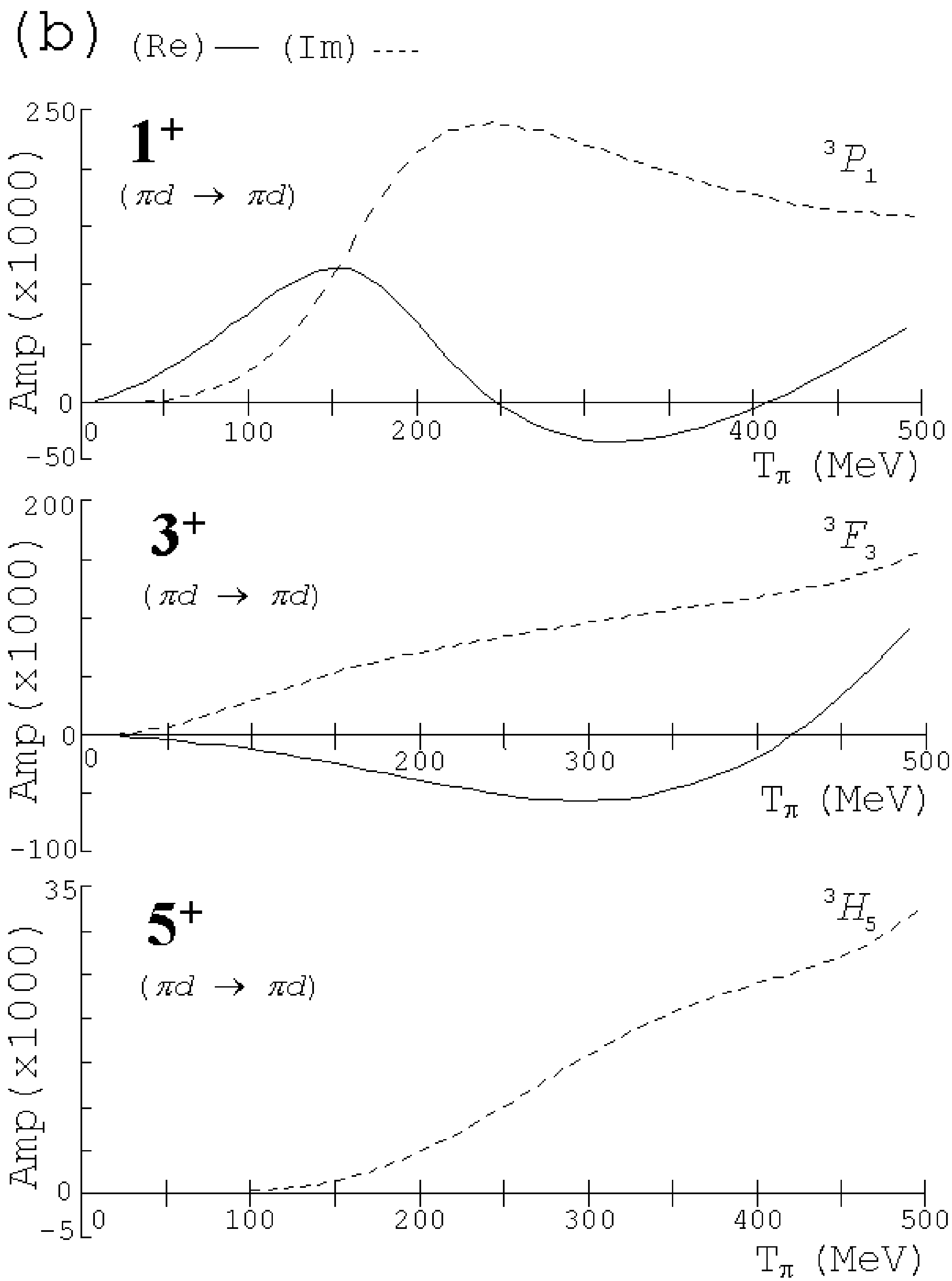

Figure 4. Continued (partial wave amplitudes for the unified system; 1^+, 3^+, 5^+; in the 5^+ system the real part of $^3H_5$ is nearly zero)

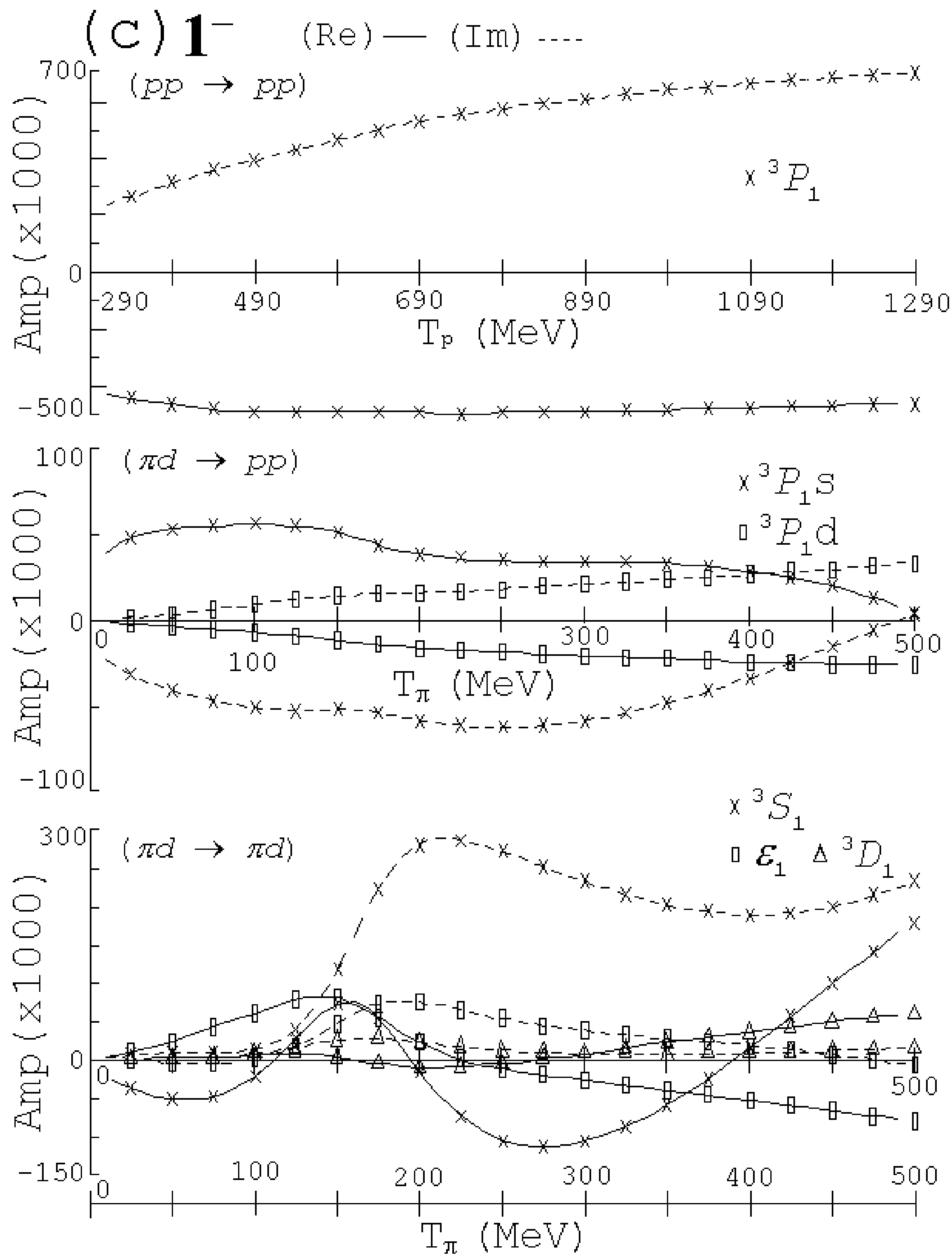

Figure 4. Continued (partial wave amplitudes for the unified system, 1^-)

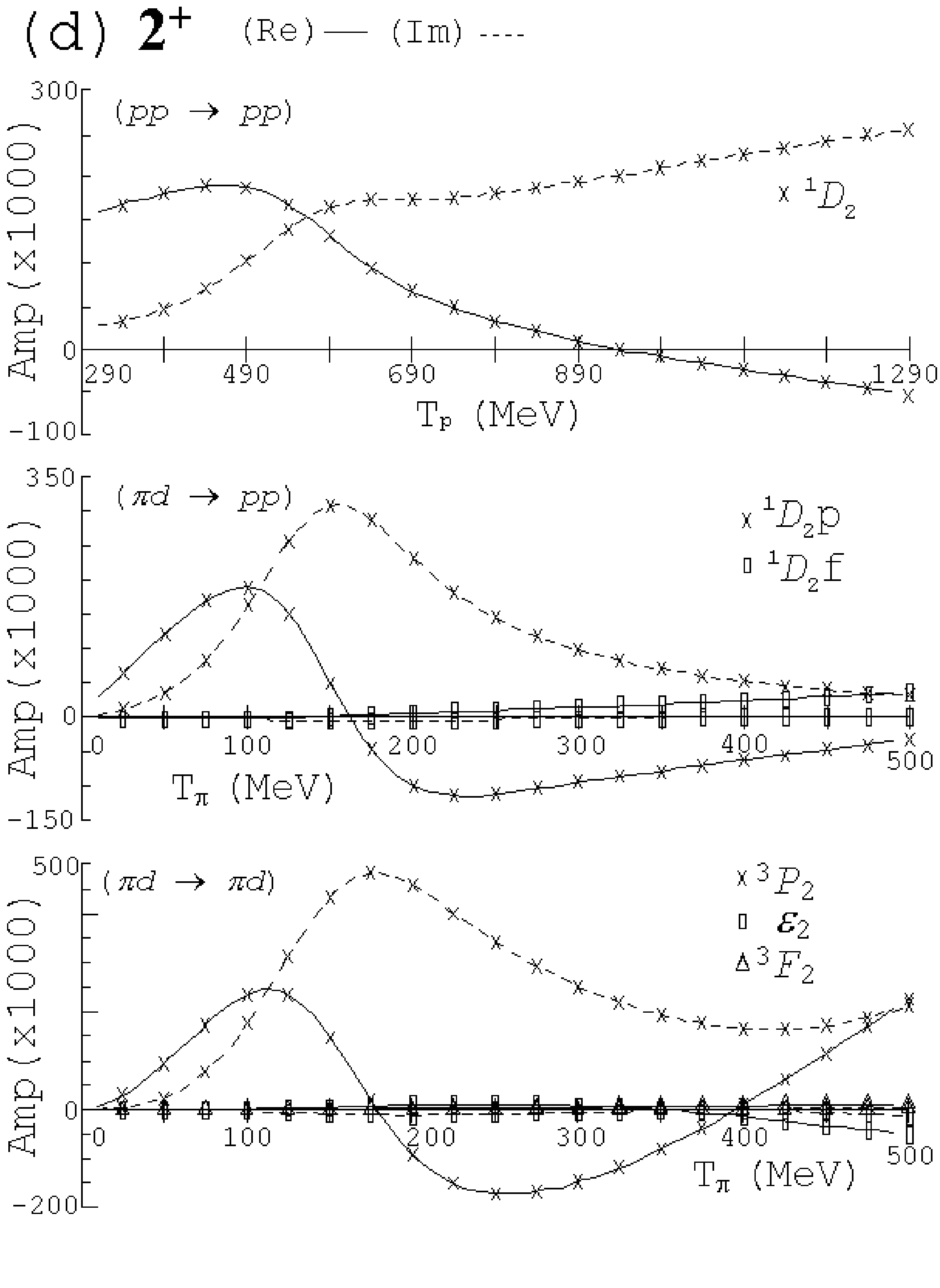

Figure 4. Continued (partial wave amplitudes for the unified system, 2^+)

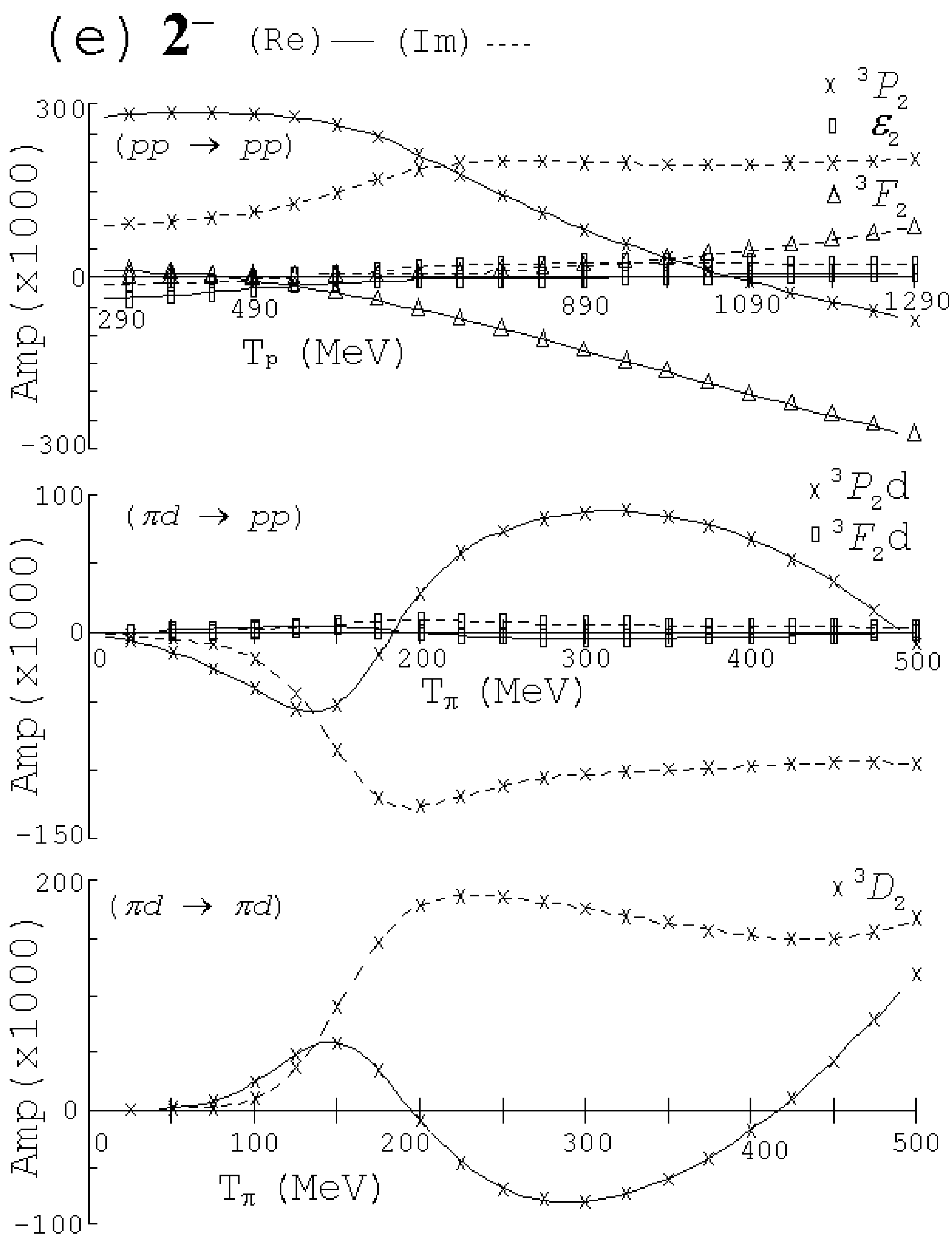

Figure 4. Continued (partial wave amplitudes for the unified system, 2^-)

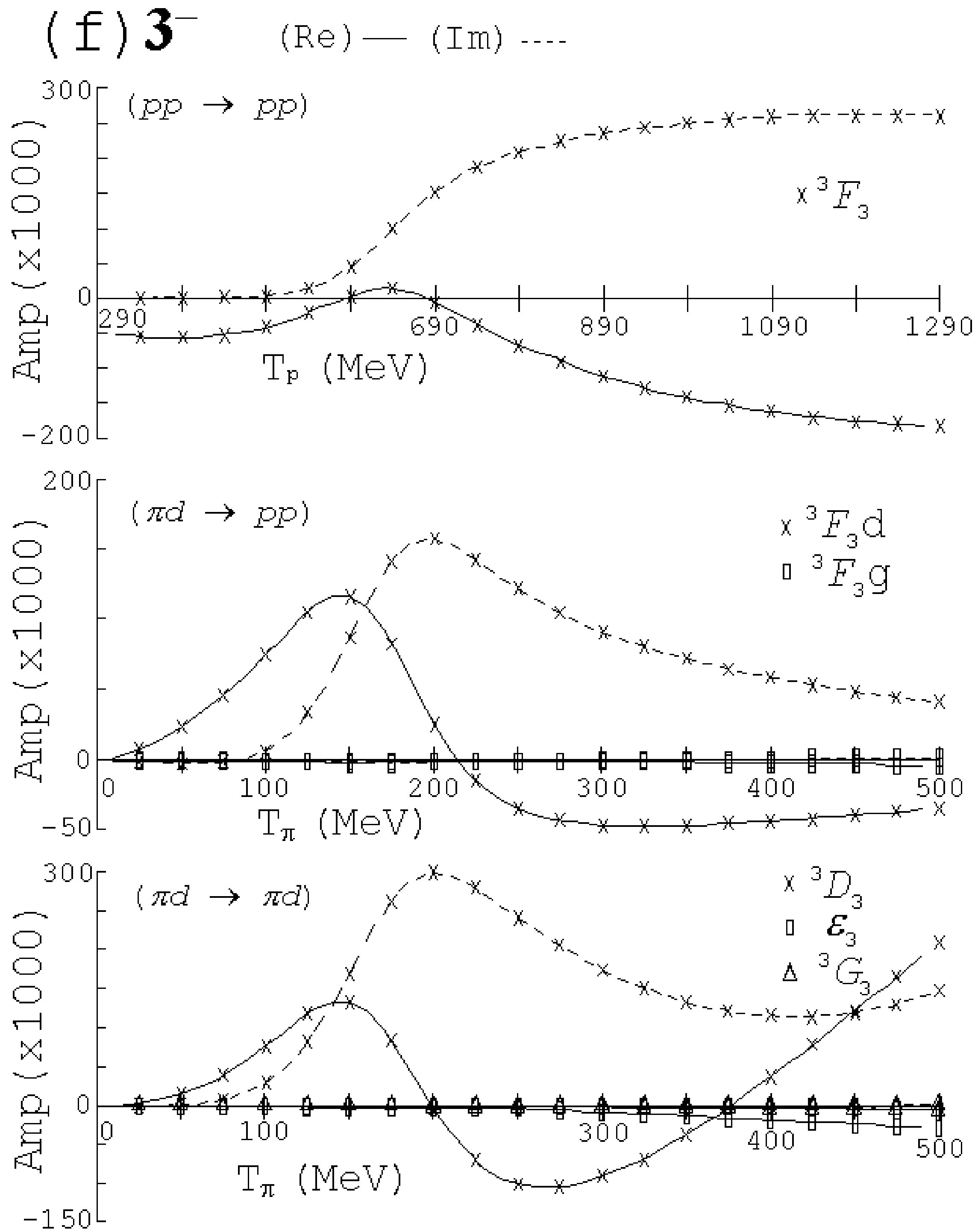

Figure 4. Continued (partial wave amplitudes for the unified system, 3^{-})

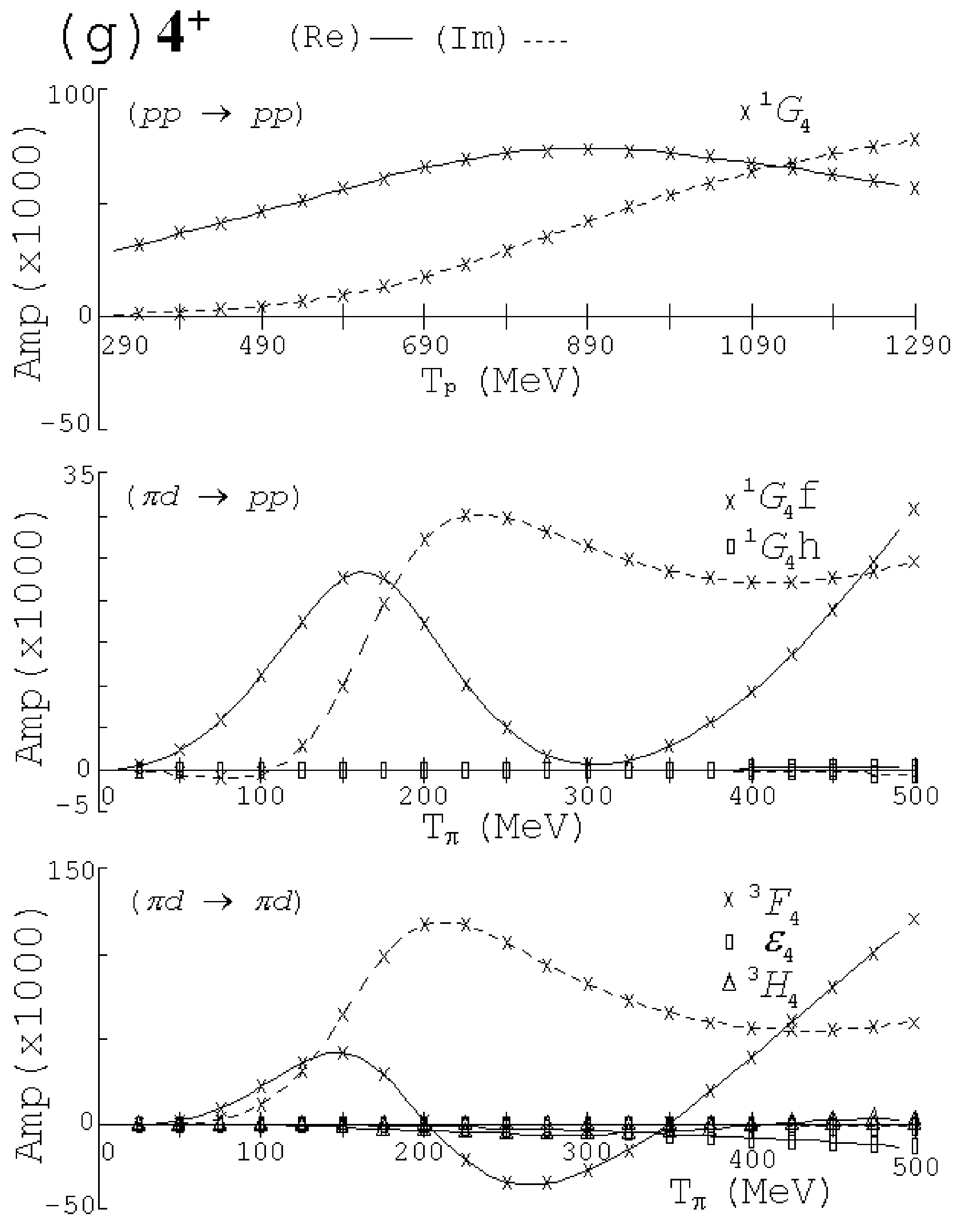

Figure 4. Continued (partial wave amplitudes for the unified system, 4^+)

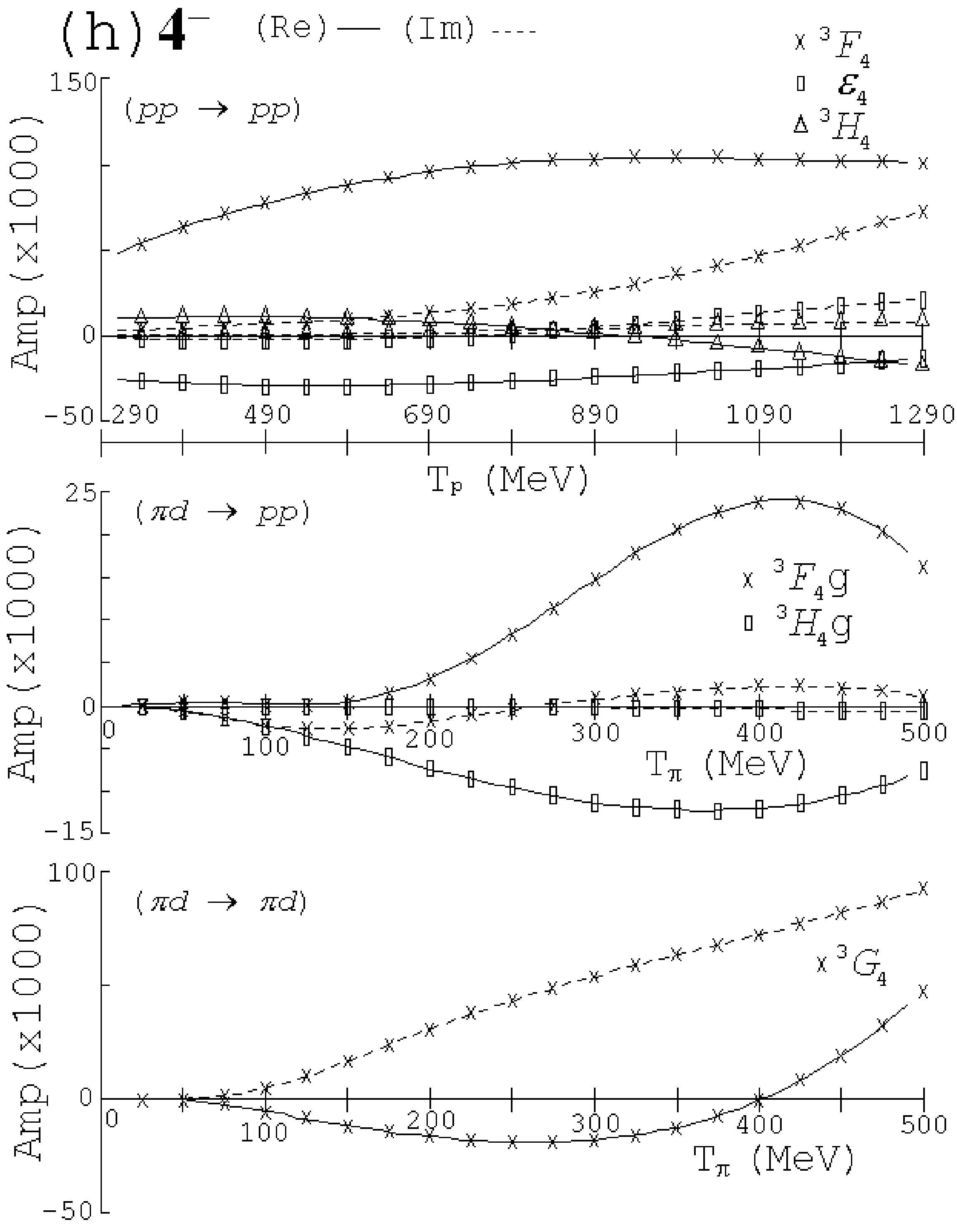

Figure 4. Continued (partial wave amplitudes for the unified system, 4^-)

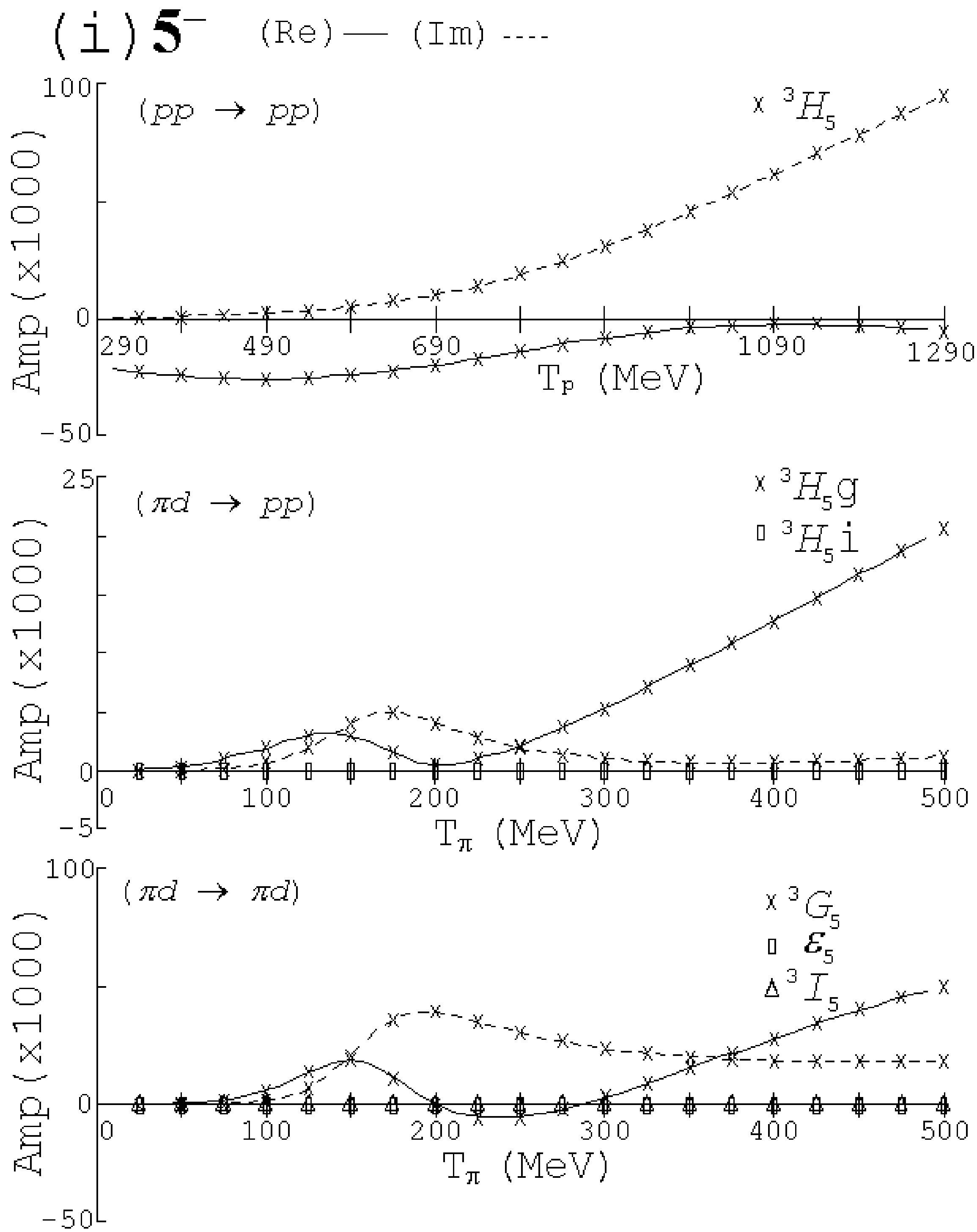

Figure 4. Continued (partial wave amplitudes for the unified system, 5^-)

systems, respectively. The solid (dashed) line shows the real (imaginary) part of amplitude. As described in Table 1, the 0^+ system contains three partial wave amplitudes. There are no elastic pp partial waves in the 1^+, 3^+ and 5^+ systems, they are presented in (b). Other systems contain six partial wave amplitudes. In (b), for the 5^+ system, the real part of ${}^3H_5$ is zero.

For spin flipped partial wave amplitudes, lower angular momentum states are dominant and higher angular momentum states are almost negligible. This also occurs in the inelastic channel.

Since we have carried out fits in which the pp partial waves were held fixed, the amplitudes for pp elastic scattering are the same as those given in WI96[4]. For this reason, we have omitted comparisons of the pp amplitudes.

Comparison of partial wave amplitudes for the elastic $\mathrm{p}d$ reaction is presented in Figure 5. We compare the dominant partial waves in each state from the single-reaction analysis (solution is SP96[4]) and the unified analysis (solution is C500). Figure 5 presents partial wave amplitudes for the elastic $\mathrm{p}d$ reaction from T_{p} = 0 to 500 MeV. Solid (dashed) curves give the real (imaginary) parts of amplitudes corresponding to the unified solution (C500 solution). The separate analysis (SP96) is plotted with long dash dotted (real part) and short dash-dotted (imaginary part) lines. The dotted curve gives the value of $\mathrm{Im}T - T^2 - T_{sf}^2$, where T_{sf}^2 is the spin-flip amplitude for the unified solution. The single energy solution (SES) which is generated using the unified analysis is presented. The real (imaginary) parts of single-energy solutions (SES) are plotted as filled (open) circles. All amplitudes have been multiplied by a factor of 10^3 and are

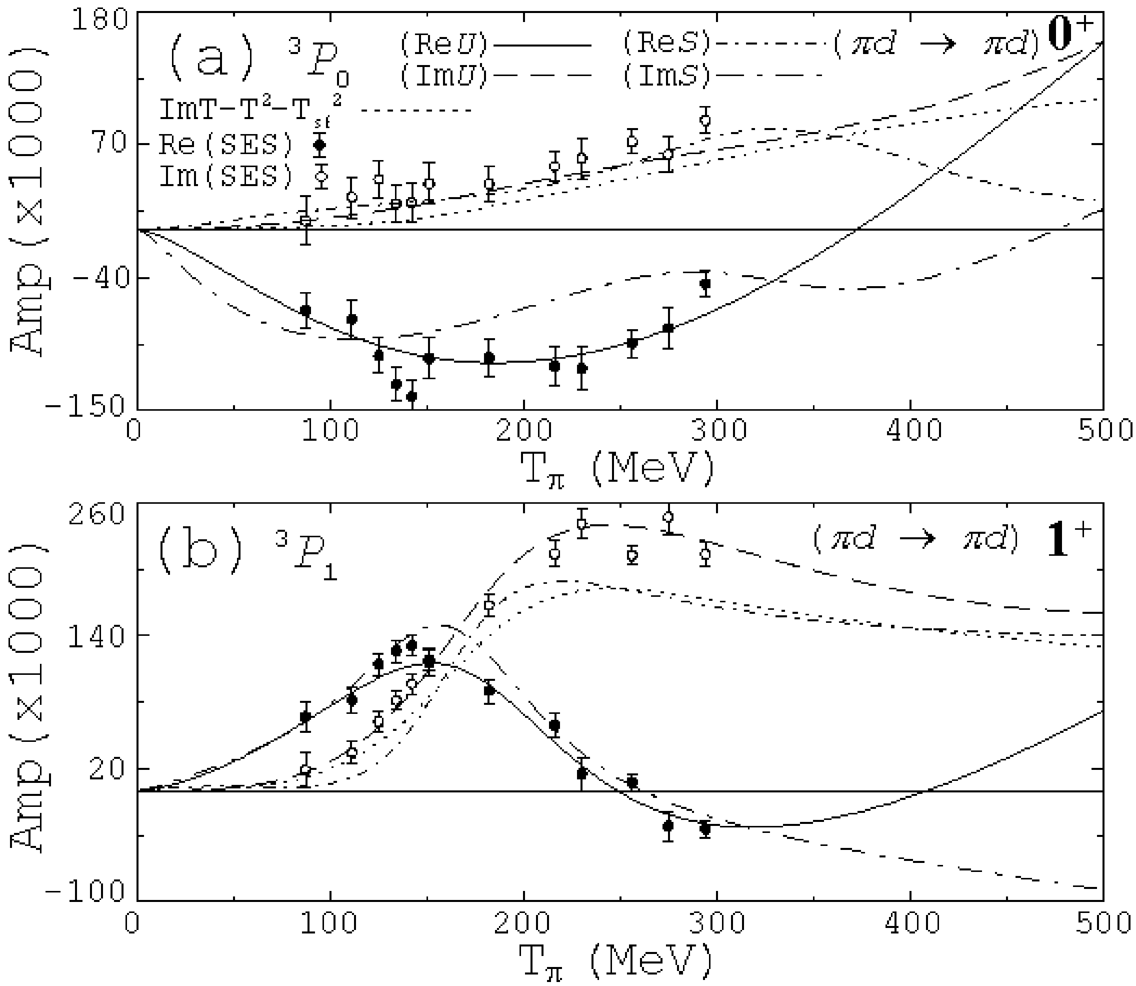

Figure 5. Partial wave amplitudes for the elastic pd reaction from T_p = 0 to 500 MeV. Solid (dashed) curves give the real (imaginary) parts of amplitudes corresponding to the unified solution (C500 solution). The separate analysis (SP96[4]) is plotted with long dash dotted (real part) and short dash-dotted (imaginary part) lines. The dotted curve gives the value of $\mathrm{Im}T - T^2 - T_{sf}^2$, where T_{sf}^2 is the spin-flip amplitude for the unified solution. The single energy solutions (SES) which are generated using the unified analysis are also presented. The real (imaginary) parts of single-energy solutions (SES) are plotted as filled (open) circles. All amplitudes have been multiplied by a factor of 10^3 and are dimensionless. Only the dominant partial waves are plotted for each states: (a) $^3P_0$ (0^+), (b) $^3P_1$ (1^+), (c) $^3S_1$ (1^-), (d) $^3P_2$ (2^+), (e) $^3D_2$ (2^-), (f) $^3F_3$ (3^+), (g) $^3D_3$ (3^-), (h) $^3F_4$ (4^+), (i) $^3G_4$ (4^-), (j) $^3H_5$ (5^+), (k) $^3G_5$ (5^-).

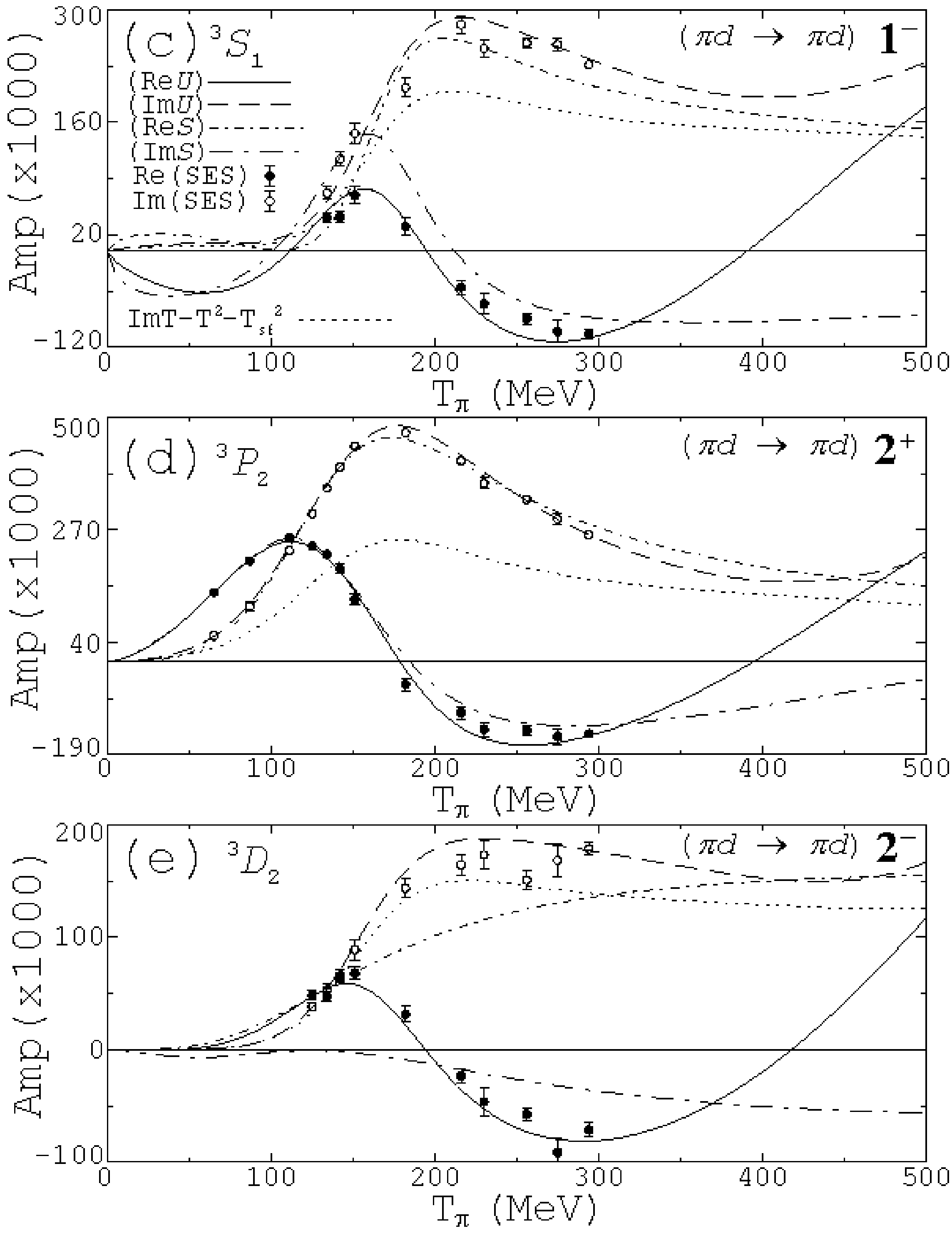

Figure 5. Continued (partial wave amplitudes for the elastic p*d* reaction)

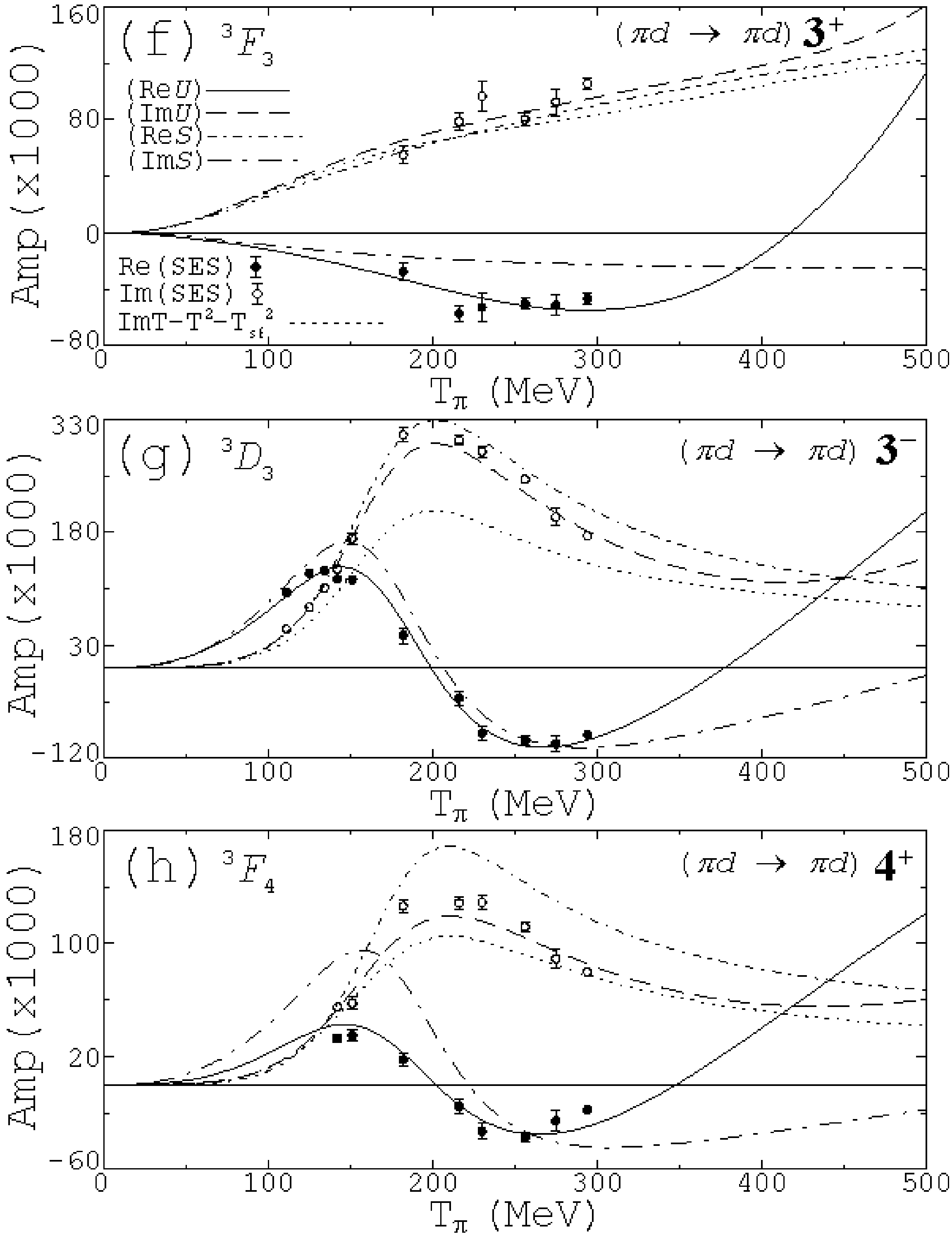

Figure 5. Continued (partial wave amplitudes for the elastic pd reaction)

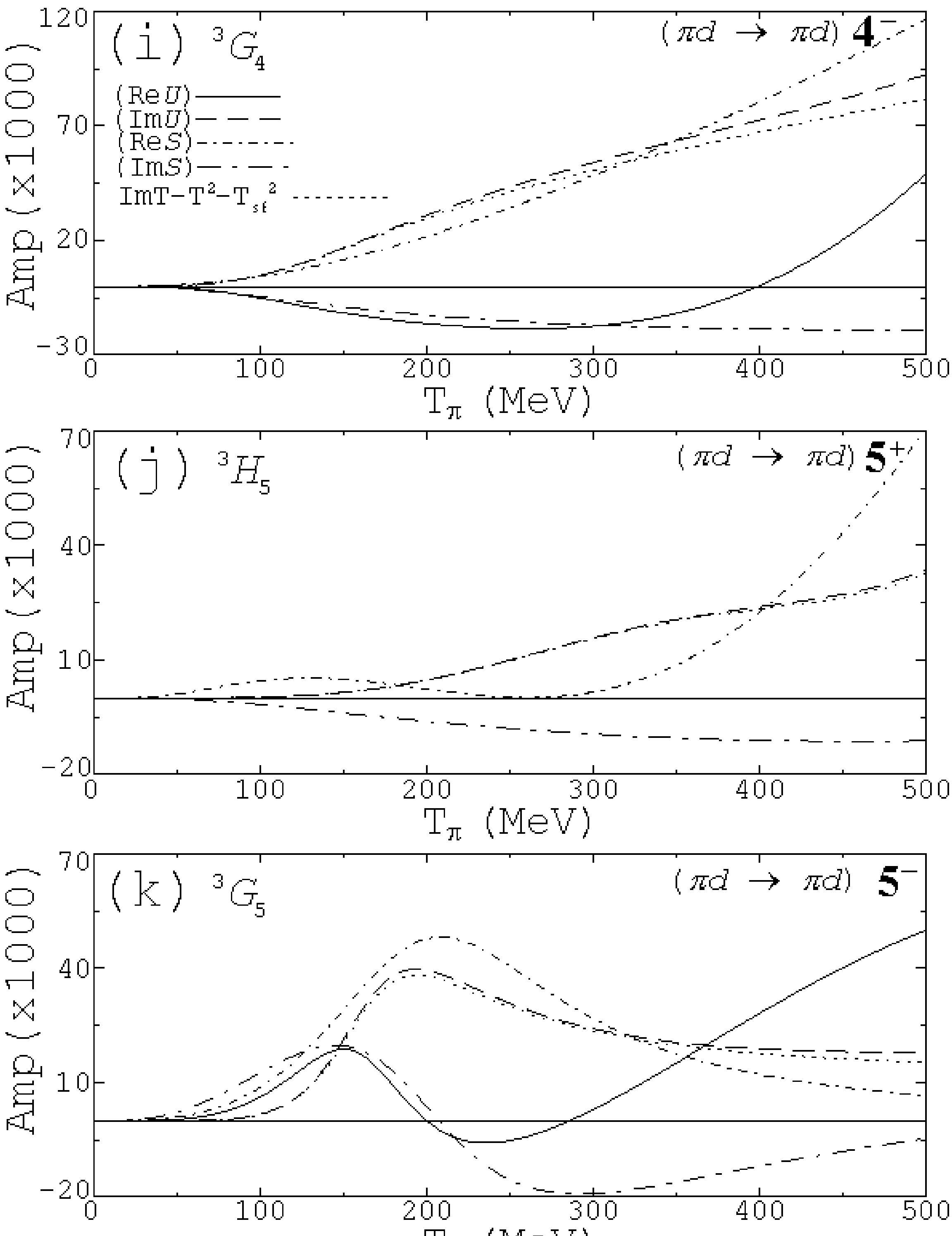

Figure 5. Continued (partial wave amplitudes for the elastic p*d* reaction)

dimensionless. Only the dominant partial waves are plotted for each state: (a) $^3P_0$ (0^+), (b) $^3P_1$ (1^+), (c) $^3S_1$ (1^-), (d) $^3P_2$ (2^+), (e) $^3D_2$ (2^-), (f) $^3F_3$ (3^+), (g) $^3D_3$ (3^-), (h) $^3F_4$ (4^+), (i) $^3G_4$ (4^-), (j) $^3H_5$ (5^+), (k) $^3G_5$ (5^-).

The results for elastic $\mathrm{p}d$ scattering in the unified and separate analyses are qualitatively similar, up to the limit of our single-energy analyses. Significant differences begin to appear above a pion laboratory kinetic energy of 300 MeV or 2.3 GeV in $\sqrt{s}$. (The $^3D_2$ partial wave from a unified analysis is an exception, departing from the single-reaction analysis near threshold.) The upper limit to our single-energy analyses is due to a sharp cutoff in the number of data. This is apparent in Figure 3-2. Much additional data above 300 MeV will be required before a stable solution to 500 MeV can be expected.

A comparison of results for $\mathrm{p}d \to pp$ reveals the most pronounced differences. One reason for this is the overall phase which was left undetermined in separate analysis[3]. There, we arbitrarily chose the $^3P_1 s$ wave to be real.

Figure 6-1 shows a comparison of the partial wave amplitudes for the $\mathrm{p}d \to pp$ reaction from T_p = 0 to 500 MeV without adjustment. The solid (dotted) curves give the real (imaginary) parts of the amplitudes. Amplitudes from the unified analysis are marked as ‘x’. Amplitudes from the separate analysis are plotted without symbols. Only the dominant partial waves are plotted for each state: (a) $^1S_0 p$ (0^+), (b) $^3P_1 s$ (1^+), (c) $^1D_2 p$ (2^+), (d) $^3P_2 d$ (2^-), (e) $^3F_3$ (3^-), (f) $^1G_4 f$ (4^+), (g) $^3F_4 g$ (4^-), (h) $^3H_5 g$ (5^-). In (b), the imaginary part of $^3P_1 s$ is zero for the separate analysis because of the arbitrary phase choice of zero. In (g), the imaginary part of $^3F_4 g$ is nearly zero for the separate analysis.

In the present analysis, the overall phase has been determined. In Figure 6-1, we see that the phase is very different in the unified and separate analyses. Given the large difference in overall phase, we have chosen to compare the partial-wave amplitudes from the separate and unified analyses in different ways. There are two ways to compare the partial wave amplitudes of the $pd \to pp$ reaction; the first is to compare the moduli of the amplitudes and the second is to match the phase.

Figure 6-2 shows a comparison of the moduli of the partial-wave amplitudes for $pd \to pp$ from T_p = 0 to 500 MeV. The solid and dashed curves give the amplitudes corresponding to the unified and separate (SP96[4]) solutions, respectively. Moduli of the single-energy solutions are plotted as filled circles. All amplitudes have been multiplied by a factor of 10^3 and are dimensionless. Only the dominant partial waves are plotted for each state: (a) ^1S_0p (0^+), (b) ^3P_1s (1^+), (c) ^1D_2p (2^+), (d) ^3P_2d (2^-), (e) $^3F_3$ (3^-), (f) ^1G_4f (4^+), (g) ^3F_4g (4^-), (h) ^3H_5g (5^-).

Figure 6-3 presents the partial wave amplitudes for $pd \to pp$ from T_p = 0 to 500 MeV. Here the phase has been matched. The ^3P_1s partial wave of the unified analysis has been adjusted to be purely real, as in the individual analysis. The single energy solutions (SES), which are generated using the unified analysis (C500 solution), are also presented. The real (imaginary) parts of the SES are plotted as ‘I‘ (‘▯‘) marks. Only the dominant partial waves are plotted for each state: (a) ^1S_0p (0^+), (b) ^3P_1s (1^+), (c) ^1D_2p (2^+), (d) ^3P_2d (2^-), (e) $^3F_3$ (3^-), (f) ^1G_4f (4^+), (g) ^3F_4g (4^-), (h) ^3H_5g (5^-).

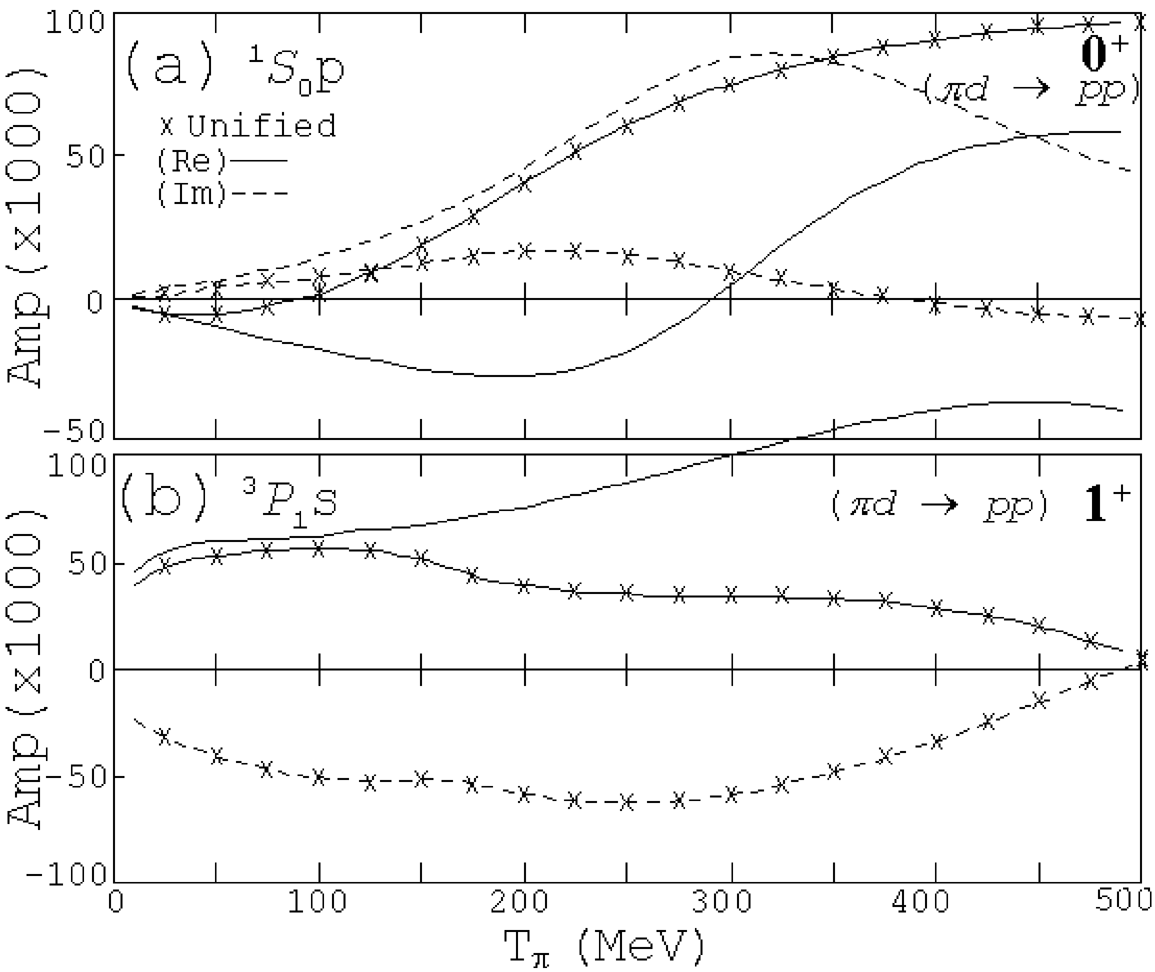

Figure 6-1. Partial wave amplitudes for $\pi d \to pp$ from T_π = 0 to 500 MeV without phase adjustment. To adjust the phase ambiguity, the ^3P_1s partial wave is assumed purely real in the separate analysis (SP96 solution[4]). The comparison of the moduli for the two analyses is presented in Figure 6-2. In Figure 6-3, the phases have been matched. The solid (dotted) curves give the real (imaginary) parts of the amplitudes. Amplitudes from the unified analysis are marked as 'x'. Amplitudes from the separate analysis have no mark. Only the dominant partial waves are plotted for each state: (a) ^1S_0p (0^+), (b) ^3P_1s (1^+), (c) ^1D_2p (2^+), (d) ^3P_2d (2^-), (e) $^3F_3$ (3^-), (f) ^1G_4f (4^+), (g) ^3F_4g (4^-), (h) ^3H_5g (5^-). In (b) the imaginary part of ^3P_1s is zero for the separate analysis because of phase adjustment. In (g) the imaginary part of ^3F_4g is zero for the separate analysis.

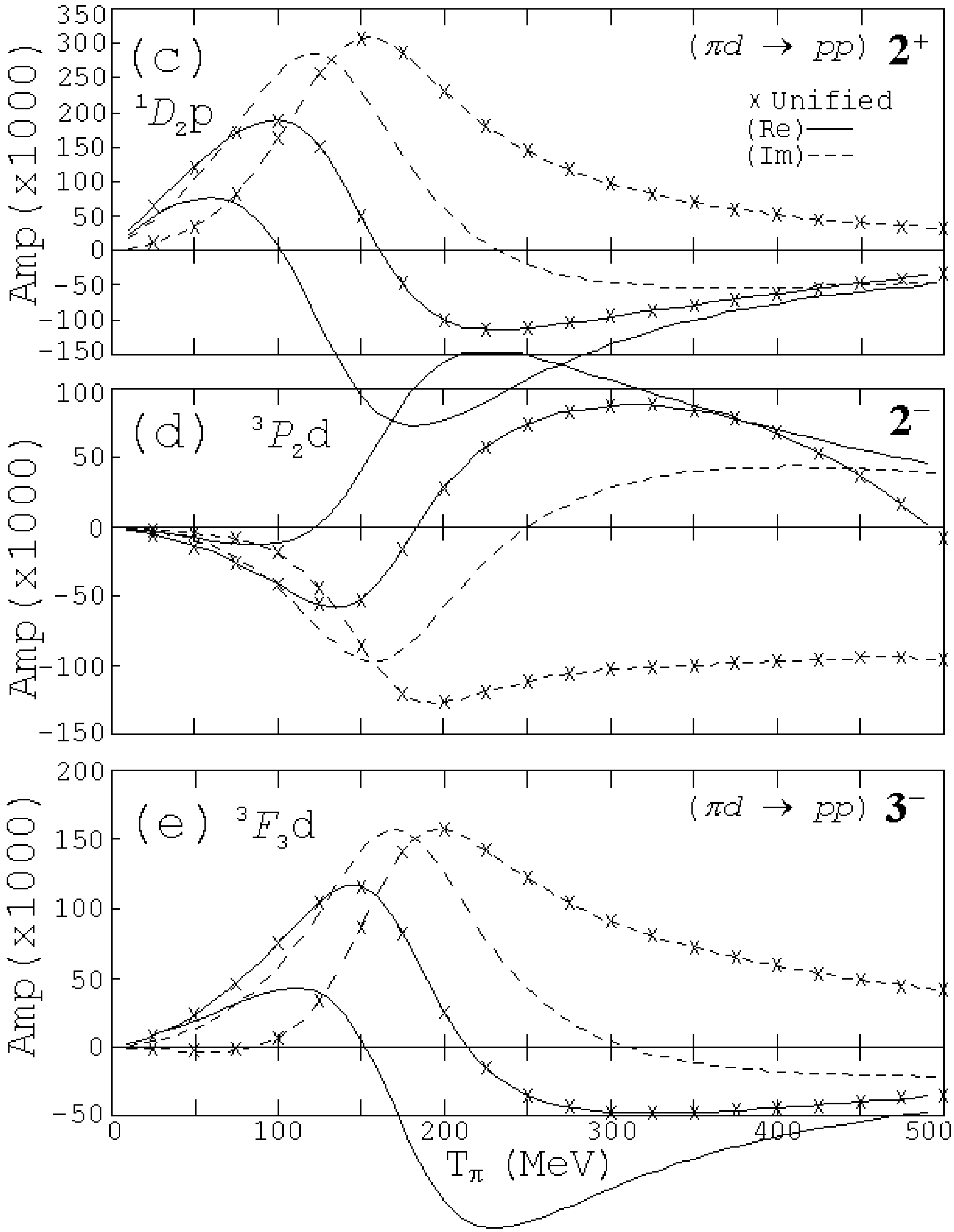

Figure 6-1. Continued (partial wave amplitudes for $\pi d \to pp$ without adjustment)

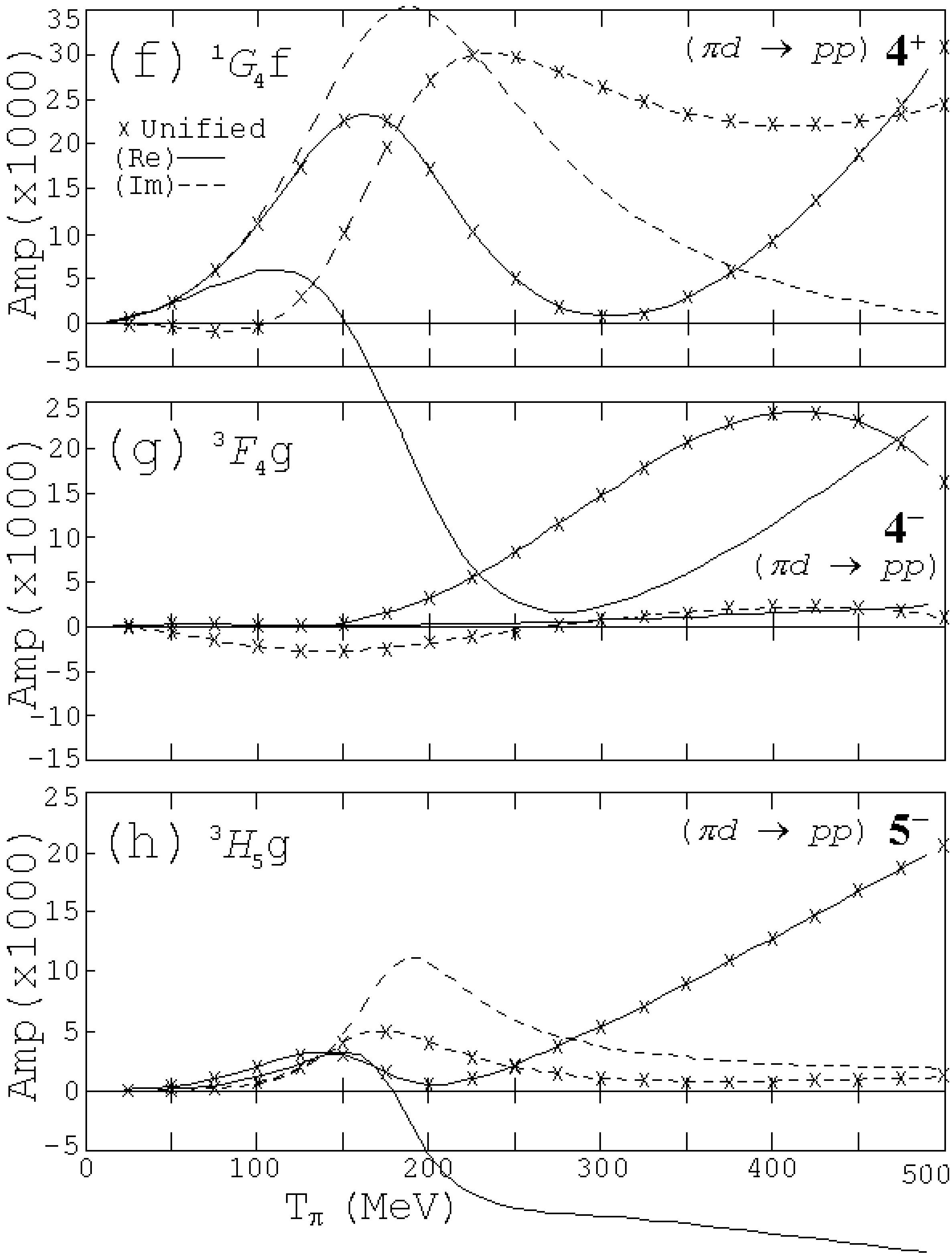

Figure 6-1. Continued (partial wave amplitudes for $\pi d \to pp$ without adjustment)

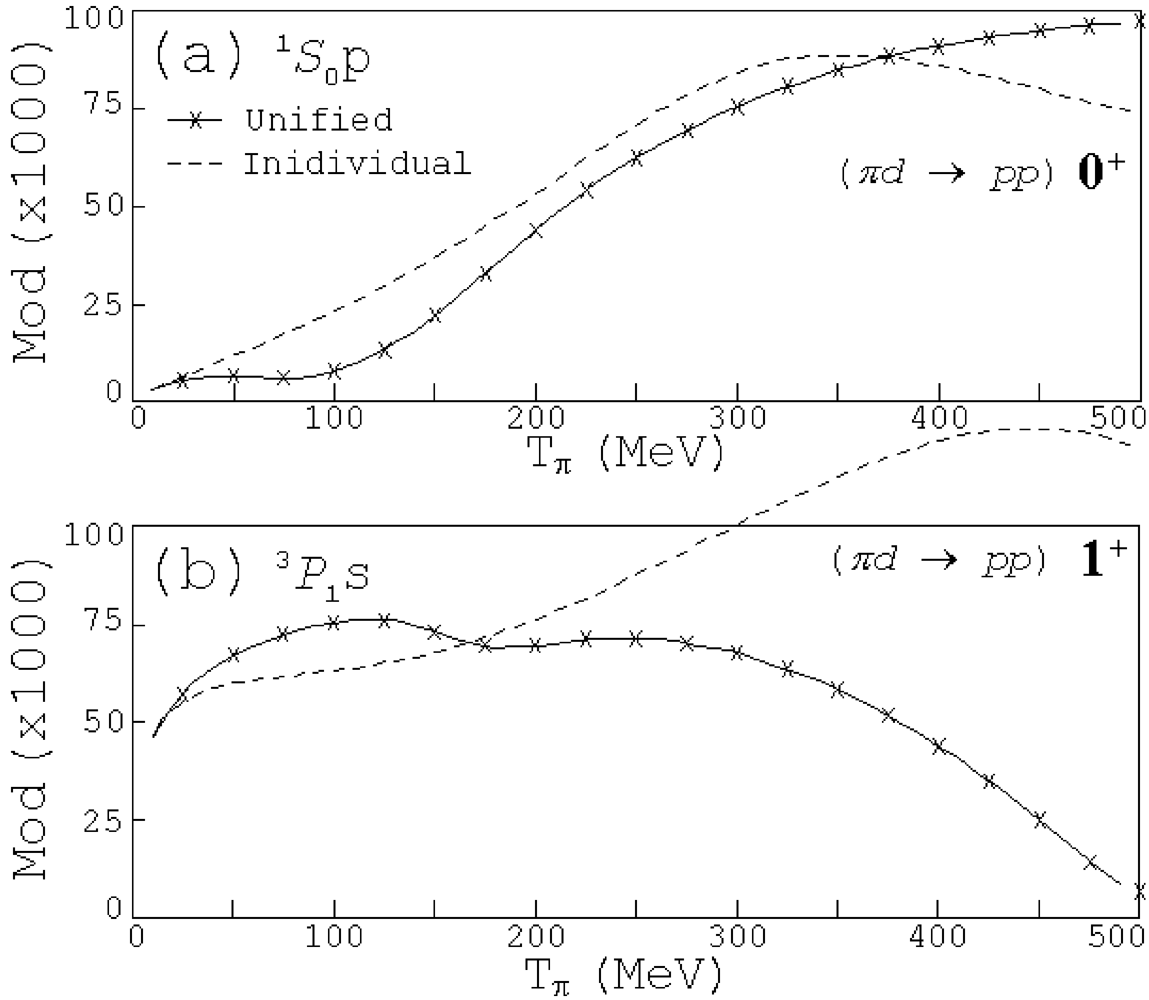

Figure 6-2. Moduli of the partial-wave amplitudes for $\pi d \to pp$ from T_π = 0 to 500 MeV. The solid and dashed curves give the amplitudes corresponding to the unified and separate (SP96[4]) solutions respectively. Moduli of the single-energy solutions are plotted as filled circles. All amplitudes have been multiplied by a factor of 10^3 and are dimensionless. Only the dominant partial waves are plotted for each state: (a) ^1S_0p (0^+), (b) ^3P_1s (1^+), (c) ^1D_2p (2^+), (d) ^3P_2d (2^-), (e) $^3F_3$ (3^-), (f) ^1G_4f (4^+), (g) ^3F_4g (4^-), (h) ^3H_5g (5^-).

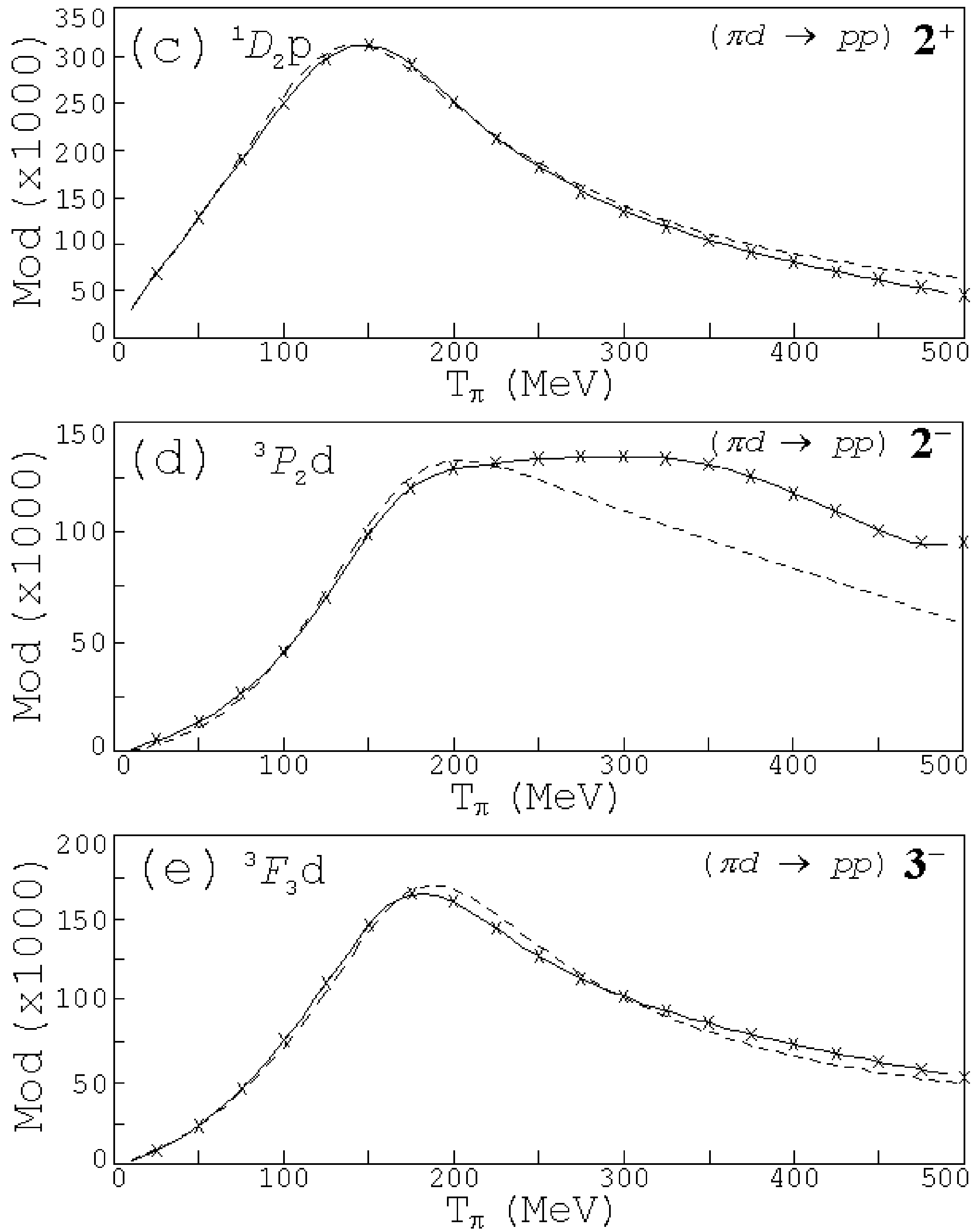

Figure 6-2. Continued (moduli of the partial-wave amplitudes for $\pi d \rightarrow pp$)

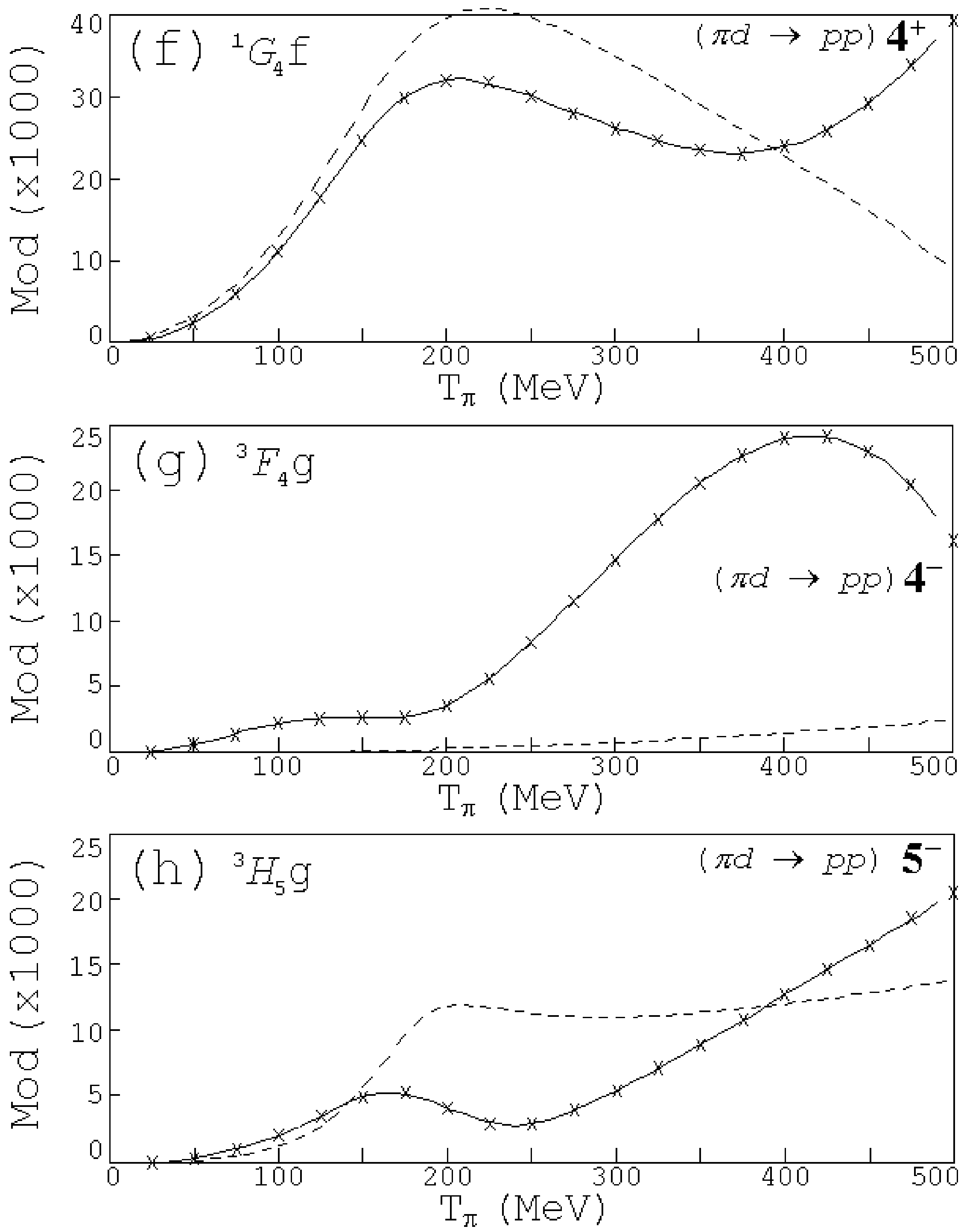

Figure 6-2. Continued (moduli of the partial-wave amplitudes for $\pi d \rightarrow pp$)

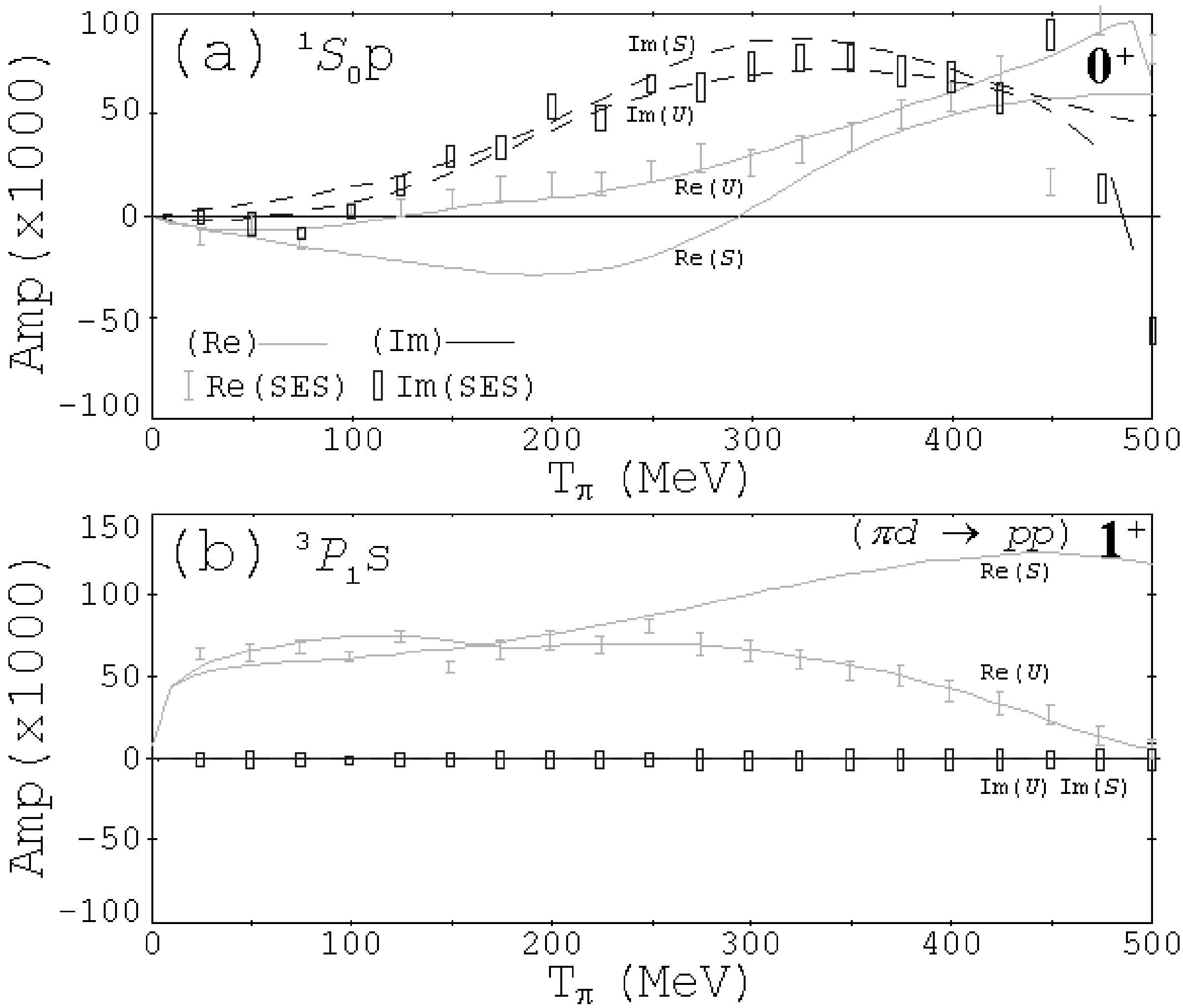

Figure 6-3. Partial wave amplitudes for p$d \rightarrow pp$ from T_{p} = 0 to 500 MeV. The phase has been matched. The ^3P_1s partial wave of the unified analysis is adjusted to be purely real as in the individual analysis. Single energy solutions (SES), which have been generated using the unified analysis (C500 solution), are also plotted. The real (imaginary) parts of the SES are plotted as ‘ I ‘ (‘ ▯‘) marks. Only the dominant partial waves are plotted for each state: (a) ^1S_0p (0^+), (b) ^3P_1s (1^+), (c) ^1D_2p (2^+), (d) ^3P_2d (2^-), (e) $^3F_3$ (3^-), (f) ^1G_4f (4^+), (g) ^3F_4g (4^-), (h) ^3H_5g (5^-).

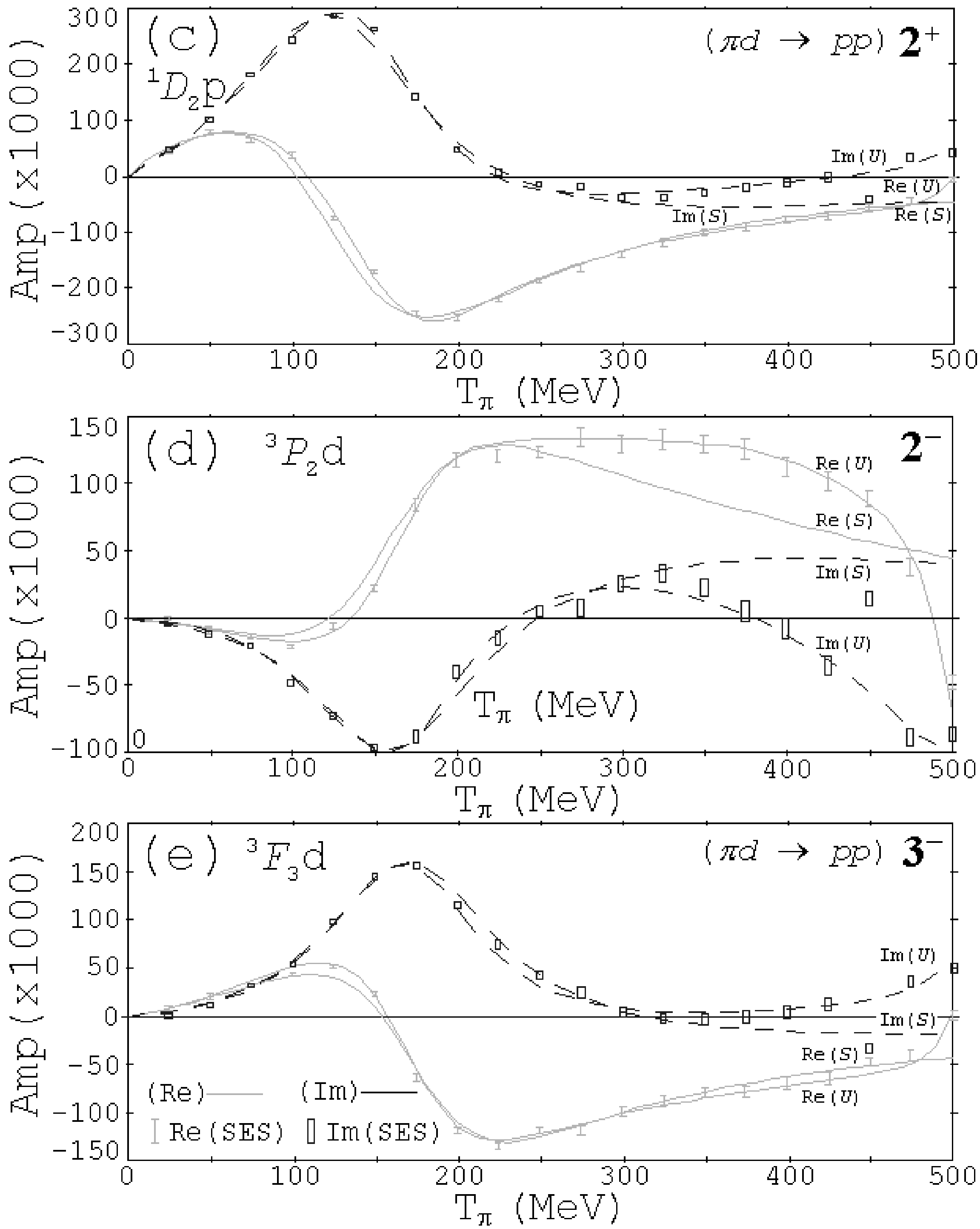

Figure 6-3. Continued (phase matched partial wave amplitudes for $\pi d \rightarrow pp$)

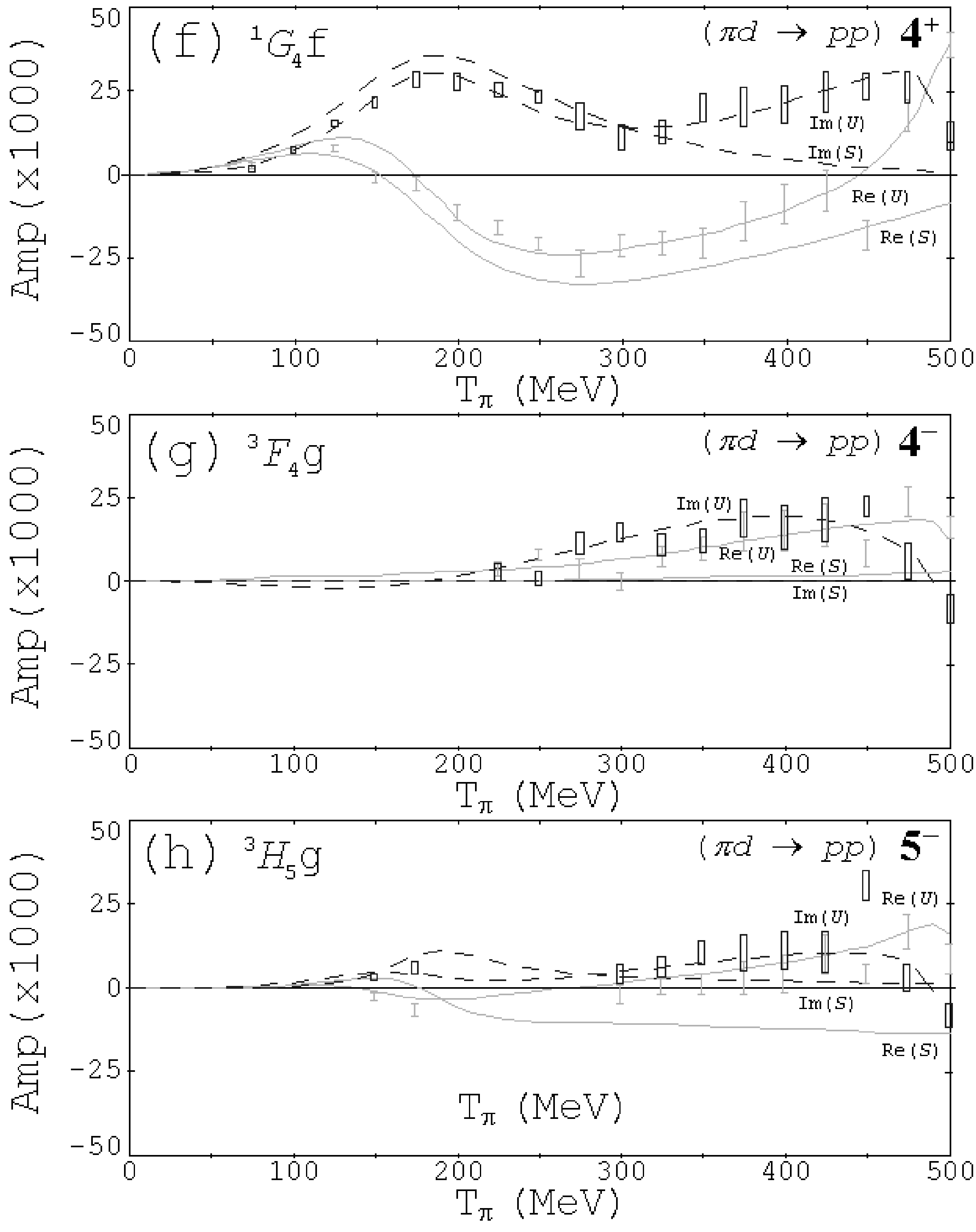

Figure 6-3. Continued (phase matched partial wave amplitudes for $\pi d \rightarrow pp$)

The overall phase difference for the $\pi d \to pp$ reaction is presented in Figure 7. In the individual analysis the overall phase of ${}^3P_1 s$ is adjusted to zero (dashed line). The phase of the ${}^3P_1 s$ from the unified solution is denoted by an '✕' mark. The difference of the two phases indicates the overall phase difference in the individual analysis.

As the case for πd elastic scattering, differences are most significant above approximately 2.3 GeV in $\sqrt{s}$. A similar lack of data exists above this energy in the $\pi d \to pp$ reaction data as shown in Figure 3-3.

In general we see a good agreement for the dominant amplitudes found in the separate and unified analyses. In Figures 5 and 6-3, we display our single-energy analyses which were done in order to search for structure which may be missing from the energy-dependent fit. (Details of the single-energy analyses are given in references [2] and [3].) A comparison of the single-energy and energy-dependent fits is given in Table 5.

Table 5-1 gives a comparison of single-energy (binned) and energy-dependent combined analyses of elastic πd reaction data. Table 5-2 gives a similar comparison for the $\pi d \to pp$ reaction data. N_{prm} is the number of parameters varied in the single-energy fits. χ_E^2 is due to the energy-dependent fit (C500) taken over the same energy interval.

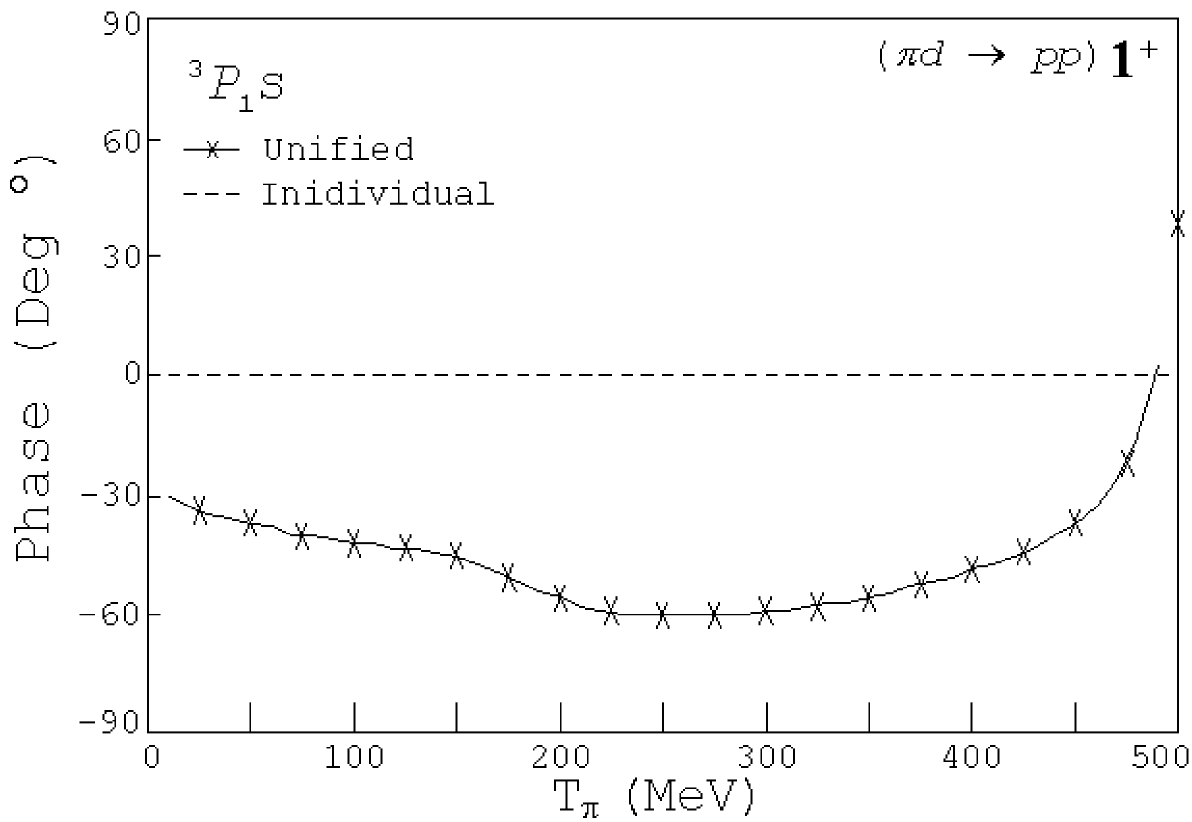

Figure 7. Overall phase difference for p$d \rightarrow pp$. In the individual analysis the overall phase of $^{3}P_{1}s$ is adjusted to zero (dashed line). The phase of the $^{3}P_{1}s$ from the unified solution is shown by the ‘X’. The difference of the two phases indicates the overall phase ambiguity in the individual analysis.

Table 5-1. Comparison of single-energy (binned) and energy-dependent unified analyses of πd elastic scattering data. N_{prm} is the number of parameters varied in the single-energy fits. χ^2_E is due to the energy-dependent fit (C500) taken over the same energy interval.

T_π (MeV)	Range (MeV)	N_{prm}	χ^2 / data	χ^2_E
65	58.0 – 72.0	2	2106/54	102
87	72.0 – 92.0	6	620/24	21
111	107.5 – 125.2	10	68/82	66
125	115.0 – 134.0	12	155/170	184
134	124.0 – 142.8	14	315/258	344
142	133.0 – 152.0	16	356/284	397
151	141.0 – 160.6	16	193/154	216
182	174.0 – 189.5	18	302/168	396
216	206.0 – 220.0	18	158/99	200
230	220.0 – 238.0	18	64/53	111
256	254.0 – 260.0	16	132/125	185
275	270.5 – 284.4	16	22/40	42
294	284.4 – 300.0	16	267/132	324

Table 5-2. Comparison of single-energy (binned) and energy-dependent unified analyses of $\mathrm{p}d \to pp$ reaction data. N_{prm} is the number of parameters varied in the single-energy fits. χ^2_E is due to the energy-dependent fit (C500) taken over the same energy interval.

T_{p} (MeV)	Range (MeV)	N_{prm}	χ^2 / data	χ^2_E
25	12.8 – 37.4	10	527/241	542
50	37.6 – 60.7	12	188/168	205
75	62.9 – 87.3	14	590/426	628
100	91.0 – 114.0	14	1263/611	1379
125	113.8 – 137.1	16	729/512	756
150	140.0 – 162.0	20	743/630	792
175	165.0 – 187.3	22	343/280	426
200	191.3 – 210.3	20	120/193	153
225	217.9 – 235.9	22	217/229	291
250	238.9 – 262.0	22	595/483	685
275	264.9 – 285.1	22	204/109	280
300	291.6 – 307.4	24	198/212	235
325	318.9 – 330.0	24	142/161	234
350	341.4 – 360.3	24	201/185	233
375	371.4 – 375.7	24	32/26	42
400	390.0 – 400.0	24	19/28	34
425	417.0 – 420.0	24	50/28	55
450	437.6 – 456.5	22	122/48	231
475	473.8 – 487.4	22	24/24	39
500	495.9 – 506.5	22	49/45	281

A comparison of the Argand plots is given in Figure 8. Only the three dominant partial waves are plotted for each reactions. The Argand plots from the unified solution are marked as '*U*'. Argand plots from the individual solution are marked as '*S*'.

Figure 8-1 gives the Argand plot comparison of the elastic πd reaction for T_π = 0 to 500 MeV: the Argand plots of ${}^3P_2$ (2^+), ${}^3D_3$ (3^-), and ${}^3D_2$ (2^-) for $\pi d \rightarrow \pi d$ are displayed. In Figure 8-2, the Argand plots of ${}^1D_2 p$ (2^+), ${}^3F_3$ (3^-), and ${}^3P_2 d$ (2^-), for $\pi d \rightarrow pp$ are displayed. Since the comparison of the two analyses for $\pi d \rightarrow pp$ requires a phase adjustment, Argand plots for $\pi d \rightarrow pp$ are displayed in Figure 8-2 (a) and phase matched Argand plots for $\pi d \rightarrow pp$ are displayed in Figure 8-2 (b). The Argand plots for the unified solution are slightly different in (a) and (b), because of the different phases.

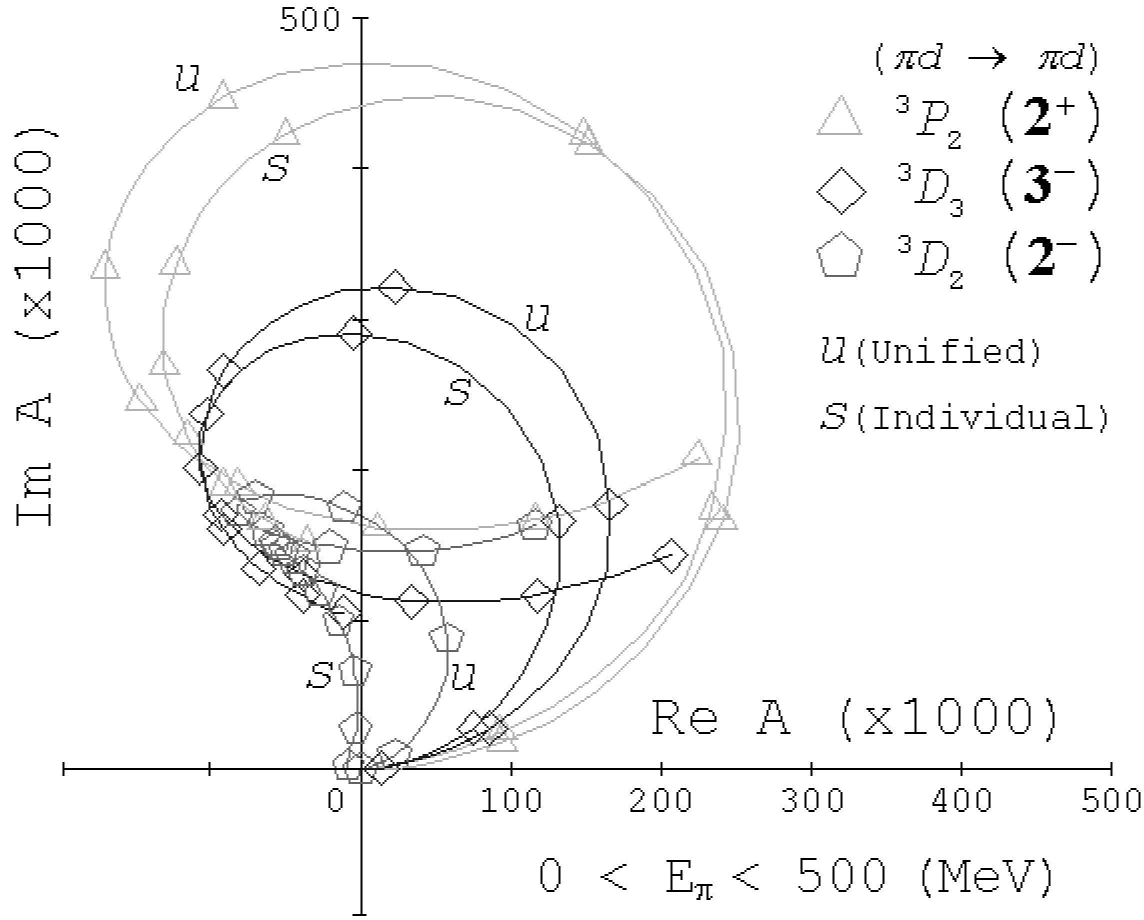

Figure 8-1. Argand plots for the elastic pd reaction for T_p = 0 to 500 MeV. Only the three dominant partial waves are plotted in each reactions. The Argand plots from the unified solution are marked as 'U'. Argand plots from the individual solution are marked as 'S'. The Argand plots of $^3P_2$ (2^+), $^3D_3$ (3^-), and $^3D_2$ (2^-) for elastic pd reaction are displayed.

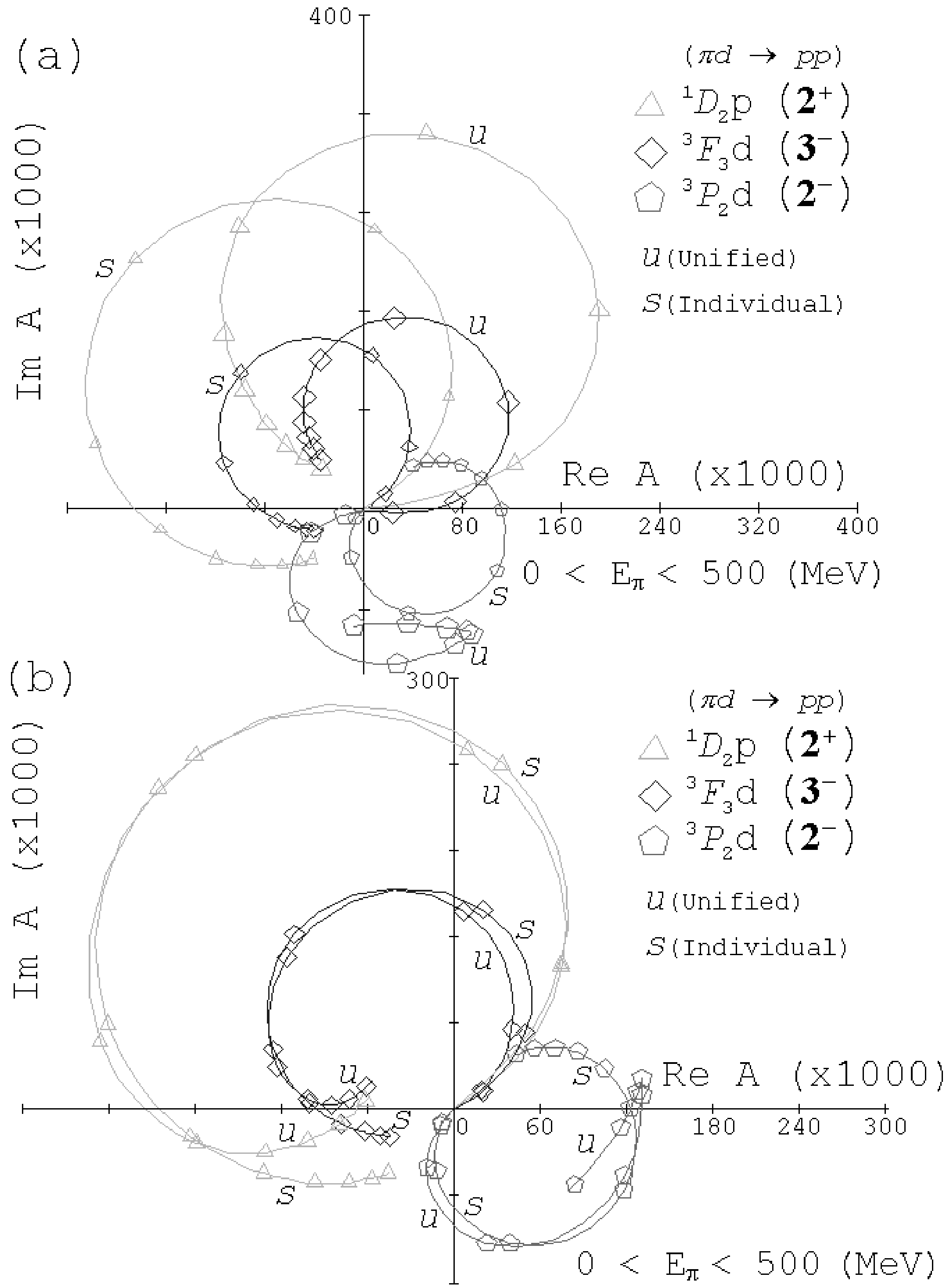

Figure 8-2. Argand plots of $^1D_2\,p\ (2^+)$, $^3F_3d\ (3^-)$, and $^3P_2d\ (2^-)$ for $\pi d \to pp$. Phase matched Argand plots for $\pi d \to pp$ are displayed in (b).

Chapter 7

RESONANCE-LIKE BEHAVIOR IN THE B = 2 SYSTEM

As briefly mentioned in Chapter 2, there are resonance-like states in the three reactions $pp \to pp$, $\pi d \to pp$, and $\pi d \to \pi d$; and the very existence (or non-existence) of a dibaryon system has been one of the hottest issues of debate in the Nuclear Physics community in last half century.

The question is whether two nucleons, when they react together, can comprise a super multiplet as a bound state (quasi-stable particle) or not.

The nucleon pair has isospin 0 or 1. A nucleon pair with the total isospin equal to zero is known as deuteron. As described in Chapter 2, the deuteron is a simplest multi-nucleon system and the only known dibaryon in the nature.

A second case, with total isospin equal to one, is the testing ground of the controversial dibaryon resonance, a possible manifestation of sub-hadronic degrees of freedom.

Another possible state is total isospin equal to two. As a two baryon system, the N-Δ pair has isospin 1 or 2. The possible existence of the total isospin two system is conjectured to be a stable πNN bound state such as $\pi^- nn$ and $\pi^+ pp$. Specially, the existence of bound states of negative pions and two neutrons (pineuts) has been predicted[24]. These systems decay through only weak interactions. This implies these system should be stable and have lifetimes comparable to that of the charged pion. However, in spite of all the experimental[25] and theoretical[26] efforts, current information points toward the nonexistence of pNN bound states, thus the evidence in favor of pNN bound states has now disappeared.

The question is whether the resonance-like behaviors seen in the isospin one system correspond to true resonances or not: that is, are there actual *S*-matrix poles in the second Riemann sheet (resonances) or not ?

Some models suggest the need for dibaryon resonances. From the study of the static *quark* model, R.J. Oakest[27] examined the role of the deuteron in the eightfold way and found it must belong to a ten dimensional representation of $SU(3)$, and he raised a question - in the limit of exact unitary symmetry, are two baryon states bound. Or if unitary symmetry is not exact in the physical world, some of these might not occur as actual bound states. However, if the symmetry is not broken too badly, Oakest suggested nearly bound, or resonant, states should occur in baryon-baryon channels. He used “resonance” in its loosest sense to denote a relative enhancement of an interaction at a reasonably well-defined energy. To fill out the missing parts in eightfold symmetry, he suggested that dibaryon states are necessary condition. R.L. Jaffe[28] presented the bag model for the exotic multi-quark systems; and P.J. Mulders[29] predicted the possibility of the hidden-color resonances in the six-quark system.

The other alternative, to explain the structure in these two nucleon system, is pseudo-resonance effects. A pseudo-resonance is understood as a threshold effect arising from the opening of the inelastic *N*-Δ coupling. *N*-Δ threshold effect is strong enough to generate counterclockwise loops on the Argand diagrams (nonresonant Argand loops).

Generally, this idea has been used in the p*d* system, when there is smearing of the p*N* resonances (mostly Δ-resonance) over several partial waves - they are, mostly, angular momentum L = 0, 1, and 2 states - in the p*d* system[30]. Then no pole resonance is expected in the nucleon-nucleon system. The resonance-like behaviors in the p*d* system are connected with the opening up of the *N*-Δ channel[30] and the influence of an intermediate *N*-Δ state (resulting in a "pseudo-resonance") that enter through so called *N*-Δ box diagrams (involving *N*Δ in *NN* scattering) and create resonance-like loops in the Argand diagram without resonance poles actually existing[31].

On the other hand, L. Fonda *et al*. [32] showed that one should be able to fit all the elementary particle resonances without *S*-matrix poles. They performed a fit to the Δ (1236) with no pole *S*-matrix.

Compared to no-pole resonances in the p*d* system, the study of real dibaryon resonances has been performed mostly in nucleon-nucleon system and some in the p*d* system.

In 1968, R. A. Arndt predicted a $^1D_2$ nucleon-nucleon resonance from the partial-wave analysis of elastic *pp* data below 700 MeV[33].

F. Furuichi and H. Suzuki raised a question of dibaryon resonances[34] based on purely polarised proton-proton cross sections near T_L = 180 MeV measured by J.P. Auer *et al* and de Boer *et al*[35].

J.A. Niskanen showed a peak near the $N\Delta$ threshold in the cross section and in polarization for $\pi^+ d \to pp$ reaction[36]. Also T. Kamae and T. Fujita showed an irregularity, at a somewhat higher energy, in the proton polarization for $\gamma d \to pn$[37].

A. Yokosawa found that strong energy dependence was unexpectedly observed in pp polarization experiments at Argonne[38]. He found pronounced structures in the spin-dependent cross section difference $\Delta\sigma_T$ and $\Delta\sigma_L$ in elastic pp scattering.

H.G. Dosch and E. Ferreira attempted to get πd-dibaryon coupling parameters and expected possible dibaryon resonances in the 4^+ system where compared to previous 2^+ and 3^- systems[39]. They extracted information on the short range part of the nucleon-nucleon and nucleon-delta interaction[40]. H. Garcilazo showed that the decomposition of the pion-nucleon P_{11} amplitude into pole and non-pole parts did not generate large spurious effects as a result of the application of the Pauli principle in intermediate NN states when the relativistic Faddeev theory was applied to the πNN system for πd scattering[41].

The idea of dibaryon existance has been applied to multi-channel systems that contain both nucleon-nucleon system and the πd system. These studies of multi-channel systems are described in Chapter 2.

The studies of resonance free nucleon-nucleon scattering amplitudes were performed by I. Duck and Ver West[42]. W.M. Kloet *et al*. examined pseudo resonance behavior in nucleon-nucleon scattering[43]. R.L. Shypt *et al*. claimed the evidence against broad dibaryons[44].

However, W.M. Kloet and J.A. Tjon found that N-Δ box diagram itself contains poles resulting from the square-root singularity of the N-Δ branch cut[45]. Near the N-Δ branch point there are poles that originate from left-hand singularities in the unphysical sheet. They tried to find the pole positions for the ${}^3F_3$ and ${}^1D_2$ nucleon-nucleon resonance poles.

Also R.L. Shypt *et al*.[46] raised a question again about the requirement of an additional bound or virtual state in the nucleon-nucleon channel or whether the threshold alone accounts for the data to explain the rapid phase variation quantitatively in the phase $\mathrm{d}_{N\Delta}$ for ${}^1D_2(NN) \to {}^5S_2\ (N\Delta)$ that has obtained similar result from $\mathrm{p}d$ elastic reaction[40].

For dibaryon studies, the pole positions and residues were obtained from elastic NN scattering data by analytic continuation of the "production" piece of the T-matrix obtained in the energy dependent solution SM86[4] by R.A. Arndt *et al*[47]. The positions (residues) of poles extracted from the WI96 solution are 2144.6 – i75 MeV (17.3 – i33.4 MeV) for the ${}^1D_2$ partial wave, 2165.5 – i55.9 MeV (5.4 – i78.9 MeV) for the ${}^3F_3$ partial wave, and 2161.0 – i87.7 MeV (13.0 – i61.2 MeV) for the ${}^3P_2$ partial wave states in elastic pp reaction.

Argand plots of the dominant partial wave amplitudes in each system from T_{p} = 0 to 500 MeV are presented in Figure 9: (a) 0^+, (b) 1^+, (c) 1^-, (d) 2^+, (e) 2^-, (f) 3^+, (g) 3^-, (h) 4^+, (i) 4^-, (j) 5^+ and (k) 5^- system. Each plot for $pp \to pp$ is marked as '△', $\mathrm{p}d \to pp$ is marked as '□' and $\mathrm{p}d \to \mathrm{p}d$ is marked as '⌘'. The mark points denote 25MeV steps. All amplitudes have been multiplied by a factor of 10^3. All amplitudes are dimensionless.

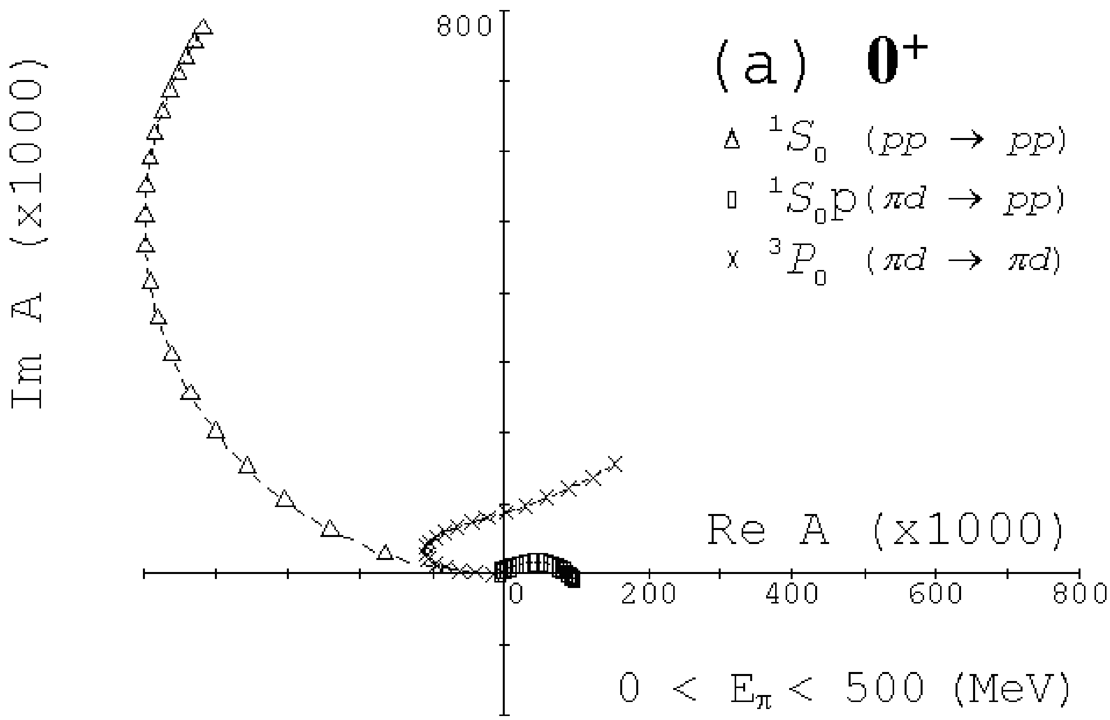

Figure 9. Argand plots of the dominant partial wave amplitudes in each system from T_p = 0 to 500 MeV: (a) 0^+, (b) 1^+, (c) 1^-, (d) 2^+, (e) 2^-, (f) 3^+, (g) 3^-, (h) 4^+, (i) 4^-, (j) 5^+ and (k) 5^-. Each plot for $pp \to pp$ is marked as '△', $\pi d \to pp$ is marked as '□', and $\pi d \to \pi d$ is marked as '×'. The marked points denote 25MeV steps. All amplitudes have been multiplied by a factor of 10^3. All amplitudes are dimensionless.

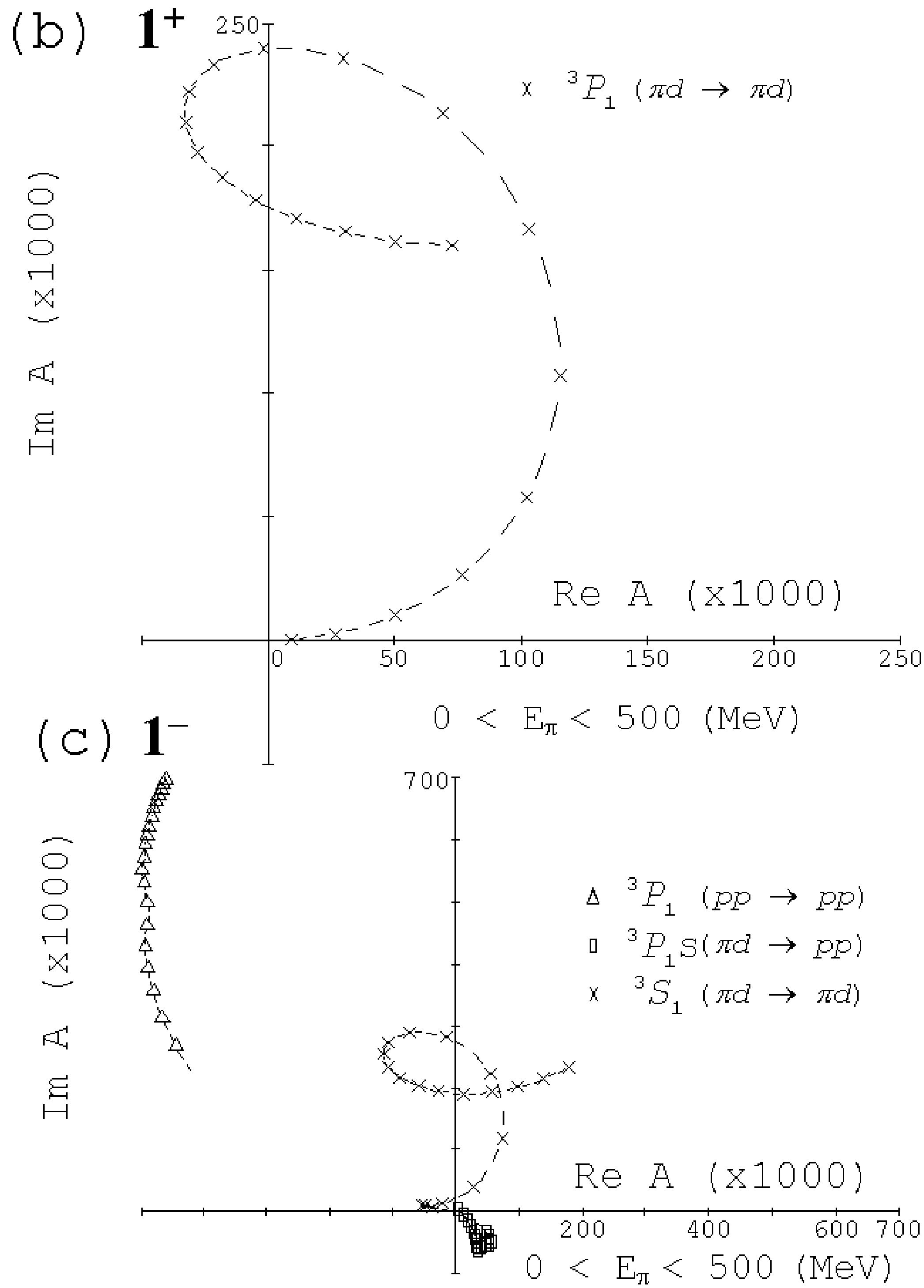

Figure 9. Continued (Argand plots)

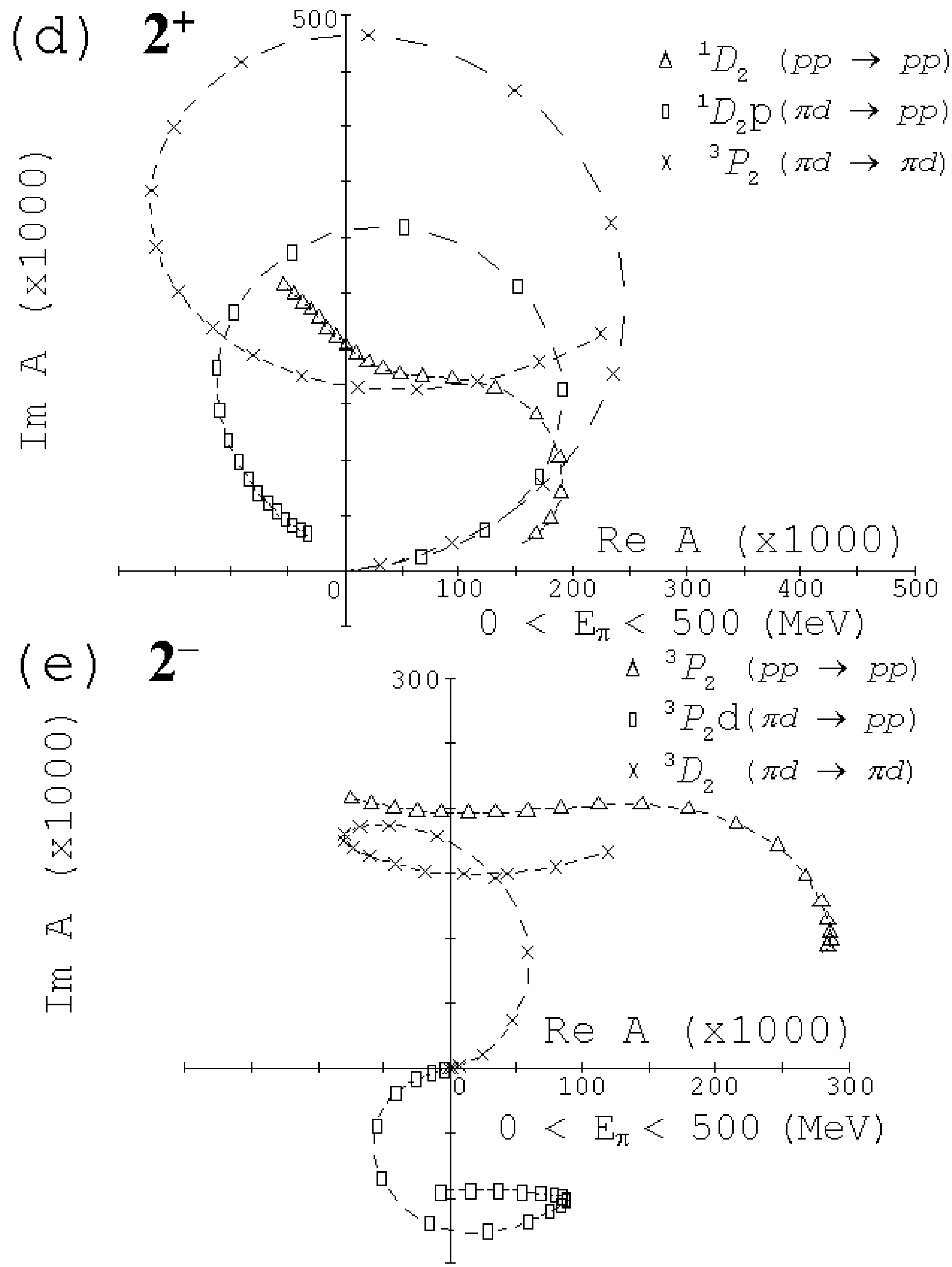

Figure 9. Continued (Argand plots)

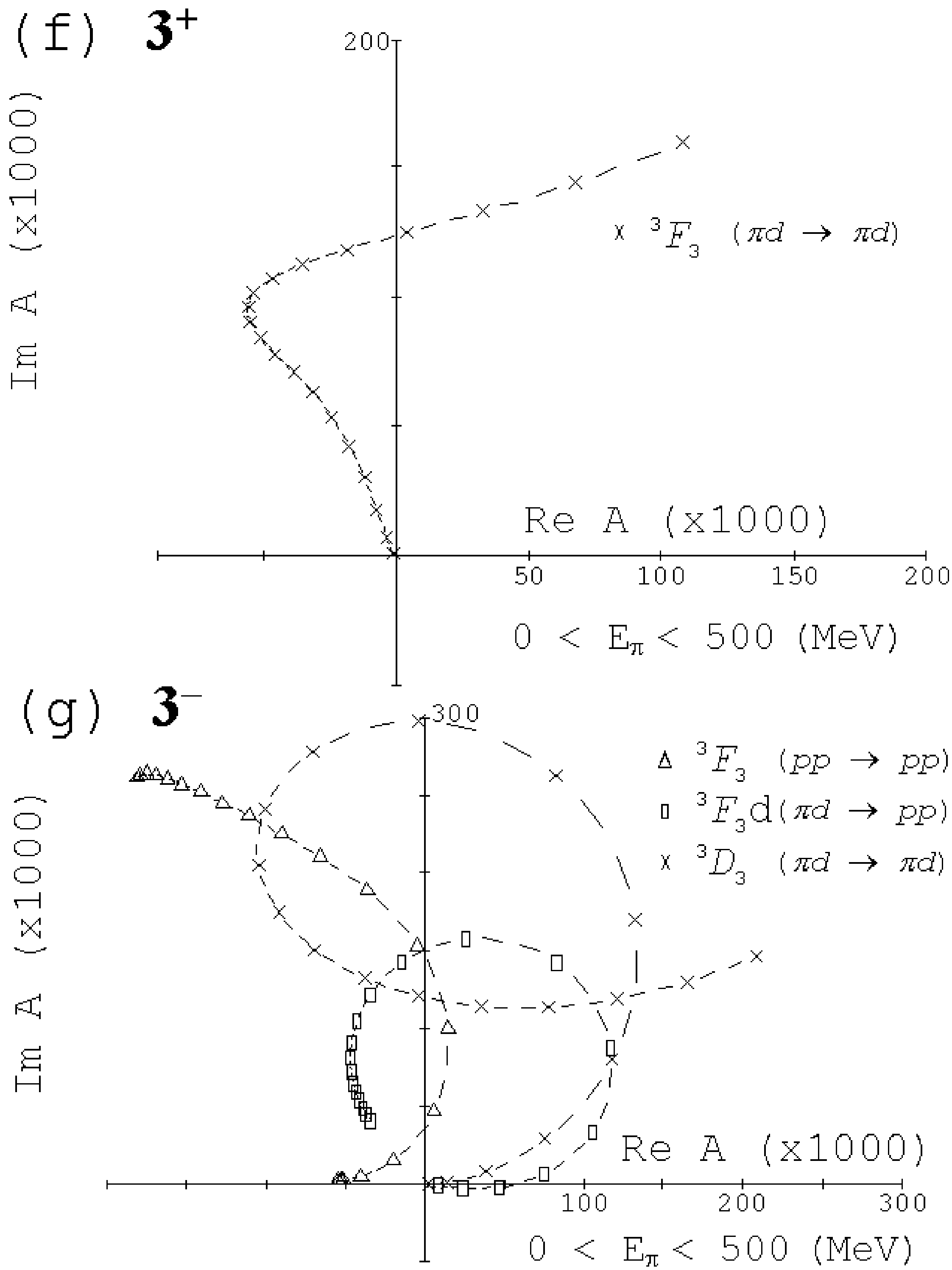

Figure 9. Continued (Argand plots)

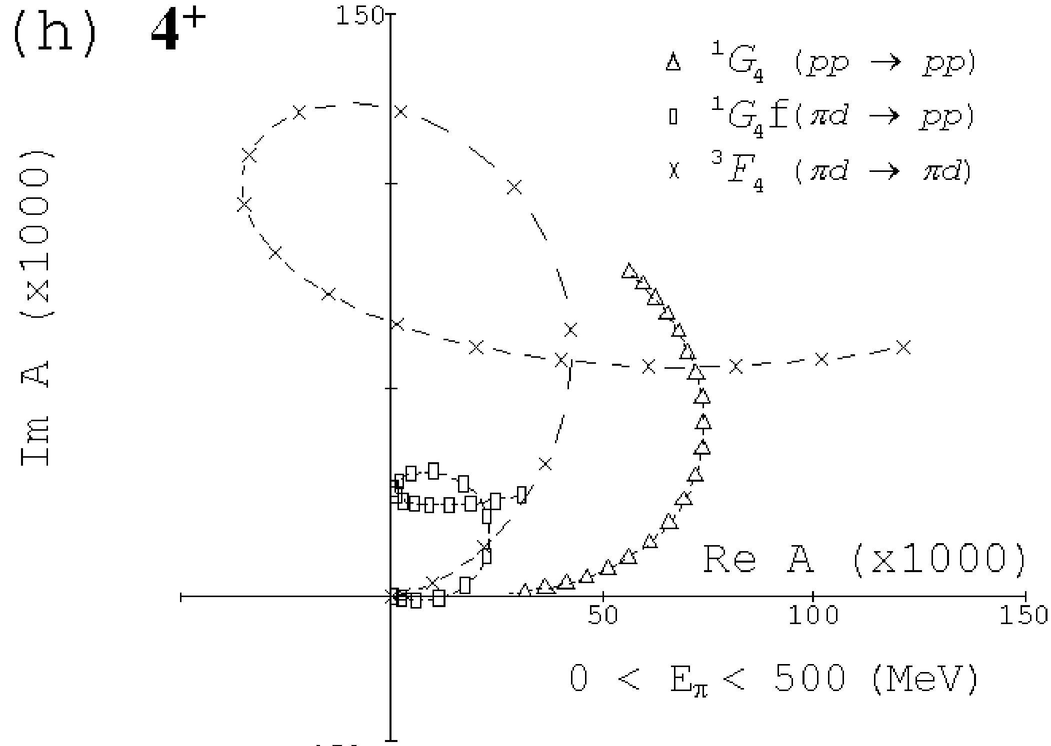

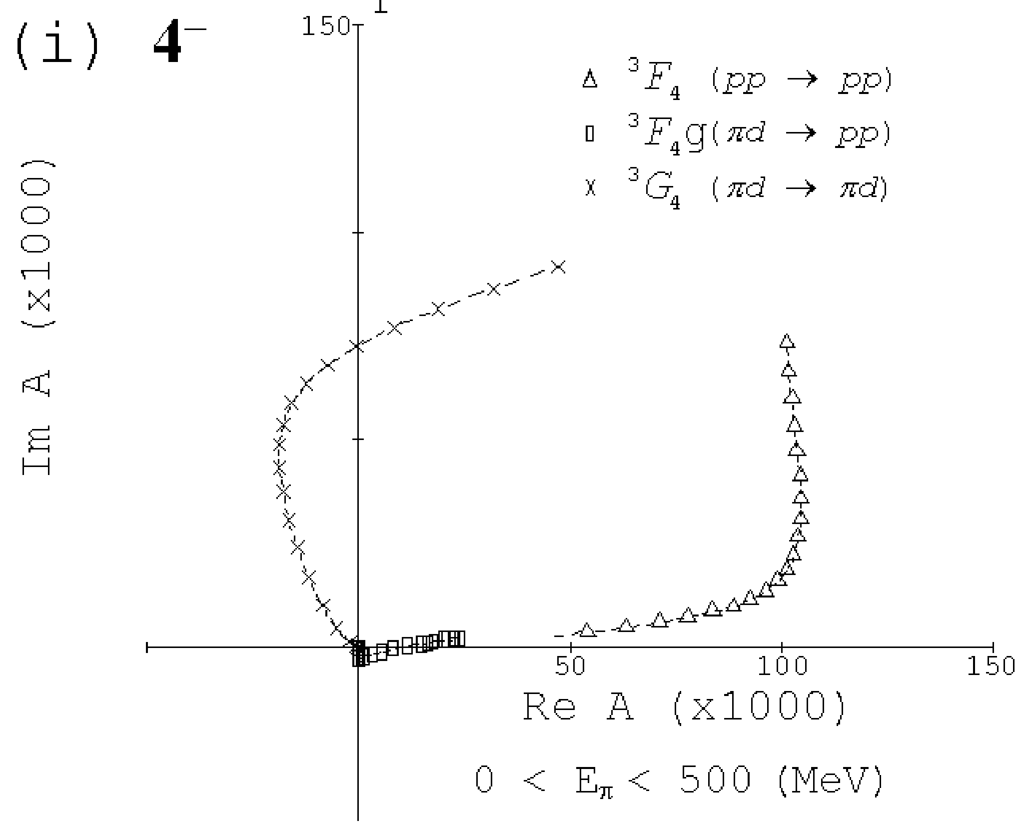

Figure 9. Continued (Argand plots)

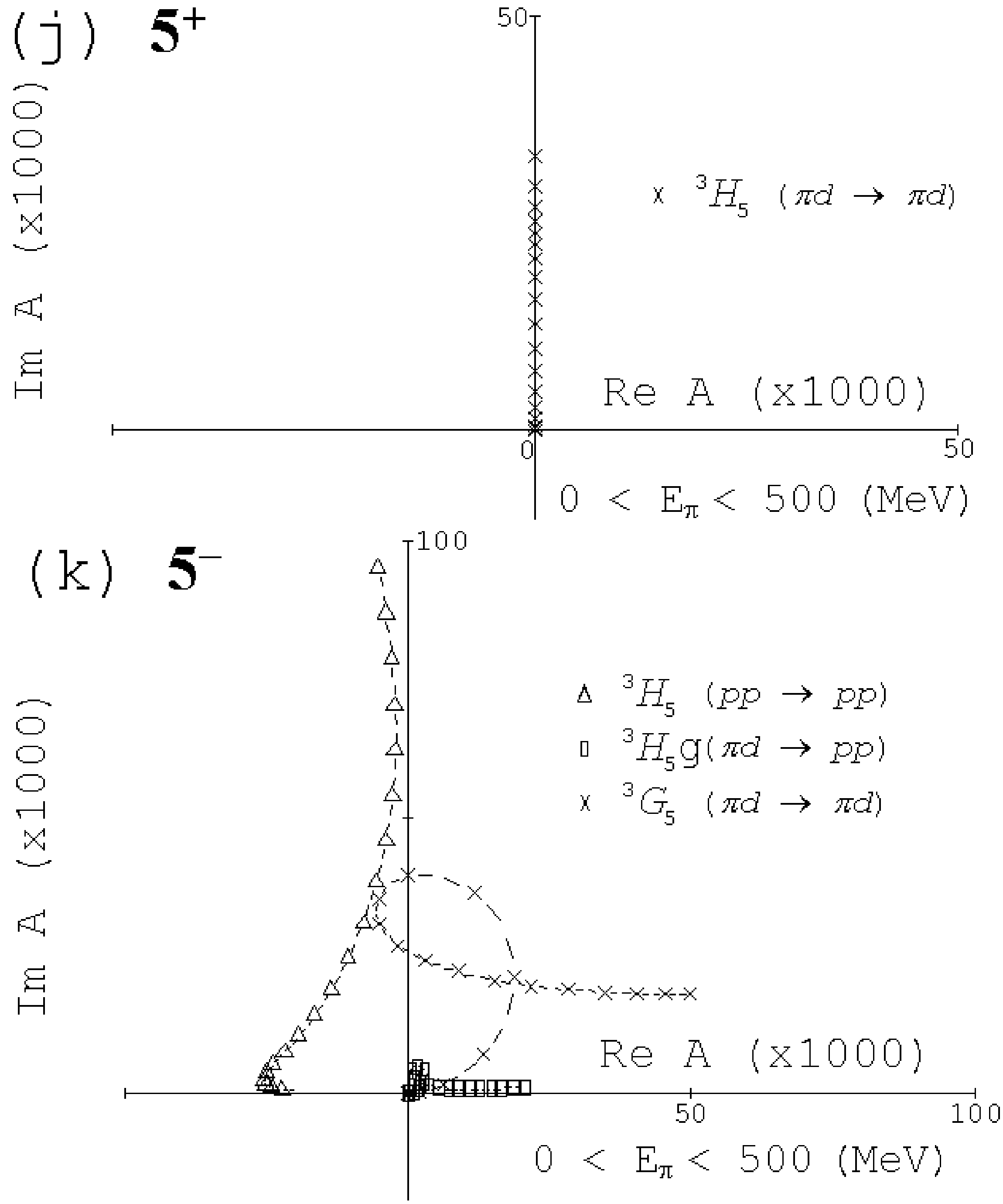

Figure 9. Continued (Argand plots)

In the present analysis, we fit the data of the elastic $\mathrm{p}d$ and $\mathrm{p}d \rightarrow pp$ reactions based on the elastic pp amplitudes that contains poles. Most systems show clear resonance-like behaviors except 0^+, 3^+, 4^-, and 5^+ system. This implies the elastic $\mathrm{p}d$ and $\mathrm{p}d \rightarrow pp$ reactions actually contain poles. There appear to be dibaryon resonances in these two baryon systems.

Predictions for observables are presented in Figure 10. Figure 10-1 presents the predictions for observables of the elastic $\mathrm{p}d$ reaction. (a) is at T_{p} = 256 MeV and (b) is at T_{p} = 180 MeV. Figure 10-2 presents the predictions for observables of the $\mathrm{p}d \rightarrow pp$ reaction. (a) is at T_{p} = 143 MeV and (b) is at T_{p} = 180 MeV. In Figure 10-2, $d\mathrm{s}/d\Omega$, A_{xx}, A_{yy}, A_{zz}, T_{20}, and T_{22} are symmetric about 90°. iT_{11}, T_{21}, and K_{yy} are antisymmetric about 90°. Solid (dashed) curves give the predictions from the unified (separate) analysis. Data have been normalized.

Predictions for observables of the elastic $\mathrm{p}d$ reaction show there are also rapid phase changes around 90°. There is a very different angular dependence in the separate and unified analyses, as can be seen in Figure 10-1. This is particularly true near 60° and 120°. The differential cross section and iT_{11} are exceptions. There is a sharp cutoff in the data base below about 60° as shown in Figure 3-2. For larger angle, around 120°, both solutions agree within error bars.

Predictions for observables of the $\mathrm{p}d \rightarrow pp$ reaction show there are also rapid phase changes around 90°. The predictions for observables in the $\mathrm{p}d \rightarrow pp$ reaction are similar in both the unified and separate analyses, apart from iT_{11}.

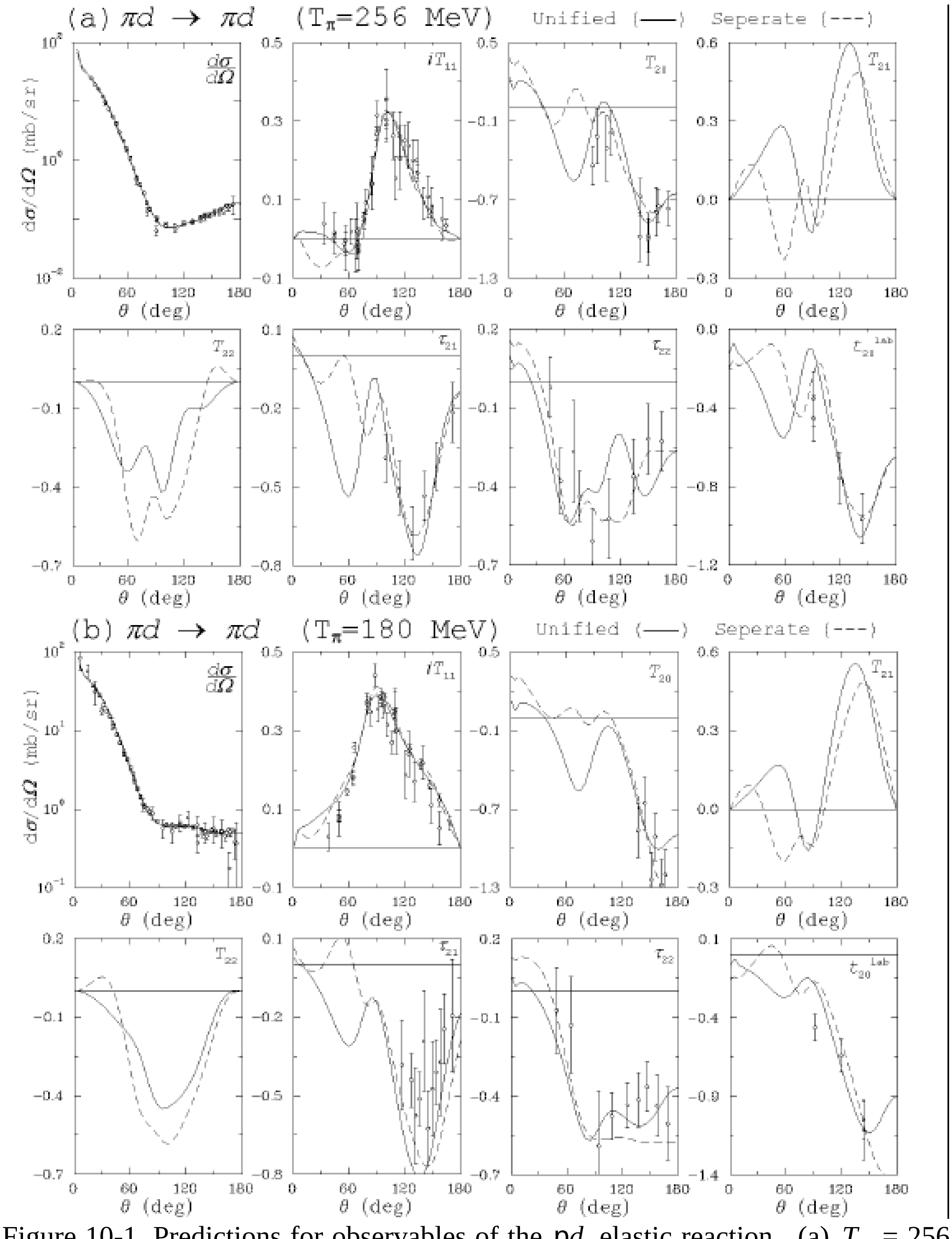

Figure 10-1. Predictions for observables of the pd elastic reaction. (a) T_p = 256 MeV and (b) T_p = 180 MeV. Solid (dashed) curves give the predictions from the unified (separate) analysis. Data have been normalized.

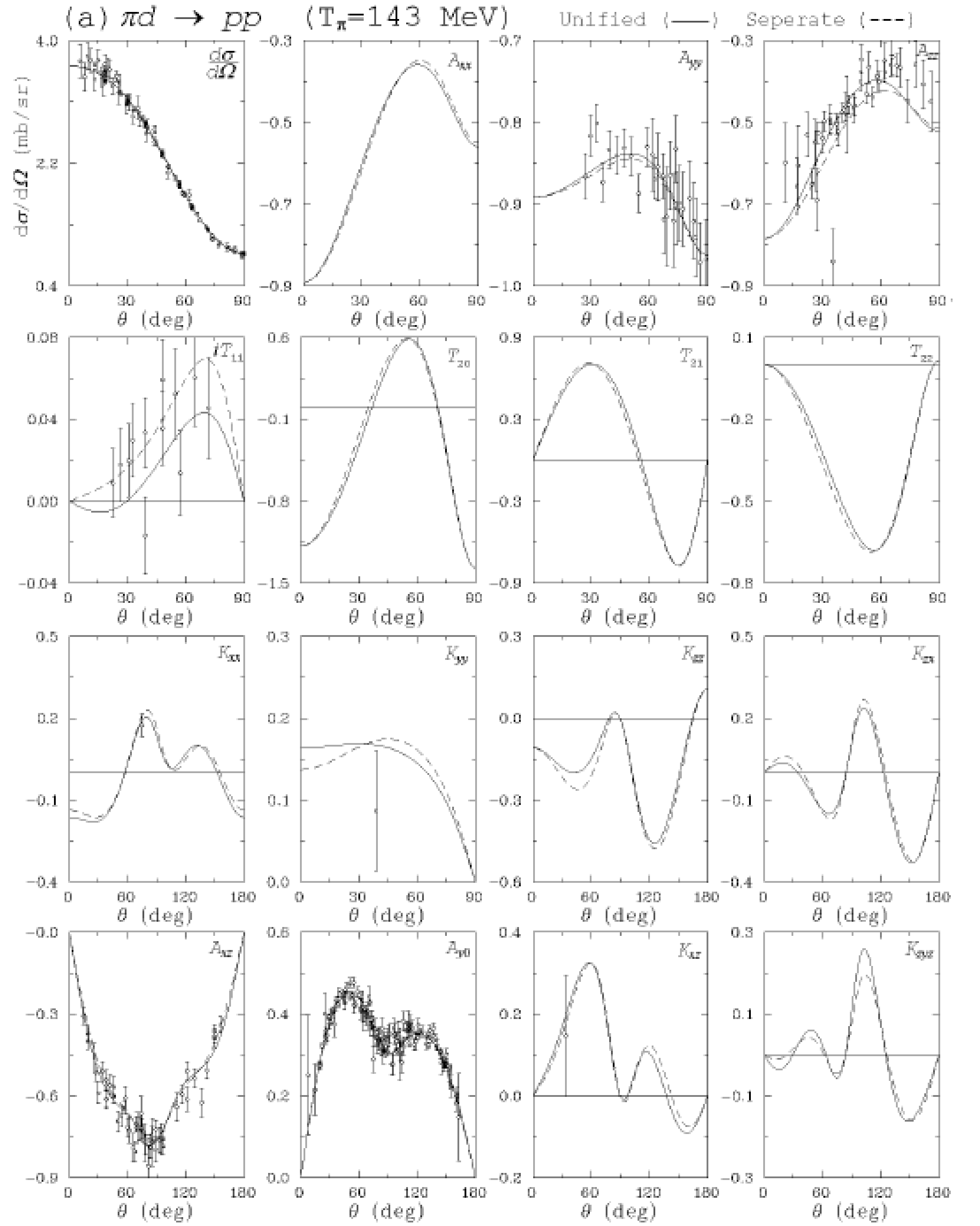

Figure 10-2. Predictions for observables of the p$d \rightarrow pp$ reaction. (a) T_p = 143 MeV and (b) T_p = 180 MeV. Solid (dashed) curves give the predictions from the unified (separate) analysis. Data have been normalised. $d\sigma/d\Omega$, A_{xx}, A_{yy}, A_{zz}, T_{20}, and T_{22} are symmetric about 90°. iT_{11}, T_{21}, and K_{yy} are antisymmetric about 90°.

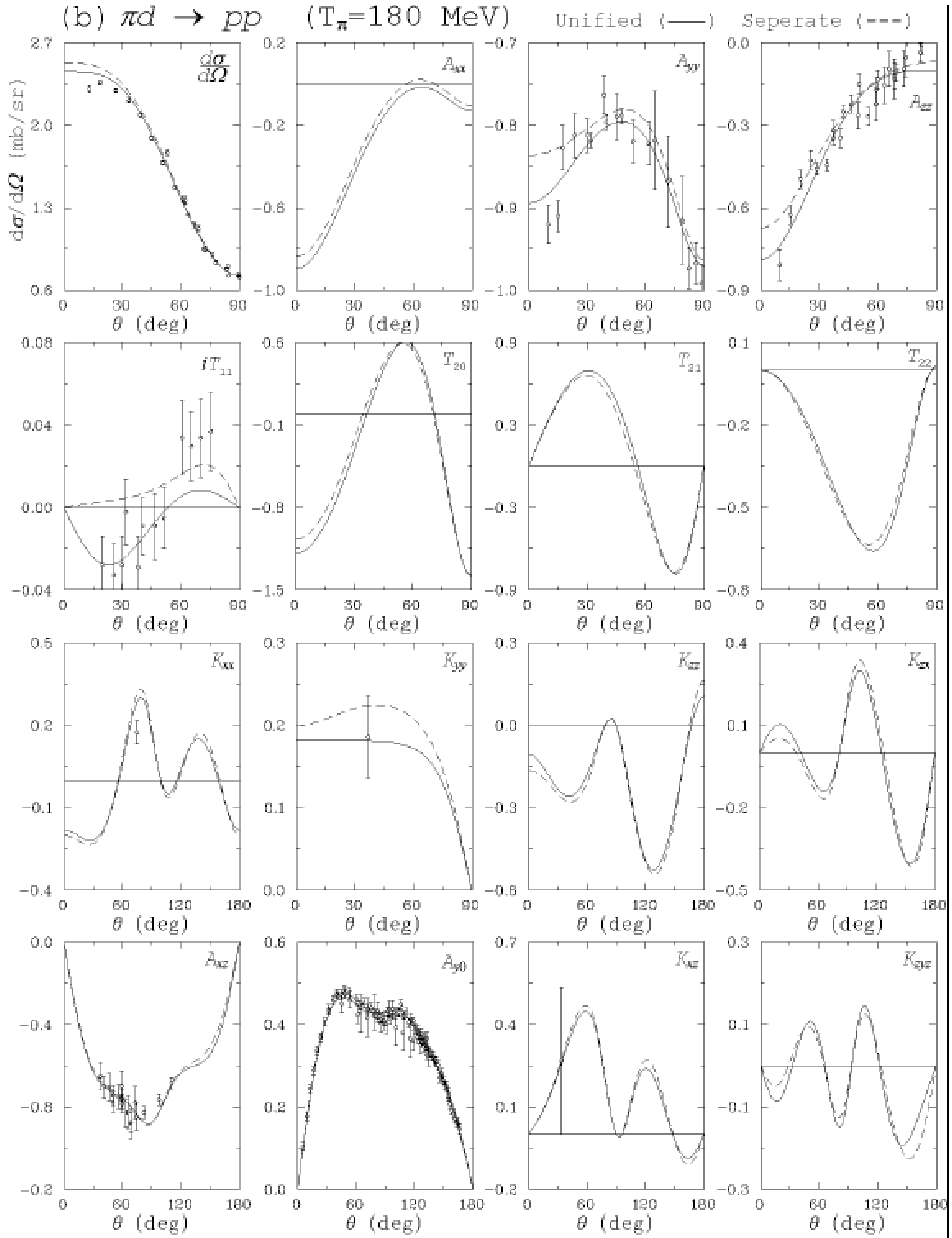

Figure 10-2. Continued (predictions for observables of the p$d \rightarrow pp$ reaction at T_{p} = 180 MeV)

Chapter 8

SUMMARY AND CONCLUSIONS

We have obtained new partial-wave amplitudes for πd elastic scattering and the reaction $\pi d \to pp$, using a *K*-matrix method which utilized information from previous VPI elastic pp scattering analysis. In addition to producing amplitudes more tightly constrained by unitarity, we have resolved the overall phase ambiguity existing in a previous analysis of $\pi d \to pp$ data alone.

As mentioned in Chapter 6, the unified analysis has resulted in a slightly improved fit to the πd elastic and $\pi d \to pp$ data bases. The most noticeable differences, at the partial-wave level, appear at higher energies where the existing data are sparse. It is difficult to find cases where the fit has been dramatically improved. One exception is the set of πd total cross section data between 300 and 500 MeV. Here the unified analysis is much more successful in reproducing the energy dependence. The unified analysis gives total cross sections which begin to rise at 500 MeV, whereas the separate analysis shows a fairly monotonic decrease from 400 to 500 MeV. The behavior seen in the unified analysis seems reasonable, as the πd total cross sections do begin to rise just beyond the upper energy limit of our analysis. Many of the individual partial-wave amplitudes from the unified solution show rising imaginary parts near 500 MeV, a feature absent in the analysis of πd elastic data alone.

The present analysis has also resulted in a unified description of the resonance-like behavior previously noted in separate analyses of pp [1] and pd [2] elastic scattering, and the reaction p$d \to pp$ [3].

We extracted poles from elastic pp analysis[47]. Since our new partial-wave amplitudes for pd elastic scattering and the reaction p$d \to pp$ are tightly constrained from elastic pp scattering by unitarity, it is a necessary condition that actual dibaryon poles exist in pd elastic scattering and in the reaction p$d \to pp$. It is clear that our predictions for the observables in elastic pd reaction show very rapid phase changes around 90° that can not be explained by the N-Δ contributions alone. Predictions for the reaction p$d \to pp$ show very similar rapid phase changes.

Resonance-like behaviors in the Argand plots suggest one should look for dibaryon poles in the 1^+, 1^-, 2^+, 2^-, 3^-, 4^+, and 5^- systems.

We expect that our unified analysis will further constrain models based on these two mechanisms - actual dibaryon resonances and N-Δ intermediate threshold effects.

Appendix A

Some Useful Kinematic Relations

In the laboratory system, consider a nuclear reaction as a general binary scattering in which a particle of mass m_1 strikes a particle of mass m_2 initially at rest and, after the collision, particles of masses m_3 and m_4 emerge. And their four momentum are p_1, p_2, p_3, and p_4, respectively.

Mandelstam's variable s of this system is

$$s = (p_1 + p_2)^2 = p_1{}^2 + 2p_1 \cdot p_2 + p_2{}^2 = m_1{}^2 + 2\left(p_1^0, \mathbf{p}_1\right) \cdot \left(p_2^0, \mathbf{p}_2\right) + m_2{}^2$$

Since a particle of mass m_2 initially at rest, $\boldsymbol{p}_2 = 0$ and $T_2 = 0$ where T is kinetic energy of the particle. So

$$s = m_1{}^2 + 2p_1^0 p_2^0 + m_2{}^2.$$

Since $p_1^0 = E_1 = T_1 + m_1$ and $p_2^0 = E_2 = m_2$,

$$s = m_1{}^2 + 2(T_1 + m_1)m_2 + m_2{}^2 = (m_1 + m_2)^2 + 2m_2 T_1.$$

Now consider the specific reaction, $pp \rightarrow \mathrm{p}d$, with $m_1 = m_2 = m_p$ and

$$s = 4m_p{}^2 + 2m_p T_p.$$

For $\mathrm{p}d \rightarrow pp$, we have $m_1 = m_\mathrm{p}$, and $m_2 = m_d$, and

$$s = (m_\mathrm{p} + m_d)^2 + 2m_d T_\mathrm{p}.$$

This leads to the relation

$$s = m_p{}^2 + 2m_p T_p = (m_\mathrm{p} + m_d)^2 + 2m_d T_\mathrm{p}.$$

The proton laboratory kinetic energy and pion laboratory kinetic energy are

$$\therefore \qquad T_p = \frac{s - 4m_p{}^2}{2m_p} \qquad \text{and} \qquad T_\pi = \frac{s - \left(m_\pi + m_d\right)^2}{2m_d}.$$

Applying $s = \left(m_\pi + m_d\right)^2 + 2m_d T_\pi$ and $m_d = m_p + m_n \approx 2m_p$, gives

$$T_p = \frac{\left(m_\pi + m_d\right)^2 + 2m_d T_\pi - m_d{}^2}{2m_p} = \frac{m_\pi\left(m_\pi + 4m_p\right)}{2m_p} + 2T_\pi .$$

Using m_p = 938.2723 MeV, m_π = 139.5679 MeV, and m_d = 1875.6134 MeV,

$$\frac{m_\pi\left(m_\pi + 4m_p\right)}{2m_p} \approx 290 \text{ MeV}.$$

$$\therefore \qquad T_p = 2T_\pi + 290\text{MeV}$$

In the center of mass system of the above reaction, $\boldsymbol{p}_1 = -\,\boldsymbol{p}_2$.

Mandelstam's variable *s* evaluated in the center-of-mass system is

$$s = (p_1 + p_2)^2 = \left(p_1^0 + p_2^0\right)^2 + \left(\boldsymbol{p}_1 + \boldsymbol{p}_2\right)^2 = \left(p_1^0 + p_2^0\right)^2$$

$s = \left(E_1 + E_2\right)^2 = W^2$, where *W* is total center of mass energy.

$$\therefore \qquad W = \sqrt{s}$$

The relation between center of mass momentum $\boldsymbol{q}$ **(=** $\boldsymbol{p}_1 = -\,\boldsymbol{p}_2$) and *s* is the following;

From $s = \left(E_1 + E_2\right)^2$ and $E_1 = \sqrt{\boldsymbol{q} + m_1{}^2}$ or $\boldsymbol{q}^2 = E_1{}^2 - m_1{}^2 = E_2{}^2 - m_2{}^2$.

$$E_1 = \frac{s + m_1{}^2 - m_2{}^2}{2\sqrt{s}} \qquad \text{and} \qquad E_2 = \frac{s - m_1{}^2 + m_2{}^2}{2\sqrt{s}}.$$

So the relation between center of mass momentum $\boldsymbol{q}$ and *s* is

$$\boldsymbol{q}^2 = E_1{}^2 - m_1{}^2 = \frac{\left\{s - \left(m_1 + m_2\right)^2\right\}\left\{s - \left(m_1 - m_2\right)^2\right\}}{4s}.$$

Appendix B

Partial Wave Decomposition for Three Reactions

The proton is a spin half ($s = 1/2$) particle. Elastic *pp* scattering can occur with total spin singlet ($S = 0$) or triplet ($S = 1$) states. This leads to five basic angular momentum states to describe the elastic *pp* system. :

for spin singlet,	$S = 0$	$L = J$
for spin triplet,	$S = 1$	$L = J$
		$L = J \pm 1$

and there is spin mixture state ε of two spin flipped states for $L = J + 1$ and $L = J - 1$. Here, L is the orbital angular momentum and J is the total angular momentum.

Another important restriction for the elastic *pp* reaction is parity (P) conservation. Elastic *pp* scattering occurs between two identical particles.

The Pauli principle requires the overall wave function to be odd under exchange of identical particles. That is $P_r P_\sigma P_\tau = -1$, where P_r is the space exchange operator which interchanges two particles. P_σ and P_τ are $P_\sigma = \frac{1}{2}\left(1 + \vec{\sigma}_1 \cdot \vec{\sigma}_2\right)$ and $P_\tau = \frac{1}{2}\left(1 + \vec{\tau}_1 \cdot \vec{\tau}_2\right)$, respectively, the exchange operators for spin and isospin for each particles[13]. So only spin singlet (odd under exchange) even angular momentum states (even under exchange) or spin triplet (even under exchange) odd angular momentum states (odd under exchange) can be present for the elastic pp system.

Possible partial wave states for elastic pp system are given in below, using the notation $^{2S+1}L_J$, where S is the total spin and J is the total angular momentum of the system.

For the spin singlet state ($S = 0$), the elastic pp reaction occurs only with even angular momentum states. So the possible partial wave states are $2S + 1 = 1$ and $L = J =$ even :

$$^1S_0,\ ^1D_2,\ ^1G_4,\ ^1I_6,\ \ldots$$

For the spin triplet state ($S = 1$), the elastic pp reaction occurs only with odd angular momentum states. So the possible partial wave states are $2S + 1 = 3$, $L = J =$ odd ;

$$^3P_1,\ ^3F_3,\ ^3H_5,\ \ldots \qquad ;$$

or $2S + 1 = 3$, $L = J \pm 1$, and L has odd values :

$$\begin{array}{lll}
L = 1 : L = J - 1 = 1 \rightarrow & J = 2 & ^3P_2,\ e_2, \\
 L = J + 1 = 1 \rightarrow & J = 0 & ^3P_0, \\
L = 3 : L = J - 1 = 3 \rightarrow & J = 4 & ^3F_4,\ e_4, \\
 L = J + 1 = 3 \rightarrow & J = 2 & ^3F_2,\ e_2, \\
L = 5 : L = J - 1 = 5 \rightarrow & J = 6 & ^3H_6,\ e_6, \\
 L = J + 1 = 5 \rightarrow & J = 4 & ^3H_4,\ e_4, \\
\ldots & &
\end{array}$$

Since there is no $L = J - 1$ state for $J = 0$, e_0 cannot occur.

Spin coupled states will be

$$^3P_2,\ e_2,\ ^3F_2 \qquad ^3F_4,\ e_4,\ ^3H_4 \qquad ^3H_6,\ e_6,\ ^3J_6 \qquad \ldots$$

Parity conservation implies there is no transition between the different parity states. The total angular momentum(J) of the system is a good quantum number and it is convenient to describe possible partial waves in terms of the invariant variable J, because there is no transition between states of different J either. Spin triplet states of possible partial waves in elastic pp reaction in terms of J are follows:

$J = 0$: $^3P_0$

$J = 2$: $^3P_2$, e_2, $^3F_2$

$J = 4$: $^3F_4$, e_4, $^3H_4$

…

Possible partial wave decompositions for the pp elastic system are given in Table A-1.

The pion (p) is a spinless (s = 0) particle and the deuteron is a spin one (s = 1) particle. The total spin of the pd elastic system is one (S = 1) and only spin triplet states are available. Four basic angular momentum states are required to describe the pd elastic system. Details of possible partial wave decompositions for the pd elastic system are given in Table A-2.

Table A-1. Possible partial wave decompositions for the *pp* elastic system. State symbol is described by f_{JL}. J is total angular momentum of the system and L is orbital angular momentum. f_J is spin singlet state. f_{JJ} is spin triplet with $J = L$. f_{JJ-1} is spin triplet with $J = L + 1$. e_J is spin flipped mixture state of $J = L + 1$ and $J = L - 1$ state. $f_{J\,J+1}$ is spin triplet with $J = L - 1$.

States	$J = 0$	$J = 1$	$J = 2$	$J = 3$	$J = 4$	$J = 5$	$J = 6$
f_J	$^1S_0$	-	$^1D_2$	-	$^1G_4$	-	$^1I_6$
f_{JJ}	-	$^3P_1$	-	$^3F_3$	-	$^3H_5$	-
f_{JJ-1}	-	-	$^3P_2$	-	$^3F_4$	-	$^3H_6$
e_J	-	-	e_2	-	e_4	-	e_6
$f_{J\,J+1}$	$^3P_0$	-	$^3F_2$	-	$^3H_4$	-	$^3J_6$

Table A-2. Partial wave decompositions for the p*d* elastic system. Symbols are equivalent to those used in Table A-1. For the p*d* elastic system, there is no spin singlet system (no f_J state).

States	$J = 0$	$J = 1$	$J = 2$	$J = 3$	$J = 4$	$J = 5$
f_{JJ}	(x)	$^3P_1$	$^3D_2$	$^3F_3$	$^3G_4$	$^3H_5$
f_{JJ-1}	(x)	$^3S_1$	$^3P_2$	$^3D_3$	$^3F_4$	$^3G_5$
e_J	(x)	e_1	e_2	e_3	e_4	e_5
$f_{J\,J+1}$	$^3P_0$	$^3D_1$	$^3F_2$	$^3G_3$	$^3H_4$	$^3I_5$

For the $\mathrm{p}d \to pp$ reaction, the $\mathrm{p}d$ states are spin triplet only and pp states are spin singlet, even angular momentum states, or spin triplet, odd angular momentum states. This allows six possible transitions between the two system. Since $\mathrm{p}d \to pp$ is an inelastic reaction, we need to consider the intrinsic parity for initial and final states. The intrinsic parity of proton is even (+1), this gives even intrinsic parity (+1) for the pp system. Intrinsic parity of pion is odd (–1) and that of deuteron is even (+1), this gives odd intrinsic parity (–1) for the $\mathrm{p}d$ system.

To maintain the parity conservation, the inelastic reaction must have states $\Delta L = \pm 1$. Details of possible partial wave decompositions for the $\mathrm{p}d \to pp$ system is given in Table A-3. States are denoted from pp partial waves to $\mathrm{p}d$ partial waves. Partial wave notations are ${}^{2S+1}L_J l$ where S is the total spin, J is the total angular momentum, L is the angular momentum of the pp state, and l is the angular momentum of the $\mathrm{p}d$ state.

Table A-3. Details of possible partial waves for the $\mathrm{p}\,d \to pp$ system. By time reverse, $pp \to \mathrm{p}\,d$ is identical with $\mathrm{p}\,d \to pp$. Symbols that follow have pp initial state to $\mathrm{p}d$ final state.

$f_J \to f_{J\,J-1}$	$f_J \to f_{J\,J+1}$	$f_{J\,J} \to f_{J\,J-1}$	$f_{J\,J} \to f_{J\,J+1}$	$f_{J\,J-1} \to f_{J\,J}$	$f_{J\,J+1} \to f_{J\,J}$
-	${}^1S_0 p$	${}^3P_1 s$	${}^3P_1 d$	-	-
${}^1D_2 p$	${}^1D_2 f$	${}^3F_3 d$	${}^3F_3 g$	${}^3P_2 d$	${}^3F_2 d$
${}^1G_4 f$	${}^1G_4 h$	${}^3H_5 g$	${}^3H_5 i$	${}^3F_4 g$	${}^3H_4 g$
${}^1I_6 h$	${}^1I_6 j$	${}^3J_7 i$	${}^3J_7 k$	${}^3H_6 i$	${}^3J_6 i$

The Δ has isospin $3/2$ and the nucleon has isospin $1/2$, the total isospin of the $N\Delta$ system is one or two. Since the two nucleon system has total isospin 1 or zero and the πd system has total isospin 1, only the $N\Delta$ channels with total isospin 1 will couple the two proton system to the πd system. On the other hand, the nucleon has spin $1/2$ and the delta has spin $3/2$, so $N\Delta$ channels with total spin two or one are possibly coupled to the two proton system and the πd system with appropriate angular momentum. From the nucleon, there are two possible helicity states and from the delta, there are four possible helicity states. For a combined nucleon-delta system, there are eight possible helicity states.

For total spin one states, $2S + 1 = 3$, the possible partial wave states of the $N\Delta$ are follows;

For $L = J$; $({}^3S_0)$, ${}^3P_1$, ${}^3D_2$, ${}^3F_3$, ${}^3G_4$, ${}^3H_5$, … ;

For $L = J + 1$; ${}^3P_0$, ${}^3D_1$, ${}^3F_2$, ${}^3G_3$, ${}^3H_4$, … ;

For $L = J - 1$; ${}^3S_1$, ${}^3P_2$, ${}^3D_3$, ${}^3F_4$, ${}^3G_5$, ${}^3H_6$, … ;

For total spin two states, $2S + 1 = 5$, the possible partial wave states of the $N\Delta$ are follows;

For $L = J$; $({}^5S_0)$, ${}^5P_1$, ${}^5D_2$, ${}^5F_3$, ${}^5G_4$, ${}^5H_5$, … ;

For $L = J + 1$; $({}^5P_0)$, ${}^5D_1$, ${}^5F_2$, ${}^5G_3$, ${}^5H_4$, … ;

For $L = J - 1$; $({}^5S_1)$, ${}^5P_2$, ${}^5D_3$, ${}^5F_4$, ${}^5G_5$, ${}^5H_6$, … ;

For $L = J + 2$; ${}^5D_0$, ${}^5F_1$, ${}^5G_2$, ${}^5H_3$, … ;

For $L = J - 2$; ${}^5S_2$, ${}^5P_3$, ${}^5D_4$, ${}^5F_6$, ${}^5G_7$, ${}^5H_8$, …

Here, $^5S_0$, $^5P_0$, and $^5S_1$ partial wave states are not allowed to couple to the two proton system. As mentioned, in the pp partial wave decomposition, the pp system requires an overall anti-symmetric wave function under exchange of identical particles. Possible partial waves for the $N\Delta$ system are summarized in Table A-4.

Table A-4. Partial wave decompositions for the $N\Delta$ system. Symbols are equivalent to those used in Table A-1. For the $N\Delta$ system, there is no spin singlet system (no f_J state).

Spin	States	$J = 0$	$J = 1$	$J = 2$	$J = 3$	$J = 4$	$J = 5$
$S = 1$	f_{JJ}	-	$^3P_1$	$^3D_2$	$^3F_3$	$^3G_4$	$^3H_5$
	f_{JJ+1}	$^3P_0$	$^3D_1$	$^3F_2$	$^3G_3$	$^3H_4$	$^3I_5$
	f_{JJ-1}	-	$^3S_1$	$^3P_2$	$^3D_3$	$^3F_4$	$^3G_5$
$S = 2$	f_{JJ}	-	$^5P_1$	$^5D_2$	$^5F_3$	$^5G_4$	$^5H_5$
	f_{JJ+1}	-	$^5D_1$	$^5F_2$	$^5G_3$	$^5H_4$	$^5I_5$
	f_{JJ-1}	-	-	$^5P_2$	$^5D_3$	$^5F_4$	$^5G_5$
	f_{JJ+2}	$^5D_0$	$^5F_1$	$^5G_2$	$^5H_4$	$^5I_5$	$^5J_6$
	f_{JJ-2}	$^5S_2$	$^5P_3$	$^5D_4$	$^5F_6$	$^5G_7$	$^5H_8$

Appendix C

Observables for the Elastic *pp* Reaction

Since the proton is a spin $1/2$ particle, the observables depend upon its polarization. Summary of the observables for the elastic pp reaction is presented in Table 2-1. In this Appendix, the dependence of observables on polarization is briefly discussed.

Four possible polarization conditions suggest 256 $(=4^4)$ possible observables in the elastic pp reaction. However, depending on conservation laws and the Pauli principle, the actual number of observables is reduced. A general descriptions of these observables follows[16].

For the unpolarized case (unpolarized beam and unpolarized target), the obsevables are: differential cross section ($ds/d\Omega$), total cross section (s_T), or elastic total cross section (s_T^{el}). In this case, directions are denoted as (0000), where we label the directions of four particles ($\boldsymbol{p_1}'$, $\boldsymbol{p_2}'$, $\boldsymbol{p_1}$, $\boldsymbol{p_2}$), respectively, scattered, recoiled, incident, and target particles. For example, the differential cross section ($ds/d\Omega$, I_0) is

$$(0, 0; 0, 0) = I_0 = \frac{1}{4}\mathrm{Tr}MM^* = \frac{1}{q^2}\left\{\sum_i |H_i|^2 + |H_4|^2\right\},$$

where q is the center-of-mass momentum of incident proton and M is scattering matrix. The scattering angle θ is considered 0 for the total cross section (σ_T) because of the optical theorem

$$\sigma_T = \frac{4\pi}{q} \operatorname{Im} f(0) .$$

If only one particle is polarized, there are 12 possible measurements. There are 6 possible 'Polarization'(P) measurements for one final state particle which is

$$(X,0\ ;\ 0,0) \text{ or } (0,X\ ;\ 0,0) \equiv I_0 P_X .$$

Also there are 6 possible 'Asymmetry'(A) measurements of one initial state particle (either the initial beam or the initial target) which is

$$(0,0\ ;\ X,0) \text{ or } (0,0\ ;\ 0,X) \equiv I_0 A_X .$$

Depending on the coordinate system and particles, notations of particle directions are as follows. In the laboratory system, take the z-axis($\mathbf{q}$) for the incident beam ($\boldsymbol{p}_1$) direction, then $\mathbf{q}'$ will be the direction of scattered particle ($\boldsymbol{p}_1'$) and $\mathbf{q}''$ will be the direction of recoiled particle ($\boldsymbol{p}_2'$). In the center-of-mass system take normalized directions such as

$$\mathbf{n} = \frac{\mathbf{q}_i \times \mathbf{q}_f}{|\mathbf{q}_i \times \mathbf{q}_f|} \qquad \text{(y-axis : axial vector),}$$

$$\mathbf{l} = \frac{\mathbf{q}_i + \mathbf{q}_f}{|\mathbf{q}_i + \mathbf{q}_f|} \qquad \mathbf{m} = \frac{\mathbf{q}_i - \mathbf{q}_f}{|\mathbf{q}_i - \mathbf{q}_f|} \qquad \text{(polar vector).}$$

Here, $\mathbf{q}_i$ ($\mathbf{q}_f$) is a unit vector in the direction of the incident (scattered) particle momenta in the center-of-mass system. Since $\mathbf{q}_i$ is taken as the z-axis, $\mathbf{n}$ is the norm of the y-axis. Other useful directions are the cross product of $\mathbf{n}$ with the norm of laboratory system. They are

$\mathbf{s} = \mathbf{n} \times \mathbf{q}$ (x-axis : axial vector),

$\mathbf{s}' = \mathbf{n} \times \mathbf{q}'$ $\mathbf{s}'' = \mathbf{n} \times \mathbf{q}''$ (polar vector).

Here, $\mathbf{s}$ is the vector along the x-axis.

Because of parity conservation and time reversal, only the **n** direction is non-zero and asymmetry measurements are identical with the corresponding polarization measurements. For elastic pp scattering, two final state particles are identical. So all possible measurements with one polarized particle are identical. In SAID, all the measurements of the one polarized particle case are denoted as **P**.

When two final state particles are polarized, and the incident beam and target are unpolarized, then measurement yields the correlation of the two final state spin directions.

$$(X,Y\,;\,0,0) \equiv I_0 C_{XY}$$

For this state condition, symbol C for "Polarization Correlation" is used in Table 2-1. There are nine possible spin correlated measurements. However, only C_{NN}, C_{PP}, C_{KK}, $C_{KP} = C_{PK}$ are non-zero because of the form of the scattering matrix and only C_{NN} and C_{KP} have been measured. Here, direction symbols are labeled N for **n** (y direction), K for **l**, and P for **m**. For the C_{NN} measurement, we have used a notation A_{yy} (nn00) because this is actually y-direction.

When two initial state particles (beam and target) are polarized, and if the final state polarization is not measured, then

$$(0,0\,;\,X,Y) \equiv I_0 A_{XY}\,.$$

For this state condition, the symbol A for "Asymmetry in Cross Section" is used in Table 2-1. There are nine possible doubly polarized cross-sections and these are time-reversed counterparts of the spin correlation measurements. A_{xx} (00ss), A_{zz}

(00kk), and A_{zx} (–(00sk)) are measured observables and available in SAID. Here, s labels for **s** (x-direction), k labels for z-direction, and For A_{zx}, '–' sign is used to describe the negative direction of A_{xz} (00sk).

If one particle of initial state and one particle of final state are polarized, then either an initial polarized beam or a polarized target, and the polarization of one of the final particles, are measured.

$$(X,0\ ;\ Y,0) \text{ or } (0,X\ ;\ Y,0) \text{ or } (X,0\ ;\ 0,Y) \text{ or } (0,X\ ;\ 0,Y) \equiv T_{XY}^{(12)}$$

There are 36 (= $3\times 3\times 4$) possible measurements for this case. Because of the characteristics of scattering matrix, only 9 measurements are non-zero. There are six possible measurements which are those involving two *N*'s, two *K*'s, and two *P*'s such as

$$(X,0\ ;\ Y,0) = (0,X\ ;\ Y,0),\ (X,0\ ;\ 0,Y) = (0,X\ ;\ 0,Y).$$

AT (–(0s″k0)), **DT** (0nn0), and **RT** (0s″s0) are measured observables and available in SAID. Another three possible measurements are a *K* and a *P* in each of the four groups such as

$$(0,P\ ;\ 0,K) = (0,K\ ;\ 0,P),\quad (P,0\ ;\ 0,K) = (K,0\ ;\ 0,P), \text{ etc.}$$

For these states, symbol *K* for "Polarization Transfer" is used in Table 2-1. Only **D0SK** (0s″0k) where '*D*' means "Depolarization Tensor" is measured and available in SAID.

For experimental reasons, five linear combinations of the above five non-zero quantities are used. These combinations are (for elastic pp reaction) :

$$I_0 D^{(11)} = (N,0\ ;\ N,0),$$

$$I_0 R^{(11)} = (K,0\ ;\ K,0)\cos\theta/2 + (K,0\ ;\ P,0)\sin\theta/2,$$

$$I_0 A^{(11)} = (K,0\ ;\ P,0)\cos\theta/2 - (K,0\ ;\ K,0)\sin\theta/2,$$

$$I_0 R'^{(11)} = (P,0\ ;\ K,0)\cos\theta/2 + (P,0\ ;\ P,0)\sin\theta/2\,,$$

$$I_0 A'^{(11)} = (P,0\ ;\ P,0)\cos\theta/2 - (P,0\ ;\ K,0)\sin\theta/2\,.$$

In SAID, **D** (n0n0), **R** (s′0s0), **A** (s′0k0), **RP** (k′0s0), and **AP** (k′0k0) are available.

When three particles are polarized, there are three choices for each initial and final state. The first one is to use a polarized beam and unpolarized target, then measure the polarization of both final particles (X,Y ; W,0). There are 27 possible measurements for this case and only 13 are non-zero. The second possible measurement is to use an unpolarized beam and polarized target, then measure the polarization of both final state particles (X,Y ; 0,W). There are 27 possible measurements for this case and only 13 are non-zero. The last choice is to use a polarized beam and polarized target, then measure the polarization of one of the final state particles. There are 54 possible measurements such as (X,0 ; Y,W) or (0,X ; Y,W). These are identical with the first and the second choices by time reversal invariance. For this state condition, symbol M for "Contribution to the Polarization of Scattered Particle" is used in Table 2-1. In SAID, **NNKK** (0nkk), **NSNK** (0s″nk), and **NSKN** (0s″kn) are available measurements.

When the polarizations of the beam, target, and both final state particles are measured, there are 81 possible measurements and 41 of them are non-zero. However, except for total cross sections, no experiments have been carried out for this choice of measurement. In SAID, longitudinal polarized total cross section ($\Delta\sigma^{\mathrm{L}}_{tot}$) and transverse polarized total cross section ($\Delta\sigma^{\mathrm{T}}_{tot}$) are available measurements.

Appendix D

Unitarity and Multi-Channel Matrix Formalisms

In Chapter 3, the scattered wave ψ_{sc}, for a simple spinless particles system, is given by

$$\psi_{sc} = \frac{1}{k}\sum_{l=0}^{\infty}(2l+1)\frac{\eta_l e^{2i\delta_l}-1}{2i}P_l(\cos\theta)\frac{e^{ikr}}{r}.$$

S_l is the l^{th} component of the scattering matrix and is defined as

$$S_l = \eta_l e^{2i\delta_l}.$$

For a pure elastic system, the scattering matrix S satisfies the unitarity condition

$$\mathbf{S}^{+}\mathbf{S} = \mathbf{S}\mathbf{S}^{+} = \mathbf{1}.$$

Here, η_l = 1 for a pure elastic system and $S_l^{+} = S_l{}^{*} = e^{-2i\delta_l}$.

For a multi-channel system such as two nucleon system, there are inelastic channels as described in Figure 1. The unitarity-satisfied full S-matrix contains all the possible scattering channels, such as

$$\mathbf{S} = \begin{pmatrix} NN \to NN & NN \to N\Delta & NN \to \pi d & NN \to NN\pi & \cdots \\ N\Delta \to NN & N\Delta \to N\Delta & N\Delta \to \pi d & N\Delta \to NN\pi & \cdots \\ \pi d \to NN & \pi d \to N\Delta & \pi d \to \pi d & \pi d \to NN\pi & \cdots \\ NN\pi \to NN & NN\pi \to N\Delta & NN\pi \to \pi d & NN\pi \to NN\pi & \cdots \\ \vdots & \vdots & \vdots & \vdots & \ddots \end{pmatrix}.$$

From the definition of partial wave amplitude

$$f_l = T_l = \frac{\eta_l e^{2i\delta_l} - 1}{2i},$$

the multi-channel *T*-matrix is defined as

$$\mathbf{S} = 1 + 2i\mathbf{T}.$$

If the *S*-matrix satisfies unitarity, the *T*-matrix satisfies

$$\mathrm{Im}\, T_{\alpha\alpha} = \sum_{\gamma} \left| T_{\gamma\alpha} \right|^2 \geq 0 \qquad \text{or} \qquad \mathrm{Im}\, T_{\alpha\alpha} - \sum_{\gamma} \left| T_{\gamma\alpha} \right|^2 = 0,$$

or in matrix form,

$$\mathrm{Im}\mathbf{T} = \mathbf{T}^{+}\mathbf{T} \qquad \text{or} \qquad \mathbf{T}^{+} - \mathbf{T} = 2i\mathbf{T}^{+}\mathbf{T}.$$

Another convenient matrix formalism for a multi-channel system is the *K*-matrix which is defined as

$$\mathbf{S} = \left(1 + i\mathbf{K}\right)\left(1 - i\mathbf{K}\right)^{-1}.$$

Relations between the *T*-matrix and the *K*-matrix are

$$\mathbf{T} = \mathbf{K}\left(1 - i\mathbf{K}\right)^{-1} \qquad \text{or} \qquad \mathbf{K} = \mathbf{T}\left(1 + i\mathbf{T}\right)^{-1}.$$

If the *S*-matrix satisfies unitarity, the *K*-matrix is real. Due to time reversal, the *K*-matrix is symmetric.

Generally, from pion threshold energy (290 MeV of proton laboratory kinetic energy T_p) to 1290 MeV of T_p, which is 500 MeV of T_π (pion laboratory kinetic energy), $N\Delta$ is the dominant channel. If we assume that the $N\Delta$ channel accounts for all unmeasured scattering, then we have the following real symmetric *K*-matrix that satisfies the unitarity condition.

$$\mathbf{K} = \begin{pmatrix} pp \to pp & pp \to \mathrm{p}d & pp \to N\Delta \\ \mathrm{p}d \to pp & \mathrm{p}d \to \mathrm{p}d & \mathrm{p}d \to N\Delta \\ N\Delta \to pp & N\Delta \to \mathrm{p}d & N\Delta \to N\Delta \end{pmatrix}.$$

To satisfy the conservation laws, $N\Delta$ is either $p\Delta^{+}$ or $n\Delta^{++}$.

As described in Appendix B, our two nucleon system contains spin singlet and spin triplet states and inelastic channels require parity conservation. This condition requires two 4×4 *K*-matrices that contain 2×2 spin flipped matrices. Two such 4×4 *K*-matrices follow;

When *J* is even and the parity is even, or *J* is odd and the parity is odd, the 2×2 spin flipped pp system couples to the non-spin flipped $\mathrm{p}d$ system. In this case, the 4×4 *K*-matrix formalism is

$$\mathbf{K} = \begin{pmatrix} pp_{L=J-1} \to pp_{L=J-1} & pp_{L=J-1} \to pp_{L=J+1} & pp_{L=J-1} \to \mathrm{p}d_{L=J} & pp_{L=J-1} \to N\Delta_{L} \\ pp_{L=J+1} \to pp_{L=J-1} & pp_{L=J+1} \to pp_{L=J+1} & pp_{L=J+1} \to \mathrm{p}d_{L=J} & pp_{L=J+1} \to N\Delta_{L} \\ \mathrm{p}d_{L=J} \to pp_{L=J-1} & \mathrm{p}d_{L=J} \to pp_{L=J+1} & \mathrm{p}d_{L=J} \to \mathrm{p}d_{L=J} & \mathrm{p}d_{L=J} \to N\Delta_{L} \\ N\Delta_{L} \to pp_{L=J-1} & N\Delta_{L} \to pp_{L=J+1} & N\Delta_{L} \to \mathrm{p}d_{L=J} & N\Delta_{L} \to N\Delta_{L} \end{pmatrix}.$$

Here, the relations between angular momentum *L* and total angular momentum *J* are explained in Appendix B. For the $N\Delta$ state, we assume that the lowest angular momentum state with the correct J^{P} is dominant.

When *J* is even and the parity is odd, or *J* is odd and the parity is even, the 2×2 spin flipped $\mathrm{p}d$ system couples to the non-spin flipped pp system. In this case, the 4×4 *K*-matrix formalism is

$$\mathbf{K} = \begin{pmatrix} \mathrm{p}d_{L=J-1} \to \mathrm{p}d_{L=J-1} & \mathrm{p}d_{L=J-1} \to \mathrm{p}d_{L=J+1} & \mathrm{p}d_{L=J-1} \to pp_{L=J} & \mathrm{p}d_{L=J-1} \to N\Delta_L \\ \mathrm{p}d_{L=J+1} \to \mathrm{p}d_{L=J-1} & \mathrm{p}d_{L=J+1} \to \mathrm{p}d_{L=J+1} & \mathrm{p}d_{L=J+1} \to pp_{L=J} & \mathrm{p}d_{L=J+1} \to N\Delta_L \\ \mathrm{p}d_{L=J} \to \mathrm{p}d_{L=J-1} & pp_{L=J} \to \mathrm{p}d_{L=J+1} & pp_{L=J} \to pp_{L=J} & pp_{L=J} \to N\Delta_L \\ N\Delta_L \to \mathrm{p}d_{L=J-1} & N\Delta_L \to \mathrm{p}d_{L=J+1} & N\Delta_L \to pp_{L=J} & N\Delta_L \to N\Delta_L \end{pmatrix}.$$

These 4×4 K-matrices are real, symmetric matrices and satisfy the unitarity for the whole system.

Bibliography

[1] R. A. Arndt, *et. al*., Phys. Rev. C **50**, 2731 (1994).

[2] R. A. Arndt, *et. al*., Phys. Rev. C **50**, 1796 (1994).

[3] R. A. Arndt, *et. al*., Phys. Rev. C **48**, 1926 (1993).

[4] These results and corresponding data bases can be viewed and compared with previous analyses by SAID (Scattering Analysis Interactive Dial-In) program in VPI&SU. It is provided at the WWW site http://clsaid.phys.vt.edu or through a telnet call to vtinte.phys.vt.edu with user/password: physics/quantum, or to clsaid.phys.vt.edu with user: said (no password). We have used an updated version (WI96) of the published solution (SM94) for the *NN* interaction in reference 1. Both solutions covered T_p = 0 ~ 1600 MeV (for the *np* case we analyzed T_n = 0 ~ 1300 MeV) or $\sqrt{s}$ = 1880 ~ 2560 MeV. For the $\mathrm{p}d$ elastic reaction, there is no data change from reference [2] and the solution is SM94. For the $\mathrm{p}d \rightarrow pp$ reaction, we have used an updated version (SP96) of the published solution (SP93). The SP93 solution covered T_p = 0 ~ 500 MeV ($\sqrt{s}$ = 2015 ~ 2440 MeV) and the SP96 solution covers T_p = 0 ~ 550 MeV ($\sqrt{s}$ = 2015 ~ 2480 MeV). For the unified analysis, the solution is C500.

[5] H. Garcilazo and T. Mizutani, p*NN Systems* (World Scientific, Singapore, 1990).

[6] F. Shimizu *et al*., Nucl. Phys. **A386**, 571 (1982); Nucl. Phys. **A389**, 445 (1982).

[7] G.W. Barry, Phys. Rev. D **7**, 1441 (1973). The binding energy of the deuteron can be found in any atomic or nuclear Physics text book, for example, O. Oldenberg, *Introduction to Atomic and Nuclear Physics* (McGraw-Hill, New York, 1961) p277.

[8] J. Nagata *et al*., Phys, Rev. C **45**, 1432 (1992).

[9] B.J. Edwards and Gerald H. Thomas, Phys. Rev. D **22**, 2272 (1980); B.J. Edwards, Phys. Rev. D **23**, 1978 (1981).

[10] N. Hiroshige *et al*., Prog. Theor. Phys. **72**, 1282 and 1287 (1984); **74**, 1161 (1985); Phys. Lett. **150B**, 41 (1985).

[11] R.A. Arndt *et al*., Phys. Rev. **135**, B628 (1964); **139**, B362 (1965); **139**, B380 (1965); **141**, 873 (1966); **154**, 1549 (1967); **159**, 1422 (1967); **169**, 1128 (1968); **169**, 1149 (1968);

[12] R.L. Setti and T. Lasinski, *Strongly Interacting Particles*, (U. of Chicago Press, Chicago, 1973).

[13] T. Ericson and W. Weise, *Pions and Nuclei*, (Clarendon Press, Osford, 1988) p82.; M.J. Moravcsik, "*The Two-Nucleon Interaction*", Oxford University Press (1963) p56, p70.

[14] J. Bystricky *et al*., J. de Phys. ; L. Eisenbud and E. Wigner, Proc. Nat. Acad. Sci. **27**, 281 (1941).

[15] R.A. Arndt *et al*., Phys. Rev. D **28**, 97 (1983)

[16] There are many papers and text books to describe the observables of the elastic *pp* reaction. We combined Bystricky's[13] and Moravcsik's notation. Moravcsik M. J., "*The Two-Nucleon Interaction*", Oxford University Press (1963) Chap. 1-2, pp11 - 20.

[17] W. Grein and M.P. Locher, J. Phys. G**7**, 1355 (1981).

[18] Madison convention, given in *Polarization Phenomena in Nuclear Reactions* (University of Wisconsin Press, Madison, 1971), p. XXV; Spherical tensors are given by W. Lakin, Phys. Rev. **98**, 139 (1955). Cartesian tensors are given by L.J.B. Goldfarb, Nucl. Phys. **7** 622 (1958); Also B. Blankleider and I.R. Afnan described the relationship between partial wave amplitudes and polarization observables in $pp \rightarrow d\pi^+$ and $\pi d \rightarrow \pi d$ in Phys. Rev. C **31**, 1380 (1985).

[19] H. Kamo and W. Watari, Pro. Theor. Phys. **62**, 1035 (1979); G. Cantale *et al*., Helv. Phys. Acta **60**, 398 (1987), and *ibid*. **64**, 736 (1991).

[20] J.M. Ford, VPI&SU Thesis, (1988) pp169-175.

[21] R.A. Arndt and M.H. MacGreror, *Methods in Computational Physics*, Vol6, p235-295, Academic Press, New York and London (1966).

[22] McNaughton, Phys. Rev. C **41**, 2809 (1990).

[23] (a) G. Cantale *et al*., Helv. Phys. Acta. **60**, 398 (1987); (b) G. Cantale *et al*., *ibid*, **64**, 736 (1991).

[24] H. Garcilazo, Phys. Rev. Lett. **61**, 1457 (1988); L. Mathelitsch and H. Garcilazo, Phys. Rev. C **28**, 1272 (1983) and Phys. Rev. C **32**, 1635 (1985) and Phys. Rev. C **34**, 1425 (1986); D. Ashery *et al*., **215**B, 41 (1988)

[25] E. Piasetzky *et al*., Phys. Rev. Lett. **53**, 540 (1984); J. Lichtenstadt *et al*., Phys. Rev. C **33**, 655 (1986); F.W.N. de Boer *et al*., Phys. Rev. Lett. **53**, 423 (1984)

[26] W.A. Gale and I.M. Duck, Nucl. Phys. B**8**, 109 (1968); T. Ueda, Phys. Lett. **74**B, 123 (1978); G. Kalberman and J.M. Eisenberg, J. Phys. G**5**, 35 (1979) and Phys. Lett. **211**B, 389 (1988); L. Mathelitsch and H. Garcilazo, Phys. Lett. B**234**, 234 (1990)

[27] R.J. Oakes, Phys. Rev. **131**, 2239 (1963).

[28] R.L. Jaffe, Phys. Rev. Lett. **38**, 195 (1977); Phys. Rev. D **15**, 267 and 281 (1977).

[29] P.J. Mulders *et al*., Phys. Rev. D **19**, 2635 (1979) and Phys. Rev. D **21**, 2653 (1980).

[30] M.M. Hoening and A.S. Rinat, Phys. Rev. C **10**, 2102 (1974).

[31] B.L.G. Bakker *et al*., Lett. Nuovo Cim. **19**, 265 (1977); Yu.A. Simonov and M. van der Velde, Phys. Lett. **76**B, 277 (1978) and J. Phys. G**5**, 493 (1979); I.M. Narodetsky and Yu.A. Simonov, Sov. J. Nucl. Phys. **28**, 698 (1978).

[32] L. Fonda *et al*., Phys. Rev. D **8**, 353 (1973).

[33] R.A. Arndt, Phys. Rev. **165**, 1834 (1968).

[34] F. Furuichi and H. Suzuki, Prog. Theor. Physics. **57**, 1803 (1977); H. Suzuki, Prog. Theor. Phys. **50**, 1080 and **54**, 143 (1974).

[35] J.P. Auer *et al*, *Phys. Lett.* **67B**, 113 (1977); W. de Boer *et al*, Phys. Rev. Lett. **34**, 558 (1975).

[36] J. A. Niskanen, Phys. Lett. **71B**, 40 (1977).

[37] T. Kamae and T. Fujita, Phys. Rev. Lett. **38**, 471 (1977).

[38] A. Yokosawa, Phys. Rep. **64**, 47 (1980).

[39] H.G. Dosch and E. Ferreira, Phys. Rev. C **29**, 2254 (1984) and Phys. Rev. C **32**, 496 (1985).

[40] E. Ferreira *et al*., Phys. Rev. C **34**, 226 (1986) and Phys. Rev. C **36**, 1916 (1987).

[41] H. Garcilazo, Phys. Rev. Lett. **53**, 652 (1984) and Phys. Rev. C **35**, 1804 (1987).

[42] I. Duck, Phys. Lett. **106B**, 267 (1981); B.J. VerWest, Phys. Lett. **83B**, 161 (1979).

[43] W.M. Kloet *et al*., Phys. Lett. **99**B, 80 (1981).

[44] R.L. Shypit *et al*., Phys. Rev. Lett. **60**, 901 (1988).

[45] W.M. Kloet and J.A. Tjon, Phys. Lett. **106B**, 24 (1981).

[46] R.L. Shypit *et al*., Phys. Rev. Lett. **60**, 901 (1988) and Phys. Rev. C **40**, 2203 (1989)

[47] R.A. Arndt *et al*., Phys. Rev. D **35**, 128 (1987).

Vita

Chang-Heon Oh was born on 21 October 1960, in Busan, Korea. He received his B.S. degree in 1983 and M.S. degree in 1985 in Physics from Yonsei University, Seoul, Korea.

He resumed his Physics studies at Virginia Polytechnic Institute & State University in 1991. He received another M.S. degree in 1993 in Physics from VPI&SU. He will receive his Doctor of Philosophy degree in Physics from VPI&SU in May of 1997.

Chang-Heon Oh

April 23, 1997